Supercritical Production of Biodiesel from Waste Cooking Oil

A Technical Report Submitted to the Department of Chemical Engineering

Presented to the Faculty of the School of Engineering and Applied Science

University of Virginia, Charlottesville, Virginia

In Partial Fulfillment of the Requirements for the Degree

Bachelor of Science in Chemical Engineering

By

Annika Szyniec, Felipe De Pinho, Maya Reese, Nitin Elavarasu, and Samuel Martin

May 5, 2025

On my honor as a University student, I have neither given nor received unauthorized aid on this assignment as defined by the Honor Guidelines for Thesis-Related Assignments.

ADVISOR

Eric Anderson, Department of Chemical Engineering

Table of Contents

1 Executive Summary

The purpose of this study was to create a technical design for a biodiesel plant capable of producing approximately 9,500 t/yr of B100 biodiesel from waste cooking oil (WCO). This plant also produces pharmaceutical-grade glycerol as a valuable side product. The use of a waste product as a feedstock improves the sustainability of the design as it does not require the extraction of underground carbon stores, reducing greenhouse gas emissions. Our design uses methanol in its supercritical state to eliminate the need for expensive catalysts in the reactor and to allow for lower quality feedstocks.

This report outlines how WCO is converted to fatty acid methyl esters (FAMEs) and glycerol through two reaction pathways in a singular plug flow reactor (PFR). One pathway is the hydrolysis of WCO and the subsequent esterification of free fatty acids (FFAs). The other pathway is the direct transesterification of WCO. Unreacted methanol and a propane co-solvent are recovered in the downstream separations processes to reduce raw material costs. Biodiesel and glycerol are purified to meet the ASTM D6751-24 and USP standards, respectively.

The total capital cost of the plant is $25,600,000 and the operating cash flow after startup is $8,760,000. An economic analysis resulted in an IRR of 13.7% and a net present value of $72,180,000, given a $1/gal biodiesel produced tax credit. These values represent the potential for promising economic returns. However, a sustained biodiesel tax credit cannot be guaranteed throughout the life of the plant. Without a biodiesel tax credit, the IRR drops to 5.2%, which is not an acceptable investment. Additionally, uncertainty lies with the use of weight percentage based kinetic data used for our team's conversion results and the implementation of this new supercritical reaction technology. Therefore, our team recommends that, in the case of a biodiesel tax credit, a pilot-scale reactor is built to verify the kinetic data prior to a final decision regarding the construction of a full-scale plant.

2   Abbreviations

ACGIH	American Conference of Governmental Industrial Hygienists
ALOHA	Ariel Locations of Hazardous Atmospheres (CAMEO Software Suite)
ASTM	American Society for Testing and Materials
BOD	Biochemical Oxygen Demand
CEPCI	The Chemical Engineering Plant Cost Index
COP	Coefficient of Performance
CS	Carbon Steel
EPA	Environmental Protection Agency
ERPG	Emergency Response Planning Guidelines
FAME	Fatty Acid Methyl Ester
FFA	Free Fatty Acid
G&A	General and Administrative
GHG	Greenhouse Gasses
HAZOP	Hazard and Operability Study
HETP	Height Equivalent to Theoretical Plate
HPS	High Pressure Steam
IEF	Initiating Event Frequency
IPL	Independent Protection Layer
IRR	Internal Rate of Return
ISBL	Inside Battery Limits
LMTD	Log-mean Temperature Difference
LOPA	Layer of Protection Analysis
LPS	Low Pressure Steam
MCE	Most Credible Event
NFPA	National Fire Protection Association
NIOSH	National Institute for Occupational Health and Safety
NRTL-RK	Non-random Two-liquid Redlich-Kwong Model
NPV	Net Present Value
OP	Operating Laborer
OSHA	Occupational Safety and Health Administration
PFR	Plug Flow Reactor
ROI	Return on Investment
SDS	Safety Data Sheet
SP	Supervising Laborer
SRK	Soave-Redlich-Kwong
SS	Stainless Steel
TMEF	Target Mitigated Event Frequency
TQ	Threshold Quantity
VOC	Volatile Organic Compound
WCO	Waste Cooking Oil

3   Introduction

In 2024, the growth in global energy demand almost doubled its recent average, bringing climate change and pollution control into international focus (International Energy Agency, 2025). As a result, there is growing concern about automobile emissions and the impact of greenhouse gasses (GHG), which accelerate the warming of the Earth's surface by preventing heat loss into space. To mitigate these effects, the Environmental Protection Agency (EPA) has set a goal of achieving net-zero GHG emissions across the economy by 2050 (US EPA, 2023). In 2016, the transportation sector overtook electric power in GHG emissions (Bleviss, 2021). Since then, GHG emissions from transportation have continued to rise, now encompassing over 28% of global carbon emissions (US EPA, 2015). Therefore, transitioning vehicles to cleaner and more sustainable fuels is vital to reaching the EPA's goal and protecting our planet against climate change.

Biodiesel, made from the reaction of biomass – such as vegetable oils or animal fats – and alcohols, has been seen as a potential alternative to petroleum-based diesel fuels (Sheehan et al., 1998). Traditional highway petroleum (low sulfur) diesel introduces new carbon into the atmosphere that was previously held as underground reserves, such as crude oil. However, biodiesel utilizes carbon sources that have already been in the atmosphere, including carbon absorbed by plants during photosynthesis. In America, most highway diesel sold at gas stations is a 5% biodiesel blend (Hearst Autos Research, 2020). Increasing access to higher percentage blends is key to reducing carbon emissions. While the biodiesel market is on the rise, having produced 21.8 billion gallons in 2024 compared to only 25 million gallons in 2005, its cost remains a hindrance to large-scale adoption (Greer, 2024; Hearst Autos Research, 2020).

Current methods of biodiesel production require the use of alkali, acid, or enzymatic catalysts to transesterify the triglycerides found in the lipids of biomass. This process involves using alcohols, such as methanol, to help convert these triglycerides into free fatty acid methyl esters (FAME), commonly known as biodiesel (Zeng et al., 2014). These processes have significant limitations, including slow reaction rates and sensitivity to water and free fatty acids (FFAs), which increase operation costs (Van Kasteren & Nisworo, 2007; Zeng et al., 2014). When FFAs found in waste oils react with alkali catalysts, soaps are formed. This unwanted by-product results in unsalable waste material and reduces the methyl ester yield by interfering with the transesterification reaction. Also, enzymatic catalysts, such as lipases, are expensive and deactivate in the presence of methanol (Zeng et al., 2014). Overall, due to pre-treatment costs to remove water and fatty acids, catalyst maintenance, and catalyst replacement, all catalytic transesterification methods have costly inhibitors to their full adoption in biodiesel production (Nagapurkar & Smith, 2023; Zeng et al., 2014).

However, recent developments in supercritical transesterification may result in cost reductions in biodiesel production. At supercritical conditions, changes in pressure alter the solubility of the reactant and products and cause the fluid, methanol, to exhibit properties of both

a liquid and a vapor (Zeng et al., 2014). As a result, catalysts are not required to assist in the reaction, and the separation of products is simpler (Van Kasteren & Nisworo, 2007). Furthermore, supercritical pathways are insensitive to water and fatty acids, eliminating the need for extensive pretreatment. This allows for lower-grade feedstocks, such as waste cooking oil (WCO), the focus of our project, to undergo transesterification and ultimately lower feed costs.

The goal of this project was to design a biodiesel production facility centered around a supercritical transesterification reaction of WCO. Furthermore, our team designed the necessary separation and purification steps to sell pure B100 biodiesel that meets the ASTM D6751-24 standard and pharmaceutical-grade glycerol that meets the USP standard. Finally, our team assessed the potential safety and environmental concerns of the process, the plant construction timeline, and the overall economic feasibility of the design.

4   Previous Work

Previous studies about supercritical biodiesel production processes using WCO were used to inform this design. Van Kasteren & Nisworo (2007) designed a supercritical transesterification process for continuous biodiesel production for three plant capacities: 125,000, 80,000, and 8,000 t/yr of biodiesel. The researchers found that the process was economically competitive with current alkali and acid-catalyzed biodiesel production processes. However, the researchers used the universal quasi-chemical (UNIQUAC) thermodynamic fluid package to model the transesterification, which is unsuitable for supercritical conditions.

Nagapurkar and Smith (2023) conducted a techno-economic and environmental life cycle analysis for supercritical biodiesel production from WCO based in the Midwest United States. The researchers used the Soave-Redlich-Kwong (SRK) thermodynamic fluid package to model the transesterification reaction, which is suitable for elevated pressures and temperatures. However, the researchers only modeled the single reaction pathway and did not consider the potential for competing reactions. Specifically, the hydrolysis and subsequent methyl esterification of free fatty acids (FFA) should be considered due to the presence of water in the WCO feed.

This report overcomes these gaps and makes novel contributions by:

1. Using a suitable thermodynamic package for supercritical conditions
2. Performing a kinetics-based simulation of the transesterification of triglycerides and the hydrolysis and subsequent methyl esterification of FFAs
3. Detailing information on equipment choices and plant safety considerations
4. Conducting an economic analysis and assessing the viability of the plant

5   Design Basis

Our facility is located in Lancaster, Pennsylvania, and uses WCO feedstock sourced from nearby snack food companies. Specifically, Lancaster and York counties are known for having large numbers of potato chip factories, including Utz Potato Chips, Martin's Potato Chips, Snyder's of Hanover, and Herr's Snack Factory (Beck, 2022). This location is beneficial due to its proximity to major Northeastern cities, including Philadelphia and Baltimore, which have large transportation, supply, and consumer networks. A typical potato chip factory has an output of 15,700 L WCO/day (Sourcemap, 2022). Based on this approximation, a potato chip factory can be expected to produce 5,272 t/yr of WCO (Section 13.1).

A previous economic analysis of a supercritical biodiesel process found that a plant with a 10,600 t/year capacity had a two-year payback period and a break-even selling price of $2.42/gal (Nagapurkar & Smith, 2023). Another economic analysis of an 8,000 t/yr biodiesel plant found that the required selling price was $2.04/gal (Van Kasteren & Nisworo, 2007). To reach a similar production capacity to these simulations, we are sourcing WCO from two potato chip factories. Our plant will have a total WCO feed quantity of 9,489.7 t/yr.

Using this feedstock quantity, our process resulted in a product yield of 96.9% with a total biodiesel production capacity of 9,206.1 t/yr. This capacity was reached with a continuous 24/7 production schedule, assuming the plant will be shut down for 10% of the year for repairs and maintenance. These results align with previous simulations of supercritical biodiesel production processes, which had product yields between 95% and 97% (Van Kasteren & Nisworo, 2007; Zeng et al., 2014).

6   Discussion

This section includes information regarding the chosen feedstocks, products, and the decisions that were made to design the final process plant.

6.1   Feedstocks

The raw materials required to produce biodiesel are: WCO (modeled as triolein), methanol, and propane.

6.1.1   Waste Cooking Oil

The WCO feed is prefiltered, used frying oil from potato chip factories. The most common types of frying oils used in potato chip manufacturing include corn, canola, sunflower, high oleic safflower, and cottonseed oils (Aykas & Rodriguez-Saona, 2016). However, a specific triglyceride was required for modeling. Triolein ($C_{57}H_{104}O_6$) was used as the model compound for WCO (Figure 6.1.i) (Nisworo, 2005). Triolein is a triglyceride that makes up 40-80% of the fatty acids found in common waste oils, including canola, palm, rapeseed, olive, and peanut oil. Many past studies have used it as a model for vegetable oils (Lee et al., 2011). Furthermore, triolein is available in the ASPEN Plus data bank. The filtered triolein feed does not require any additional pre-processing, such as water or free-fatty acid (FFA) removal, because the supercritical nature of the transesterification process can handle feeds with up to 36 wt% water and 30 wt% FFAs (Zeng et al., 2014). Oleic acid was selected to model the FFAs because it is the FFA that makes up triolein and is present in high concentrations in commonly used cooking oils (Bautista et al., 2009). The composition of the WCO that we will use is shown in Table 6.1.i (Anantapinitwatna et al., 2019).
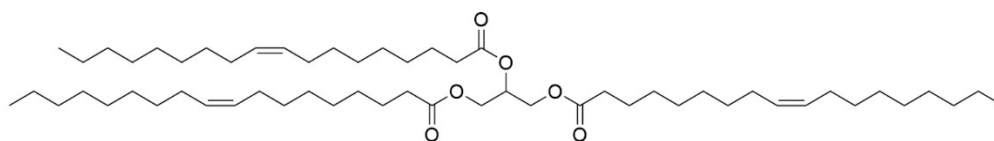
Figure 6.1.i Triolein Structure. Adapted from NIST, 2023.

Table 6.1.i WCO Feedstock Composition

Component	Weight Percent
Triglycerides	86
Oleic Acid	10
Water	4

6.1.2   Methanol

Methanol is reacted with WCO to produce biodiesel. Other low molecular weight alcohols could also have been used as reactants, including ethanol, propanol, or butanol. However, methanol is the best choice for the reactant because it is cheaper and more reactive

than the other alcohols (Gutiérrez Ortiz & de Santa-Ana, 2017; Nagapurkar & Smith, 2023). Methanol purities over 99%, such as grade A or AA, produce the highest product yield, as well as reduce the potential contamination of the biodiesel and glycerol products (Aboelazayem et al., 2018). Grade AA methanol was chosen for this process. Grade AA methanol is 99.85% pure, and the primary contaminant is ethanol at a concentration of less than 10 mg/kg (*Methanol*, 2024). Unlike grade A, which is contaminated with acetone, ethanol can also be used in the supercritical transesterification reaction, so it is a better choice (Van Kasteren & Nisworo, 2007). Furthermore, there is no substantial price differential between the grades.

6.1.3 Propane

Propane was used as a co-solvent to reduce the operating temperature, pressure, and amount of methanol required. Liquid co-solvents, such as *n*-hexane and tetrahydrofuran, could have also been used, but additional separation steps would have been required. As a gaseous co-solvent, propane can easily be separated from the products through expansion and can be directly recycled (Zeng et al., 2014). Previous studies have shown that propane can reduce methanol's supercritical temperature from 320°C to 280°C and supercritical pressure from 400 to 128 bar. Moreover, propane reduced the methanol-to-oil molar ratio from 42:1 to 24:1 (Van Kasteren & Nisworo, 2007). In our process, we used high-purity (99.5%) propane. The remaining 0.5% contained contaminants, including ethane, butane, and propylene (Scientific Solutions, n.d.).

6.2 Products

Our process produces biodiesel and pharmaceutical-grade glycerol as products.

6.2.1 Biodiesel

For commercial sale, the biodiesel produced in the process must adhere to the ASTM D6751-24 standard for biodiesel production. The diesel produced by our process is sold unblended (B100) to oil refineries, where it is likely to be blended with petroleum-based diesel into 5% or 20% biodiesel blends (Alternative Fuels Data Center, n.d). The biodiesel is formed by the transesterification of triglycerides with methanol to produce fatty-acid methyl esters (FAMEs). Furthermore, an esterification side reaction converts the FFA in the oil into FAMEs as well. More detail on the reactions is outlined in Section 6.4.1. For every one mole of triglyceride, three moles of FAMEs are produced, and for every one mole of FFA esterified, one mole of FAMEs is produced. Biodiesel is composed of four main FAMEs: methyl oleate, methyl linoleate, methyl palmate, and methyl stearate. For modeling, methyl oleate, $C_{19}H_3O_2$, was selected because it accounts for over half of the FAMEs in biodiesel (Figure 6.2.i) (Khan et al., 2021; Nagapurkar & Smith, 2023; Van Kasteren & Nisworo, 2007). Also, methyl oleate is the FAME produced when methanol is reacted with triolein; methyl oleate is available in the ASPEN Plus data bank.
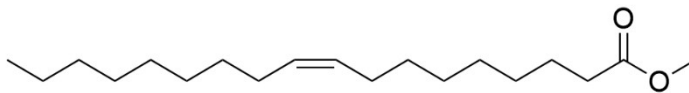
Figure 6.2.i Structure of Methyl Oleate

The requirements to meet the ASTM D6751-24 standard are listed in Section 13.3. The testing properties include water and sediment concentration, viscosity, flash point, sulfated ash, and alcohol (ASTM, 2024). Because an ASPEN Plus simulation was used to model the process, not every specification could be measured. Only water, methanol, and free glycerol concentrations were considered for this design. Other specifications, such as cloud point and acid concentration, were assumed to meet requirements because either a reliable estimate could not be produced in the simulation, or the contaminants, such as KOH, are only associated with catalyzed transesterification processes.

6.2.2 Pharmaceutical-Grade Glycerol

Pharmaceutical-grade glycerol with a 99.7% purity is a product of this process. To meet USP pharmaceutical-grade glycerol specifications, there are limits for heavy metals, sulfates, water, unreacted triglycerides, and FAMEs. The specific limits are detailed in Section 13.2 (SRS Engineering Corporation). Because of the chosen feedstock, contaminants, such as sulfur, are unlikely to appear in our final product. Furthermore, as the supercritical transesterification reaction does not require any catalysts or reagents, apart from triglycerides and methanol, the purification of the glycerol by-product is more achievable (Zeng et al., 2014). Therefore, our team focused on glycerol content, water content, fatty acid and ester content, and specific gravity as the primary metrics to meet the USP standard.

Pharmaceutical-grade glycerol is a common additive in the food, healthcare, and beauty products industries due to its high purity. Compared to crude glycerol, pharmaceutical-grade glycerol has a significantly higher market value, over $460/ton more (*Pharma Grade Glycerin, n.d*). High-purity glycerol will be sold as a high-value by-product, which increases the revenue of the biodiesel plant.

6.3 Feed and Product Quantities and Process Flow Diagram

The overall simplified block flow diagram is shown in Figure 6.3.i. The process begins with the reactor. Then, the products are separated into three streams: a recycle stream of unreacted methanol and the propane co-solvent, a biodiesel stream, and an unpurified glycerol stream. The drying and purification steps are required for the products to meet their standards. The absorption step removes the high levels of methanol from the biodiesel drying vapor.

The final process flow diagram is shown in Figure 6.3.ii. The black squares denote mixing at T-junctions. The process equipment is identified using the following nomenclature: [Equipment Type Abbreviation] – [Equipment Number]. The equipment type abbreviations are defined in Table 6.3.i.
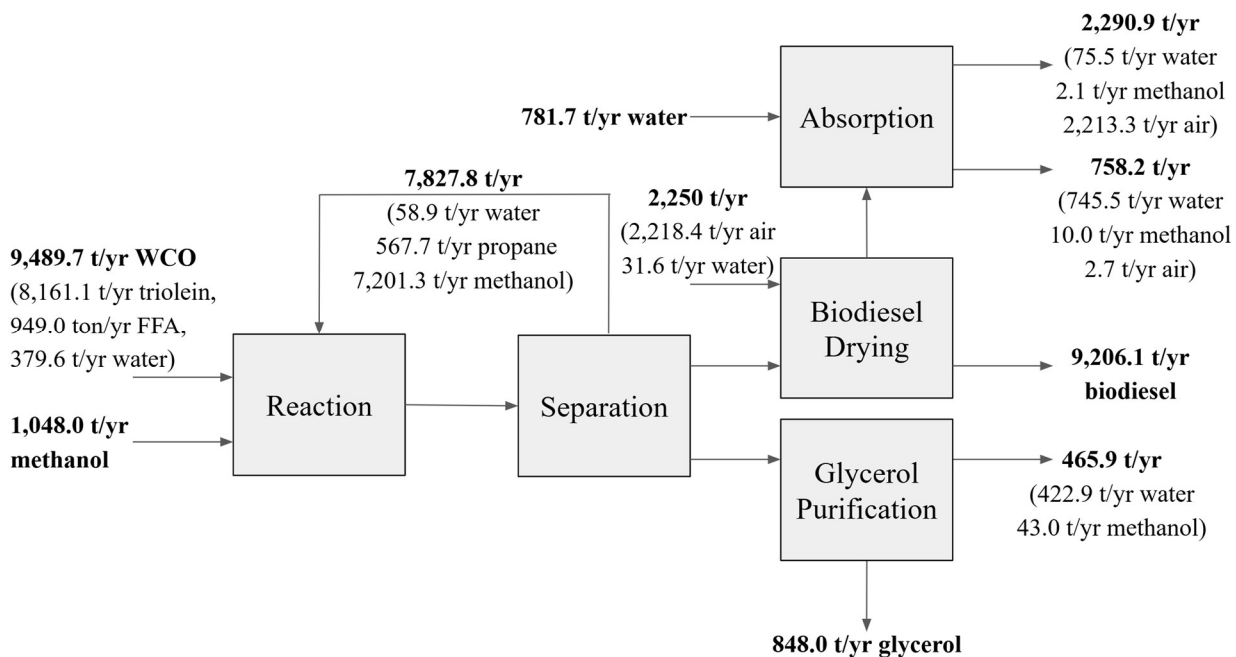
Figure 6.3.i Simplified Block Flow Diagram

Table 6.3.i Equipment Abbreviations

Equipment Type	Abbreviation
Pump	P
Heat Exchanger	HX
Reactor	R
Flash Evaporator	F
Distillation Column	D
Reflux Drum	RD
Reflux Pump	RP
Decanter	S
Absorber	A
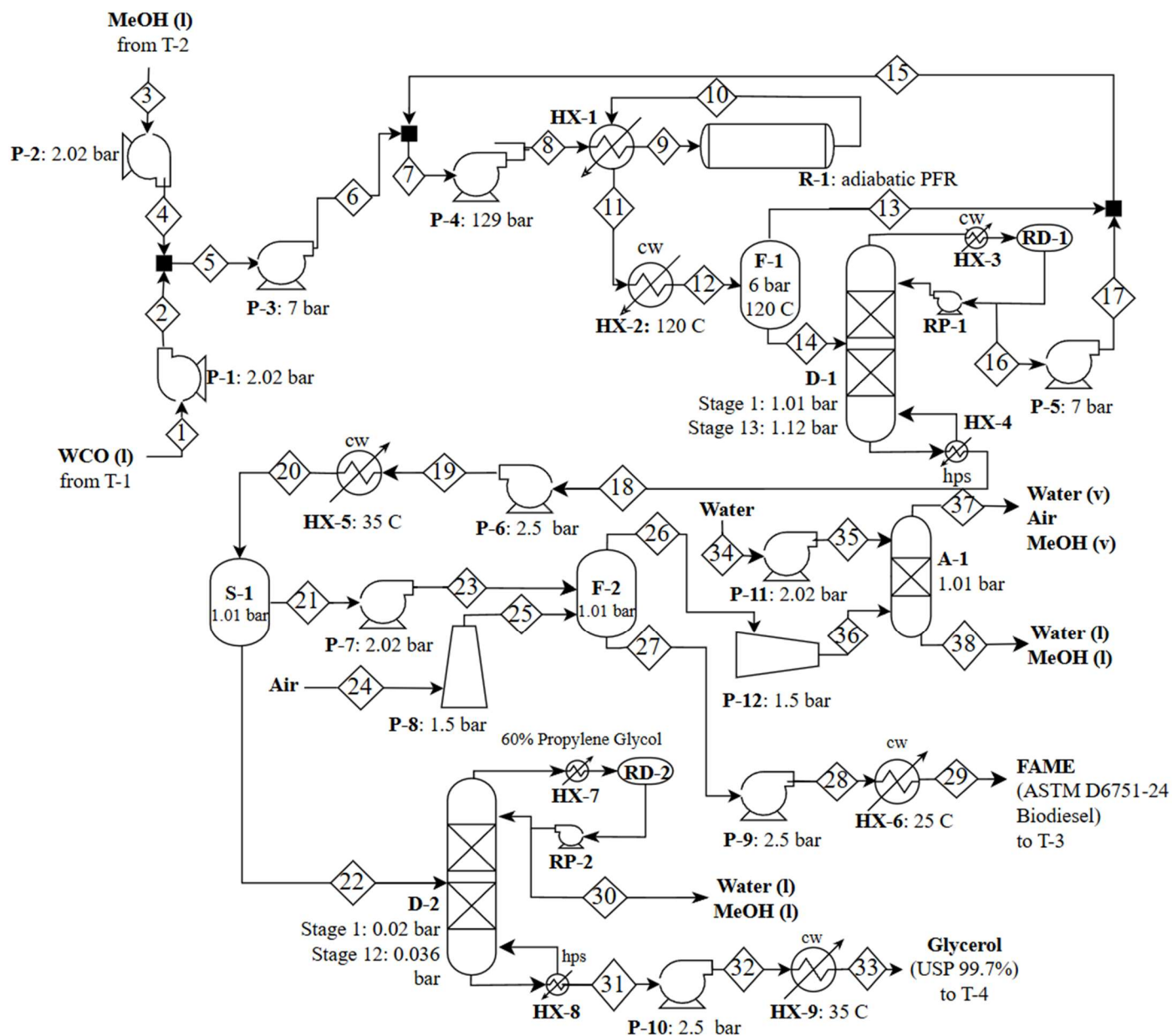
Figure 6.3.ii Process Flow Diagram

6.4   Reactor

The principal reactions for biodiesel production are the transesterification of triglycerides, hydrolysis of triglycerides, and esterification of FFAs. Because our team chose a continuous process, an adiabatic plug flow reactor (PFR) was selected. Supercritical process conditions were chosen to eliminate the need for expensive acid, alkali, or enzymatic catalysts (Van Kasteren & Nisworo, 2007; Zeng et al., 2014). Catalyzed systems incur high input costs, as well as high maintenance and separation costs due to soap generation. Moreover, higher-grade feedstocks are required because catalysts are sensitive to high water and FFA concentrations, which are present in low-grade WCO (Nagapurkar & Smith, 2023; Zeng et al., 2014).

The reactor operating conditions are summarized in Table 6.4.i. The chosen temperature and pressure values are consistent with past studies in literature (Nagapurkar & Smith, 2023; Nisworo, 2005; Okoro et al., 2018; Van Kasteren & Nisworo, 2007). These conditions have yielded high FAME concentrations without surpassing 340˚C, where fatty acids are susceptible to thermal cracking and degradation (Kusdiana & Saka, 2001; Modi, 2010).

Table 6.4.i Reactor Operating Conditions

Condition	Value
Temperature (˚C)	280
Pressure (bar)	128
Heat Transfer (J)	0

The reactor was modeled in ASPEN Plus using the Soave-Redlich-Kwong (SRK) property method. SRK is a cubic equation of state that is useful for modeling high-pressure systems. Furthermore, SRK can accurately model mildly polar hydrocarbon interactions, such as the water and methanol contained in the process (Nagapurkar & Smith, 2023).

6.4.1   Reactions

The production of biodiesel (FAMEs) from triglycerides can occur via two reaction routes: 1) transesterification of triglycerides or 2) hydrolysis and subsequent methyl esterification of FFAs (Figure 6.4.i). The first reaction pathway typically runs in a high excess of alcohol, while the second pathway runs in an excess of both water and alcohol (Kusdiana & Saka, 2004).
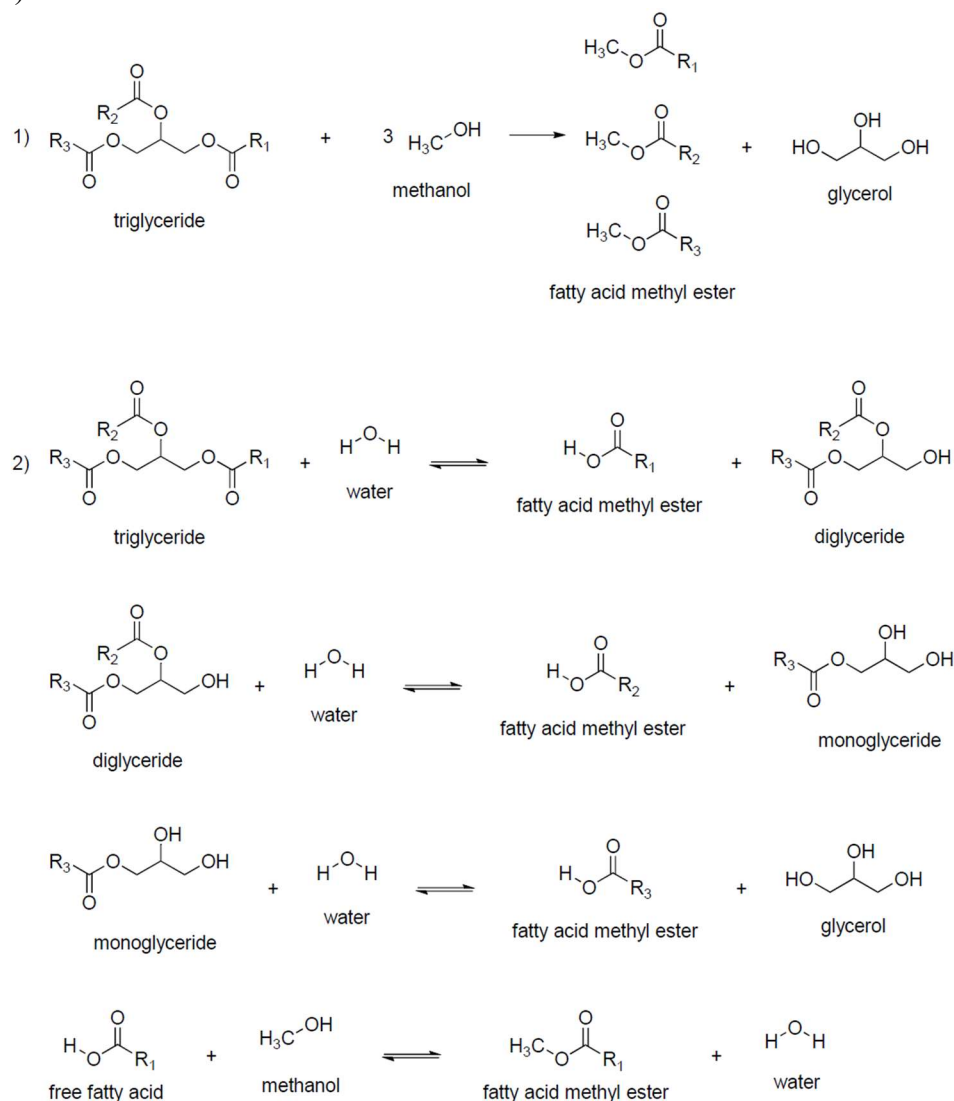
Figure 6.4.i Complete Reaction Pathway

Our system will run with a 1:24 molar ratio of WCO to methanol. The large excess of methanol ensures that triglyceride and FFA are the limiting reactants, which improves product yields. As mentioned in Section 6.1.3, previous studies on triglyceride transesterification required higher WCO-to-methanol ratios (1:42) (Kusdiana & Saka, 2001). However, the addition of a propane co-solvent lowers alcohol requirements, lowers operating temperatures and pressures, and increases oil and water miscibility. These benefits have the potential to decrease

18

operating costs, decrease safety risks, and increase reaction rates (Zeng et al., 2014). A 20:1 molar ratio of methanol to propane was selected because it yields triglyceride conversions over 95%. (Nagapurkar & Smith, 2023; Nisworo, 2005; Van Kasteren & Nisworo, 2007; Zeng et al., 2014).

Due to the excess methanol in our team's proposed system, the primary reaction pathway is triglyceride transesterification. However, due to the initial concentrations of water and FFA in the WCO, hydrolysis and esterification are likely side reactions that were considered. Our team simplified the reactions shown in Figure 6.4.i to three irreversible reactions that are shown in Figure 6.4.ii. Details on the simplification rationale are provided in the following section on reaction kinetics (Section 6.4.2).
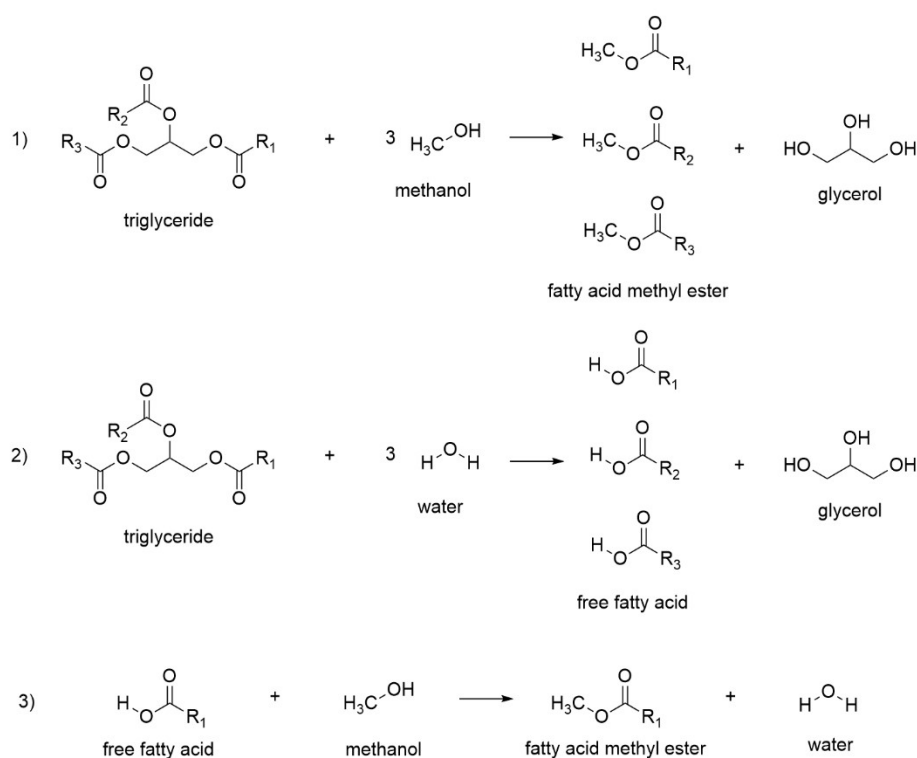
Figure 6.4.ii Simplified Reactions

6.4.2   Kinetics

Previous studies have modeled kinetics for transesterification, hydrolysis, and esterification separately (Kusdiana & Saka, 2001; Alenezi, 2009; Alenezi, 2010; Tsai, 2013). However, few studies have modeled all three reactions in a single reactor (Jebur, 2017). For this study, the kinetics were modeled using the works of Okoro et al. (2018) due to the inclusion of kinetic data for transesterification, esterification, and hydrolysis.

The supercritical transesterification of triglycerides was modeled as a first-order reaction with respect to triglyceride concentration and reaction temperature. Due to the supercritical state

of methanol and high methanol excess, the reaction was considered irreversible and was modeled using Equation 6.4.i below. Water and FFA concentrations have little effect on the transesterification reaction rate (Ma & Hanna, 1999; Nagapurkar & Smith, 2023).

Equation 6.4.i Transesterification Rate Expression

$$r_t = -\frac{dC_{TG}}{dt} \cong k_t C_{TG}$$

The hydrolysis of triglycerides using subcritical water was modeled as a first-order, irreversible reaction as a function of the triglyceride concentration (Equation 6.4.ii). Triglyceride hydrolysis has been reported to occur via a reversible, stepwise pathway, forming diglycerides and monoglycerides as intermediary molecules as depicted in Figure 6.4.i (Okoro et al., 2018). However, experimental studies have demonstrated the validity of using a pseudo-homogenous first-order, irreversible kinetic relation given an excess of water and subcritical water reaction conditions (Okoro et al., 2018; Kocsisová et al., 2006; Sturzenegge & Sturm, 1951). Alenezi et al. (2009) modeled the kinetics for the 3-step, reversible hydrolysis reaction and found that the initial hydrolysis of triglyceride was the rate-limiting step because it had the highest activation energy. In addition, the values of the reversible reaction rates were close to zero, supporting the use of an irreversible rate relation. Due to a 2:1 molar excess of water to triglycerides in our system and the subcritical water reaction conditions, our team modeled the hydrolysis reaction using the rate expression below (Equation 6.4.ii).

Equation 6.4.ii Hydrolysis Rate Expression

$$r_{hy} = -\frac{dC_{TG}}{dt} \cong k_{hy} C_{TG}$$

The supercritical esterification of FFAs was modeled as a first-order rate expression with respect to FFA concentration. Due to the high molar excess of methanol, the reaction was modeled as irreversible, as shown in Equation 6.4.iii.

Equation 6.4.iii Esterification Rate Expression

$$r_{est} = -\frac{dC_{FFA}}{dt} \cong k_{est} C_{FFA}$$

The reaction rate constants k_t, k_{hy}, and k_{est} were determined using the Arrhenius equation, where A is the pre-exponential constant (s^{-1}), E is the activation energy (kJ/kmol), R is the universal gas constant ($8.314 \frac{kJ}{kmol \cdot K}$), and T is the temperature (K) (Equation 6.4.iv). The pre-exponential constants and activation energies for each reaction reported by Okoro et al. (2018) are provided in Table 6.4.ii. These values were the inputs to the RPLUG block in ASPEN Plus.

Equation 6.4.iv Arrhenius Equation

$$k = Ae^{-[\frac{E}{RT}]}$$

Table 6.4.ii Kinetic Data (Okoro et al., 2018)

Reaction	Transesterification	Esterification	Hydrolysis
A (s^{-1})	141.8	0.1	169,227.6
E (kJ/kmol)	56,000	21,980	88,120

Almost all previous kinetic studies of biodiesel synthesis via transesterification, esterification, and hydrolysis reactions in supercritical methanol use weight percentage as each reaction compound unit. This unit is used because it is difficult to accurately determine the density and concentration of each compound under supercritical conditions (Liu, 2013). However, this results in a rate that is not in terms of concentration per time and, therefore, cannot be entered easily into ASPEN Plus models. Due to a lack of concentration-based kinetic data and the agreement between the kinetic model used and experimental results, our team proceeded to use the kinetic models determined by Okoro et al. (2018). However, future kinetic research on supercritical biodiesel synthesis reactions should prioritize the development of concentration-based kinetic models to improve the validity of reaction simulations.

6.4.3   Reactor Dimensions and Design

The reactor dimensions were selected to maximize the conversion of triglycerides and FFA in the system. Not only does increasing the conversion increase the product yields, but it also reduces the need for additional downstream processing to remove unreacted FFAs in the biodiesel product, required by the ASTM D6751-24 standard.

Approximate reaction dimensions and residence times were predicted from past studies on triglyceride transesterification. Then, ASPEN Plus conversion data was used to optimize the dimensions (Nagapurkar & Smith, 2023; Nisworo, 2005; Van Kasteren & Nisworo, 2007). These studies modeled a PFR reactor at identical process conditions to those chosen by our team, 128 bar and 280˚C. Table 6.4.iii shows a comparison of reactor dimensions from previous studies with our team's results. The reactor dimensions proposed by our team resulted in a significantly larger reactor volume and a longer residence time. This can be attributed to our team's kinetic data and the decision to model three competing reactions in a single system. A benefit of our larger tube diameter is that it reduces the pressure drop across the reactor. The volumetric flow rate in the reactor is 10.2 m³/hr.

Table 6.4.iii Comparison of Reactor Dimensions

Source	Nisworo, 2005; Van Kasteren & Nisworo, 2007	Nagapurkar & Smith, 2023	Present Study
Plant Capacity (t/yr)	8,000	10,600	9,761
Residence Time (min)	17	8.35	79
Tube Length (m)	6	55	17
Tube Internal Diameter (cm)	10	10	50
Number of Tubes	21	2	4
Tube Thickness (mm)	7	---	60
Reactor Volume (m³)	0.99	0.86	13.40
Conversion	98%	97%	>99%

Both stainless steel and carbon steel were considered for the reactor material. Compared to carbon steel, stainless steel is stronger, harder, and more corrosion resistant. Stainless steel is commonly used in food and pharmaceutical processes to prevent product contamination (*Carbon Steel vs Stainless Steel*, n.d.). Despite the benefits, stainless steel is 30% more expensive than carbon steel (Towler & Sinnott, 2022). Prior studies on supercritical biodiesel production have differing opinions on reactor material (G Doná et al., 2013; Modi, 2010.; Nagapurkar & Smith, 2023; Nisworo, 2005). Ultimately, due to cost benefits, carbon steel was chosen.

The thickness of the reactor tube walls was determined in accordance with the ASTM BPV Code Sec. VIII D.1 of the pressure vessel code. The max stress for a carbon steel vessel was determined using Table 14.2 in Towler and Sinnott (2022). The maximum stress was 8.89e7 Pa. A design pressure of 10% above the actual pressure, or 141 bar, was chosen. A conservative estimate of 0.8 for joint efficiency was selected due to the potential for imperfect welds. The equation for wall thickness was determined using Equation 6.4.v.

Equation 6.4.v Minimum Wall Thickness

$$e = \frac{0.5P_d}{2E\sigma_{max} - 1.2P_d}$$

e = wall thickness (m)
P_d = design pressure (Pa)
E = joint efficiency
σ_{max} = maximum allowable stress (Pa)

When considering the heat transfer effects of the adiabatic PFR, the heat duty within the RPLUG block was set to 0. The maximum reactor temperature was 298˚C, and the temperature exiting the reactor was 284˚C. This shows the reactions are not very exothermic, and the reactor does not have a significant heat requirement. Therefore, external heating or cooling is not required. Finally, because our team modeled the reactor using kinetic data, the final conversions accounted for the temperature changes throughout the reactor.

6.5   Separations

6.5.1   Flash Evaporator

The reactor products (stream 10) are expanded from 128 bar to 6 bar in an adiabatic flash evaporator. This pressure drop converts some of the methanol and propane from a dense supercritical fluid into a vapor, which exits in the overhead of the flash evaporator (stream 13). This stream contains 74 wt% methanol, 23 wt% propane, and the balance being water. This stream is recycled and mixed with the fresh feed of WCO and methanol to supply adequate reactant quantities into the reactor.

The dimensions of the vertical flash evaporator were determined by calculating the disengagement height, liquid level, and tank diameter. The Souders-Brown equation (Equation 6.5.i) was used to calculate the maximum allowable gas velocity and determine the minimum tank diameter.

Equation 6.5.i Souders Brown Equation

$$u_v = K_s \sqrt{\frac{\rho_L - \rho_V}{\rho_V}}$$

u_v = maximum design vapor velocity (m/s)
K_s = design parameter (m/s)
ρ_L = liquid density (kg/m^3)
ρ_V = vapor density (kg/m^3)

A height to diameter ratio between 2:1 and 4:1 is usually used to maintain the vapor velocity below the terminal velocity and ensure sufficient liquid residence time (*Flash Vessels*, n.d.). Therefore, to maintain a 2:1 aspect ratio, a tank diameter of 1.4 m was selected. A disengagement height of 1.4 m was chosen because a value equal to the tank diameter is generally the minimum space required to prevent entrainment (Nisworo, 2005). In determining the liquid level and tank volume, a 30-minute liquid hold-up time was selected to maintain smooth operation and process control for downstream separations (Nisworo, 2005). The calculated maximum vapor velocity, minimum diameter, and liquid level are depicted in Table 6.5.i. Leaving an additional 40 cm for vapor-liquid mixing between the disengagement space and liquid level, the total tank height is 2.75 m. The final tank dimensions are shown in Figure 6.5.i. Stream flows are in Table 6.5.ii. Full calculations regarding the flash drum can be found in Section 13.4. The bottoms product of the flash evaporator is sent to a distillation column to recover the remaining methanol and propane.

Table 6.5.i Flash Evaporator Design Dimensions

Design Parameter	Value
u_v (m/s)	0.38
Minimum diameter (m)	0.17
Design diameter / disengagement space (m)	1.4
Liquid level (m)	0.95
Total height (m)	2.75

Table 6.5.ii Flash 1 Stream Flows

Mass Flow (kg/hr)	Feed Stream	Vapor Recycle Stream	Biodiesel Stream
Water	63.0	5.7	57.2
Propane	71.0	57.3	14.7
Methanol	920.2	181.2	739.0
Triolein	0.1	0	0.1
FFA	4.4	0	4.4
FAME	1,160.7	0	1,160.7
Glycerol	107.6	0	107.6
Total	**2,327.0**	**244.2**	**2,803.7**
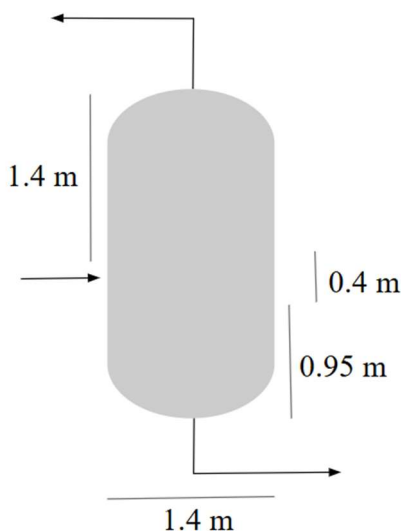
Figure 6.5.i Flash Drum Dimensions

6.5.2 Methanol and Water Distillation Column

Because the flash evaporator did not recover sufficient methanol and propane, an additional separator was required. Initially, a vacuum flash evaporator was modeled based on prior research (Van Kasteren & Nisworo, 2007). However, the desired methanol separation was not obtained, so a distillation column was used instead (Nagapurkar & Smith, 2023). The distillation column was able to achieve an overall unreacted methanol recovery of 99.2% and a 99.9% recovery of the propane in our process.

This distillation column was modeled in ASPEN Plus as a RadFrac block. NRTL-RK was used as the property method to maintain consistency across process blocks and accurately model the two liquid phases, which are present across theoretical stages 6-10. The column was modeled with 13 theoretical stages, with the feed above theoretical stage 6. ASPEN Plus design specifications were set to obtain a 99% mass recovery of methanol in the overhead stream and 97% recovery of water in the bottom. The reflux rate and distillate to feed ratio were varied in ASPEN Plus. The model converged to give the column parameters shown in Table 6.5.iii.

Table 6.5.iii Methanol Water Distillation Column Design Parameters

Parameter	Value
Top Stage Pressure (bar)	1.01
Bottom Stage Pressure (bar)	1.12
Reflux Ratio	1.49
Bottoms Rate (kmol/hr)	8.41
Distillate Rate (kmol/hr)	23.26
Distillate to Feed Ratio	0.734
Condenser Temperature (°C)	25.2
Reboiler Temperature (°C)	112.7

Random packing was used instead of trays because it is preferred for streams with two liquid phases. The packing was divided into two sections: below the feed, from stages 2-5, and above the feed, from stages 6-12. Specifically, 1.5" metal Pall rings were selected because they increase free area and improve liquid distribution compared to other packing (Sinnott, 2005). These Pall rings have an HETP of 0.675 m, which resulted in a total packing height of 7.43 m (Sinnott, 2005). The column diameter of 0.5 m was determined using ASPEN Plus. The section above the feed, CS-1, is 2.7 m in height, and the section below the feed, CS-2, is 4.73 m in height. A height of 0.75 m below the packing was calculated based on a 20-minute liquid hold-up time. These calculations are found in Section 13.6. 0.5 m of space was allowed above the packing as well as at the feed location. The total column height is 9.2 m (Figure 6.5.ii). The stream table for the distillation column is listed in Table 6.5.iv.

Table 6.5.iv Methanol/Water Distillation Column Stream Table

Mass Flow (kg/hr)	Feed Stream	Distillate Stream	Bottoms Stream
Water	57.2	1.7	55.5
Propane	14.7	14.7	0
Methanol	739.0	731.6	7.4
Triolein	0.1	0	0.1
FFA	4.4	0	4.4
FAME	1,160.7	0	1,160.7
Glycerol	107.6	0	107.6
Total	**2,083.7**	**748.0**	**1,335.7**
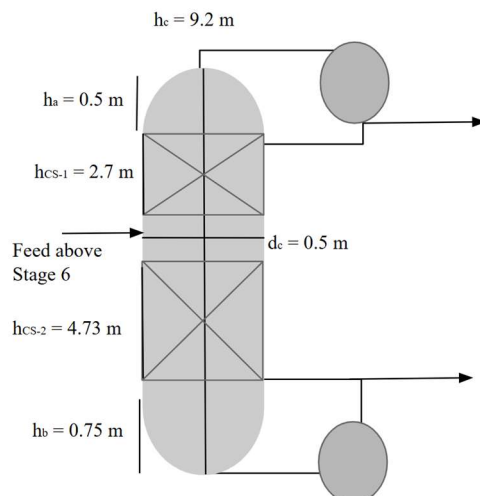
Figure 6.5.ii Methanol Water Distillation Column Dimensions

Carbon steel was selected as the material of construction because it is resistant to the limited corrosion risk presented by methanol and FFAs, and it can withstand the 120°C operating temperature. Carbon steel was chosen over stainless steel (SS) because the increased strength and corrosion resistance provided by SS were not outweighed by its higher cost. 316 SS was chosen as the material for the Pall rings because it has superior resistance to the process stream and superior wettability, which is ideal for optimal separation of the components into the different streams (Green and Southard, 2019).

A reflux pump was designed for this column based on the reflux flow rate of 1.4 m^3/hr. A single-stage centrifugal pump made of carbon steel was selected because centrifugal pumps can handle low flow rates. This pump requires 0.03 kW of power to operate.

A reflux drum was designed for this column to allow for a 30-minute hold-up time. Based on a reflux flow rate of 1.4 m^3/hr, the reflux drum volume is 0.66 m^3. A 3:1 height-to-diameter ratio resulted in a drum length of 2 m and a diameter of 0.66 m. Carbon steel was selected as the material of construction. The reflux drum calculations are detailed in Section 13.7.

A total condenser was modeled for this distillation column because the components in the recycle stream must be in a liquid phase to be pumped back through the system. The primarily methanol stream was condensed from 64.6°C to 25.2°C using a cooling water stream of 20°C. Using these values an LMTD value was calculated and utilized to determine the condenser area and overall cooling water flow rate. The LMTD calculation is actually a conservative calculation because the heat driving force across the graph is consistently higher than the values of the LMTD line from inlet to outlet.

26
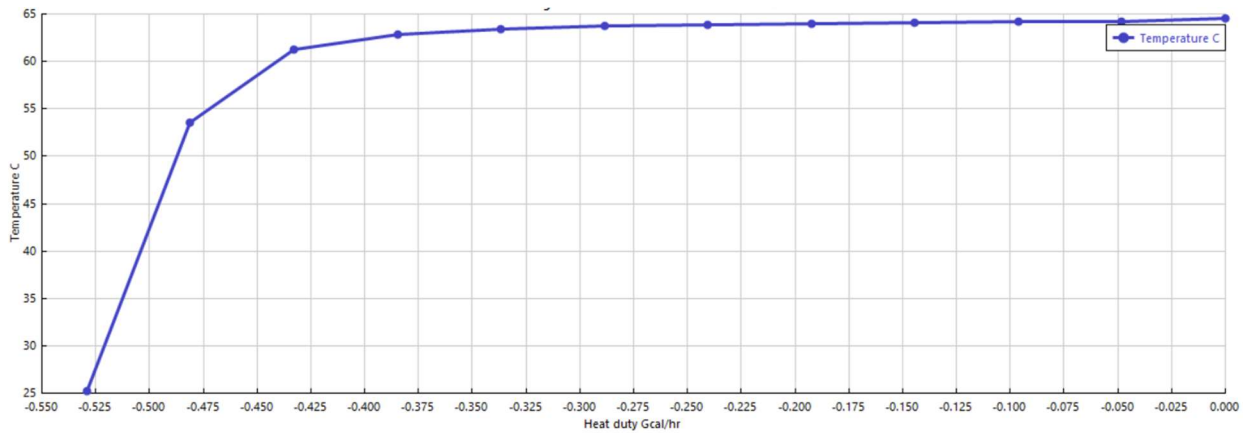
Figure 6.5.iii Methanol Water Distillation Condenser Heat Curve

A condenser area of 98.6 m² was determined using the heat transfer equation (Equation 6.5.ii). A log-mean temperature difference (LMTD) of 12.47°C was calculated assuming an inlet cooling water temperature of 20°C and an exit cooling water temperature of 40°C. The inlet cooling water temperature of 20°C is consistent across the site. An overall heat duty of 615.4 kW was determined using ASPEN Plus. An overall heat transfer coefficient, U, of 500 W/m²°C was determined based on the value for organic/water condensers in Table 12.1: Typical Overall Coefficients (Sinnott, 2005). A cooling water flow rate of 26,500 kg/hr is required to condense the stream.

Equation 6.5.ii Heat Transfer Equation

$$Q = UA\Delta T_{lm}$$

Q = Heat duty
U = Overall coefficient
A = Area of heat transfer
ΔT_{lm} = log-mean temperature difference

Equation 6.5.iii Log Mean Temperature Difference

$$\Delta T_{lm} = \frac{(T_1 - t_2) - (T_2 - t_1)}{\ln\left[\frac{T_1 - t_2}{T_2 - t_1}\right]}$$

T_1 = Temperature of hot fluid in
T_2 = Temperature of hot fluid out
t_1 = Temperature of cold fluid in
t_2 = Temperature of cold fluid out

Similar calculations were performed to design a kettle reboiler for distillation column D-1. The reboiler also contains a mixture of components: 86.9 wt% FAME, 8.1 wt% glycerol, and the balance water. The incoming stream was heated from 78.4°C to 110.7°C using 3 bar absolute saturated steam, as gathered from the ASPEN Plus simulation, and the LMTD was calculated to be 36.2°C. The overall heat transfer coefficient was estimated as a steam/heavy organic at 450

W/m^2°C using Table 12.1 in Sinnott (2005). The final heat transfer area of 33.2 m^2 was calculated using an ASPEN Plus simulated reboiler heat duty of 542.5 kW. Based on the enthalpy of the saturated steam, the required steam flow rate is 903 kg/hr. These calculations are further detailed in Section 13.5.

6.5.3 Fatty Acid Methyl Ester and Glycerol Decanter

The decanter is responsible for separating the two-phase liquid stream from the methanol-water distillation column into a primarily FAME stream and a crude glycerol stream. The exiting streams are sent to the final separation and purification steps required to meet product standards. The phase split was modeled in ASPEN Plus using the NRTL-RK property method in a decanter block. This property method was chosen for consistency with past steps, as well as its ability to model two liquid phases.

Previous research has shown similar decanters operating at atmospheric pressure and either 25 or 35°C (Nagapurkar & Smith, 2023; Nisworo, 2005). These values were used as the basis for modeling. The separation at 25 and 35°C was nearly identical. Because a lower heat duty was required to cool the distillation bottoms product, a 35°C operating temperature was selected. The ASPEN Plus simulation warned of an unstable phase split when equation component fugacities were used. When calculating the phase split using Gibbs free energy, no phase split was detected. Despite the warning, our team elected to continue to use component fugacities because the calculated liquid-liquid equilibrium K values for each component showed a strong preference towards one phase or the other, apart from methanol, which has the tendency to partition into both polar and non-polar phases (Table 6.5.v). The final product streams are summarized in Table 6.5.vi.

Table 6.5.v Liquid-Liquid Equilibrium Values

Component	Water	Methanol	Triolein	FFA	FAME	Glycerol
K	30.0	2.67	5.70e-6	1.10e-3	5.58e-6	275

Table 6.5.vi Decanter Streams

Mass Flow (kg/hr)	Feed Stream	Biodiesel Stream	Glycerol Stream
Water	55.5	1.7	53.8
Propane	0	0	0
Methanol	7.4	1.9	5.5
Triolein	0.1	0.1	0
FFA	4.4	4.4	0
FAME	1,160.7	1,160.6	0.1
Glycerol	107.6	0.4	107.2
Total	**1,335.7**	**1,169.1**	**166.6**

The physical design of the FAME and glycerol decanter assumed that the velocity of the continuous biodiesel phase was lower than the droplet settling velocity of the dispersed glycerol (Nisworo, 2005; Sinnott, 2005). This relationship is seen in Equation 6.5.iv.

Equation 6.5.iv Decanter Design Assumption

$$u_d = \frac{L_c}{A_i} < u_c$$

u_d = dispersed droplet settling velocity (m/s)
L_c = continuous phase volumetric flow rate (m/s)
A_i = area of interference (m^2)
u_c = continuous phase velocity (m/s)

The property conditions for glycerol and FAME were determined using ASPEN Plus (Table 6.5.vii). The droplet settling velocity was calculated using Stokes Law, Equation 6.5.v. An assumed droplet diameter of 150 μm was selected. This value is a conservative estimate for droplet size in the decanter (Nisworo, 2005; Sinnott, 2005). This estimation was reasonable considering the final calculated droplet diameter of 48.4 μm was less than the estimated value (Equation 6.5.vi) (Sinnott, 2005). The calculated value of droplet settling velocity is 1.13e-03 m/s.

Table 6.5.vii Density and Viscosity Data

Component	Flow Rate (kg/hr)	Density (kg/m³)	Viscosity (N*s/m²)
Glycerol	167.0	1,170	0.004221
Biodiesel	1,169.0	805	0.003972
Total	**1,336.0**		

Equation 6.5.v Droplet Settling Velocity

$$u_d = \frac{d_d^2 * g * (\rho_d - \rho_c)}{18\mu_c}$$

u_d = dispersed droplet settling velocity (m/s)
g = gravitational constant (m/s)
ρ_d = dispersed phase density (kg/m³)
ρ_c = continuous phase density (kg/m³)
μ_c = continuous phase dynamic viscosity (N*s/m^2)

Equation 6.5.vi Droplet Diameter

$$d_d = \sqrt{\frac{u_d 18\mu_c}{g(\rho_d - \rho_c)}}$$

u_d = dispersed droplet settling velocity (m/s)
μ_c = continuous phase dynamic viscosity (N*s/m^2)
g = gravitational constant (m/s)
ρ_d = dispersed phase density (kg/m³)
ρ_c = continuous phase density (kg/m³)

Our group selected a vertical, cylindrical decanter. This shape is commonly produced, so it is inexpensive. Furthermore, previous studies have shown this shape and orientation are effective for FAME and glycerol separations (Nagapurkar & Smith, 2023; Nisworo, 2005;

Sinnott, 2005). The continuous glycerol phase volumetric flow rate of 4.03e-04 m³/s was calculated using Equation 6.5.vii. The area of phase interference is 0.36 m (Equation 6.5.viii). The interfacial area was used to approximate the tank diameter to 0.7 m. The decanter will have a height of 1.4 m, based on a standard 1:2 tank diameter to height ratio.

Equation 6.5.vii Continuous Phase Volumetric Flow Rate

$$L_c = \frac{\dot{m}_c}{3600\rho_c}$$

L_c = continuous phase volumetric flow rate (m³/s)
$\dot{m}_c$ = continuous phase mass flow rate (kg/hr)
ρ_c = continuous phase density (kg/m³)

Equation 6.5.viii Interface Area

$$A_i = \frac{L_c}{u_d}$$

A_i = area of interference (m²)
L_c = continuous phase volumetric flow rate (m³/s)
u_d = dispersed droplet settling velocity (m/s)

The droplet residence time in the dispersion band is typically kept between 2 and 5 minutes (Sinnott, 2005). Our calculated value of 2.07 min is within this range (Equation 6.5.ix) (Sinnott, 2005).

Equation 6.5.ix Dispersion Band Residence Time

$$\tau_d = \frac{0.1h}{u_d}$$

τ_d = dispersion band residence time (s)
h = tank height (m)
u_d = dispersed droplet settling velocity (m/s)

The height of the dispersion band is typically 10% of the total tank height (Sinnott, 2005). The feed enters at the center of the dispersion band. To minimize glycerol entrainment in the biodiesel, the mixture was fed at a velocity of 1 m/s (Sinnott, 2005). The feed pipe diameter was calculated using Equation 6.5.x, which determines the average volumetric flow rate of the feed. The inlet feed pipe is 2.4 cm in diameter (Equation 6.5.xi).

Equation 6.5.x Feed Volumetric Flow Rate

$$L_f = \left(\frac{\dot{m}_c}{\rho_c} + \frac{\dot{m}_d}{\rho_d}\right)\frac{1}{3600}$$

L_f = feed volumetric flow rate (m³/s)
$\dot{m}_c$ = continuous phase mass flow rate (kg/hr)
$\dot{m}_d$ = dispersed phase mass flow rate (kg/hr)
ρ_c = continuous phase density (kg/m³)
ρ_d = dispersed phase density (kg/m³)

Equation 6.5.xi Decanter Feed Pipe Diameter

$$d_p = \sqrt{\frac{4(L_f/v)}{\pi}}$$

d_p = pipe diameter (m)
L_f = feed volumetric flow rate (m³/s)
v = inlet flow velocity (m/s)

The piping arrangement is based on standard vertical decanter piping locations: feed halfway up the vessel, light liquid take-off at 90% the height, and heavy liquid take-off based on a pressure balance of the tank contents (Equation 6.5.xii) (Sinnott, 2005). The final tank dimensions and piping locations are summarized in Figure 6.5.iv. Final decanter operating conditions are outlined in Table 6.5.viii. Full calculations are included in Section 13.8.

Equation 6.5.xii Take-off Pipe Mass Balance

$$z_2 = \frac{(z_1 - z_3)\rho_c}{\rho_d} + z_3$$

z_2 = glycerol take-off (m)
z_1 = biodiesel take-off (m)
z_3 = interface height (m)
ρ_c = continuous phase density (kg/m³)
ρ_d = dispersed phase density (kg/m³)
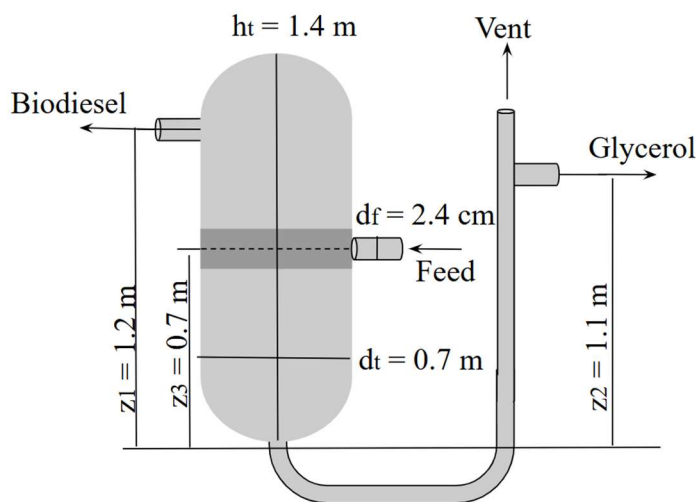
Figure 6.5.iv Decanter Dimensions

Table 6.5.viii Decanter Design Parameters

Parameter	Value
Temperature (°C)	35
Pressure (bar)	1.01
Feed Velocity (m/s)	1.0
Dispersion Band Residence Time (min)	2.07

6.5.4 Glycerol-Water Vacuum Distillation

The bottoms product of the decanter is sent to a vacuum distillation column to remove water and methanol so that the glycerol product meets the USP glycerol standard (Section 13.2). The distillation was run at a vacuum of 0.02 bar due to glycerol's high boiling point of 290°C at atmospheric pressure (Attarakih et al., 2001). A packed bed distillation column with structured

packing was chosen for this separation due to its low pressure drop, small liquid holdup, and large surface area per unit volume of packing (Attarakih et al., 2001). A low pressure drop is necessary to maintain vacuum conditions throughout the column. Specifically, Koch Flexipac HC 1Y packing was selected due to its low HETP value of 8.3 in (*Structured Packing*, n.d.). Although the cost per cubic meter for structured packing is much higher than for random packing, the additional cost is partially offset by its higher efficiency.

The distillation column was modeled using the NRTL-RK property method in ASPEN Plus. The column was modeled with 12 theoretical stages, with the feed stream at 35℃ and 1 atm entering above stage 8. The resulting design parameters for the column are shown in Table 6.5.ix. These design parameters were chosen to meet the USP grade glycerol content requirement of 99.7% and keep the temperature of the reboiler below 166℃. Above this temperature, glycerol begins to degrade (Attarakih et al., 2001). The column diameter is 0.55 m, the packed height below the feed is 0.84 m, and the packed height above the feed is 1.27 m. Allowing space equal to one column diameter at the feed location, above the packing, and below the packing resulted in a total column height of 3.75 m. The dimensions of the distillation column are depicted in Figure 6.5.v. The material of construction for the distillation column is 304 SS. 304 SS meets the Food and Drug Administration's sanitary regulations for food preparation and is commonly used in the medical industry, making it suitable to produce pharmaceutical-grade glycerol (*Know the Differences Between 304 Stainless Steel vs 316*, 2021).

Table 6.5.ix Vacuum Distillation Column Design Parameters

Parameter	Value
Top Stage Pressure (bar)	0.020
Bottom Stage Pressure (bar)	0.036
Reflux Ratio	3
Bottoms Rate (kmol/hr)	1.175
Distillate Rate (kmol/hr)	3.146
Bottoms to Feed Ratio	0.272
Condenser Temperature (℃)	11.98
Reboiler Temperature (℃)	164.6
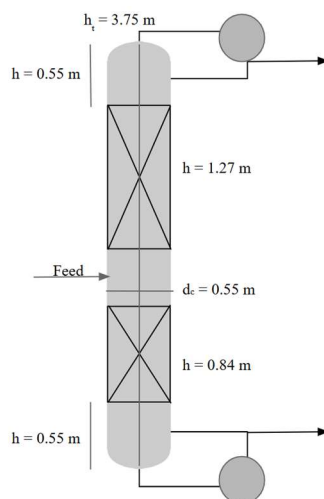
Figure 6.5.v Vacuum Distillation Column Dimensions

For this column, a total condenser was chosen to condense the methanol-rich wastewater distillate. A liquid stream allows the waste to be disposed of as wastewater, rather than releasing additional methanol vapor into the atmosphere, against national environmental regulations. The waste stream leaving the condenser must be cooled to 12°C, which is below our plant's 20°C cooling water temperature. Therefore, refrigerated antifreeze must be used as the cooling fluid to achieve sufficiently low temperatures without the risk of freezing. A 60% propylene glycol and 40% water mixture will be used as the cooling fluid in the condenser, which has a freezing point of -48°C. Propylene glycol is commonly used as a heat transfer fluid in food processing systems instead of ethylene glycol because it is non-toxic (*Propylene glycol based heat-transfer fluids*, n.d.). Since we are producing pharmaceutical grade purity, propylene glycol was selected. The propylene glycol mixture will be cooled in a glycol chiller to 2°C. A heat transfer area of 51.7 m^2 was calculated using Equation 6.5.ii.

The process side fluid is composed of 90.8 wt% water and 9.2 wt% methanol, which has a freezing point of -7°C (Verein Deutscher Ingenieure, 2010). Therefore, the methanol in this stream lowers the freezing point sufficiently to avoid the risk of freezing on the process side. The reflux drum was designed using a 30-minute liquid hold-up time and an L/D ratio of 3:1. The diameter of the drum is 0.23 m, and the length is 0.70 m.

An LMTD of 10.0°C was calculated using Equation 6.5.iii. 11.7 kg/s of the cooling fluid is required, which enters the condenser at 2°C and leaves at 6°C. The overall heat transfer coefficient, U, was estimated using Table 12.1: Typical Overall Coefficients for vacuum condensers presented in Sinnott (2005). The full calculations are outlined in Section 13.10.

Similar calculations were completed to design a kettle reboiler for the column. Since the fluid being vaporized is a single component (glycerol) and the heating medium is steam, the shell and the tube side processes will both be isothermal. Therefore, the mean temperature difference is the difference between the saturation temperatures (Sinnott, 2005). 297.3 kg/hr of saturated

steam at 15 bar was used as the heating fluid, which resulted in a mean temperature difference of 10.1°C. Using an overall coefficient of 200 W/m²°C, the area of heat transfer was determined to be 79.6 m². The full calculations can be found in Section 13.10.

107 kg/hr of the glycerol product exits the bottom of the distillation column. The composition is listed in Table 6.5.x. This stream meets the USP grade specifications for glycerol content, water content, specific gravity, and fatty acid and ester content (Table 6.5.xi). A methanol and water waste stream exits the top of the column at a flow rate of 59.1 kg/hr (Table 6.5.x).

Table 6.5.x Vacuum Distillation Column Streams

Mass Flow (kg/hr)	Feed Stream	Glycerol Product	Waste Stream
Water	53.8	0.2	53.6
Propane	0	0	0
Methanol	5.5	0	5.5
Triolein	0	0	0
FFA	0	0	0
FAME	0.1	0.1	0
Glycerol	107.2	107.2	0
Total	**166.6**	**107.5**	**59.1**

Table 6.5.xi Comparison of the USP Standard and Glycerol Product

Component	Specification	Calculated Value
Glycerol content (mass%)	99.7 min	99.75
Water (mass%)	0.3 max	0.19
Specific Gravity	1.2612 min	1.2638
Fatty Acid & Ester	1.000 mL per 0.5 N NaOH consumed max	Typical result: pass Weight %: 4.73e-05

To reach the required vacuum pressure of 0.02 bar, a 2-stage steam jet ejector system was chosen. Steam jet ejectors are easy to operate, require little maintenance, and have low installation costs. In addition, they have a long life, sustained efficiency, and low maintenance costs since they have no moving parts (Green & Southard, 2019). In this case, 3 bar saturated steam is sent through a venturi-shaped diffuser that converts velocity energy to pressure energy, evacuating the column (Green & Southard, 2019). The ratio of suction pressure to motive pressure and the ratio of suction pressure to steam pressure were used to determine the optimal area ratio of the venturi diffuser using Figure 6.5.vi (Green & Southard, 2019). The specific diameter and area of the venturi openings were selected based on specifications for steam jet ejector nozzles given in work by Bauer & German (1961). The steam consumption of the system was determined using the Venturi Flow Equation (Equation 6.5.xiii). The final design parameters and steam consumption results are outlined in Table 6.5.xii. The full calculations are shown in Section 13.11.
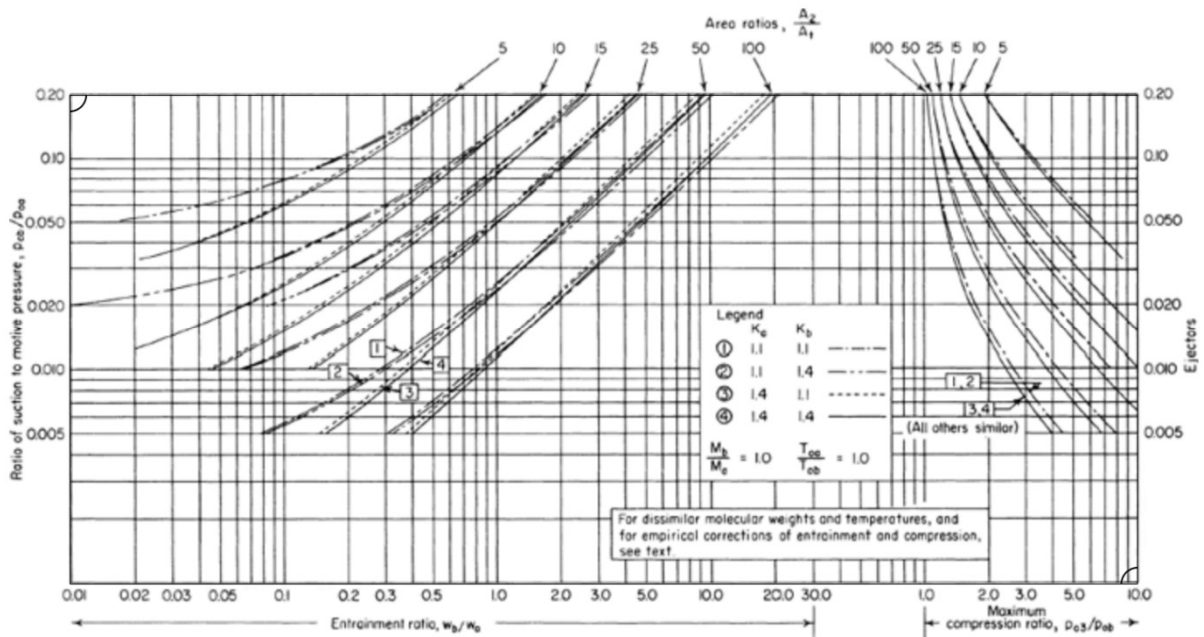
Figure 6.5.vi Design Curves for Optimum Ejectors. Taken from Perry's Chemical Engineering Handbook 9th Edition (Green & Southard, 2019).

Equation 6.5.xiii Venturi Flow Equation

$$Q = A_2 \sqrt{\frac{2}{\rho} \cdot \frac{P_1 - P_2}{1 - (\frac{A_2}{A_1})^2}}$$

Q = volumetric flowrate (m³/s)
A_1 = Area at smaller opening (m²)
A_2 = Area at larger opening (m²)
P_1 = Pressure at A_1 (Pa)
P_2 = Pressure at A_2 (Pa)
ρ = density (kg/m³)

35

Table 6.5.xii Steam Jet Ejector Design Parameters

Parameter	Stage 1	Stage 2
Initial Pressure (bar)	0.02	0.123
Final Pressure (bar)	0.15	1.01
Suction to Motive Pressure Ratio	7.5	8.2
Suction to Steam Pressure Ratio	0.007	0.041
$\frac{A_2}{A_1}$	25	5
d_1 (cm)	2.29	4.78
d_2 (cm)	11.4	10.7
Q (kg/h)	306.4	3,561

This design provides a reasonable estimation of steam consumption for initial economic assessments. However, specific design parameters vary depending on temperature and molecular weight differences of the fluids and should be determined with the assistance of a steam jet ejector manufacturer.

6.5.5   Biodiesel Flash Separator

The purpose of the second flash separator is to dry the biodiesel stream leaving the decanter so that the biodiesel product complies with the ASTM D6751-24 standard (Section 13.9). The key contaminants to meet specifications are the volume percent of methanol, volume percent of water, and weight percent of free glycerol. While water washing was initially considered prior to the flash separator drying steps, the methanol concentration leaving the decanter was sufficiently low, thus eliminating the need for a washer.

An adiabatic flash drum at atmospheric pressure was modeled in ASPEN Plus. NRTL-RK was chosen as the property method. This is a change from the SRK property method used in the prior supercritical pressure steps. However, any phase changes caused by this switch is masked by the calculated vapor phase in the flash drum. The biodiesel feed stream was fed at atmospheric pressure and 35°C. To remove the water from the biodiesel, compressed air at 1.5 bar (Section 6.7.5) and 73.7°C is sent through a porous sparger at the bottom of the flash drum to bubble air into the biodiesel. The small bubbles increase the interfacial area for mass transfer between the air and the biodiesel. As the bubbles rise, water preferentially transfers from the biodiesel phase to the air due to the difference in partial pressures, effectively stripping moisture from the liquid phase. The high surface area-to-volume ratio of small bubbles improves the efficiency of water removal, ensuring the biodiesel is sufficiently dry (Song, Zhao, Cao & Li, 2022). The air flow rates were varied until the liquid stream exiting the flash evaporator met the specifications. The final stream compositions are listed in Table 6.5.xiii. Verification of ASTM biodiesel specifications is shown in Table 6.5.xiv.

Table 6.5.xiii Flash Separator 2 Streams

Mass Flow (kg/hr)	Feed Stream	Air In	Air Out	Biodiesel
Water	1.7	4.0	5.0	0.7
Methanol	1.9	0	1.5	0.4
Triolein	0.1	0	0	0.1
FFA	4.4	0	0	4.4
FAME	1,161.0	0	0	1,161.0
Glycerol	0.4	0	0	0.4
Air	0	281.2	280.9	0.3
Total	**1,169.1**	**285.2**	**287.4**	**1,166.9**

Table 6.5.xiv ASTM Biodiesel Specification Verification

Component	Specification	Actual Value
Max Water (vol%)	0.05	0.049
Max Methanol (vol%)	0.20	0.036
Max Free Glycerol (wt%)	0.24	0.032

The dimensions of the flash drum were calculated using the same method described in Section 6.5.1. This can be seen in Section 13.9. A 5 min liquid hold-up time was selected for this vessel because it provides sufficient residence time for moisture removal while minimizing the vessel size (Miyatake, Hashimoto & Lior, 1992). A longer 10 min hold-up time would require a larger vessel, increasing equipment costs and footprint without significantly increasing moisture removal. Carbon steel was chosen as the construction material because it offers high mechanical strength and durability at a relatively low cost, making it ideal for atmospheric pressure operation. Additionally, since the biodiesel and residual contaminants in the system are not highly corrosive under the given process conditions, carbon steel provides adequate resistance without the need for more expensive alloys. The flash drum design dimensions and the final design are shown in Table 6.5.xv and Figure 6.5.vii respectively.

Table 6.5.xv Flash Drum Design Dimensions

Design Parameter	Value
u_v (m/s)	1.32
Minimum diameter (m)	0.49
Design diameter / disengagement space (m)	1.0
Liquid level (m)	0.56
Total height (m)	1.2
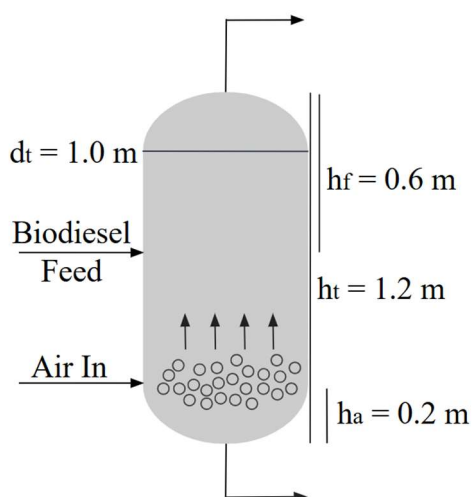
Figure 6.5.vii Flash Drum 2 Dimensions

6.6 Absorber Column

The biodiesel flash evaporator effectively reduced the water content of the biodiesel below the specified limit of 0.05 vol%. However, 12.1 t/yr of methanol were released in the vapor stream leaving the top of the flash drum (stream 26). Pennsylvania's volatile organic compound (VOC) emission regulations restrict methanol emissions to a maximum of 2.7 tons (2,455 kg) over a 12-month rolling period, regardless of plant size (Pennsylvania Code and Bulletin, 2018). Therefore, this methanol emission rate would have exceeded the limit. An absorber column was designed to transfer the methanol into a wastewater stream before venting the air to the atmosphere.

The absorber column was modeled as a RadFrac – ABSRBR1 block with no condenser or reboiler in ASPEN Plus using the NRTL-RK property method. The methanol-air stream was fed to the bottom of the column, and 781.7 t/yr of water at 20°C and atmospheric pressure was fed to the top of the column. Five theoretical stages were required to reduce the amount of methanol in the air stream leaving the column to below the legal threshold. The column was packed with 16 mm 304SS Pall rings to increase the surface area for gas-liquid contact. The Pall rings have an HETP value of 0.40 m (Sinnott, 2005). The total packed height of the column is 2.0 m, and the diameter is 0.25 m. The absorber dimensions are depicted in Figure 6.6.i. The pressure at the top of the column is 1.01 bar, and the pressure at the bottom of the column is 1.02 bar. The final amount of methanol released by the plant in the air stream is 2.1 t/yr. The water exiting the bottom of the column contains 10.0 t/yr of methanol. Information on wastewater removal is in Section 8.6.1. The stream flow rates around the absorber column are listed in Table 6.6.i.

38
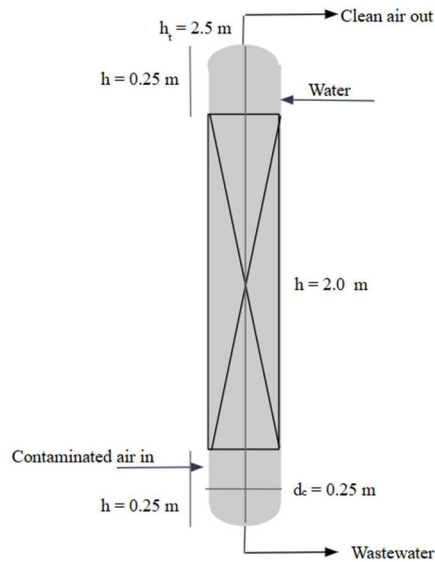
Figure 6.6.i Absorber Column Dimensions

Table 6.6.i Absorber Streams

Mass Flow (kg/hr)	Feed Stream	Water In	Air Out	Wastewater
Water	5.0	99.1	9.6	94.5
Propane	0	0	0	0
Methanol	1.5	0	0.3	1.3
Air	280.9	0	280.6	0.3
Total	**287.4**	**99.1**	**290.5**	**96.1**

6.7   Ancillary Equipment

6.7.1   Pumps

Within the plant, pumps were separated into three categories: pumps with large pressure changes, pumps for friction loss, and distillation column reflux pumps. Pumps with large pressure changes were designed using ASPEN Plus. Detailed information on the four pumps designed in ASPEN Plus is provided in Sections 6.7.2 to 6.7.5.

The reflux pumps and pumps for friction loss were all designed as centrifugal pumps, due to the low fluid flow rates. The hydraulic power of each pump was calculated according to Equation 6.7.i. All the pumps in the process have an identical, parallel backup pump. The total power of each pump was determined by assuming a pump efficiency of 70% and an electric motor efficiency of 90%.

Equation 6.7.i Pump Power

$$P = \Delta P * \dot{V}$$

P = Hydraulic Power (kW)
ΔP = Differential Pressure (kPa)
$\dot{V}$ = Volumetric Flow Rate (m³/s)

The differential pressure is the sum of the actual pressure difference, the gravity head, and the frictional losses from the pipes, heat exchanger, and control valves. Apart from the distillation column reflux pumps, all the pumps were assumed to have no height change. 0.5 atm was assumed for the pressure losses in the pipes and the heat exchangers. A conservative estimate of 0.5 atm was applied for frictional losses through the control valves of centrifugal pumps. The total pump power and designs are in Table 9.3.vi.

6.7.2   Preliminary Feed Pump (P-3)

P-3 is responsible for increasing the pressure of the feed stream from atmospheric pressure to 7 bar. Other studies recommended a pump at 5 bar, followed by a heat exchanger to preheat the methanol and WCO to 40˚C (Nisworo, 2005). This was to increase the solubility of propane and prevent phase separation when mixed with the recycle stream.

However, pumping the fluid to 7 bar, instead of 5 bar, increases the outlet temperature high enough to eliminate the need for an additional heat exchanger and accounts for the pressure drop through the pipe and control valves. By elevating the pressure early in the process, we ensured stable liquid-phase operation and decreased the required heat duty later in the process. The pump was modeled in ASPEN Plus; Table 6.7.i outlines the pump specifications.

Table 6.7.i Mixed Feed Pump Specifications

Specifications	Data
Electricity (kW)	1.7
Outlet Pressure (bar)	7
Outlet Temperature (°C)	29.8
Efficiency	0.30
Volumetric Flow Rate (m^3/hr)	3.1
Property Method	NRTL-RK

A carbon steel reciprocating pump was selected due to its ability to handle high-pressure differentials with low flow rates (Ruhrpumpen, 2025).

6.7.3   Supercritical Pressure Pump (P-4)

A pump is required to take the stream of the mixed recycle and feed streams to 129 bar before the plug flow reactor. This pump increases the stream to methanol's supercritical pressure, 128 bar, before the reactor. The operating pressure of 129 bar accounts for the frictional losses through the pipes and heat exchanger. The pump was designed in ASPEN Plus using SRK as the property method due to the high operating pressure. When we changed the property method from NRTL-RK for the low pressure parts of the process to SRK for supercritical conditions, ASPEN Plus changed the phases that are present in the stream. A heater block was added before the supercritical pressure pump to maintain a constant liquid phase in the stream. Although this heater shows a duty of 134.1 kW, this block does not represent a real heater or phase change. This is due to the different calculation methods used by the different property

method packages. The inlet stream for this pump has an inlet temperature of 78.0°C, which increases to 103.9°C. Table 6.7.ii shows the specifications for this pump.

A carbon steel reciprocating pump was selected. This specific pump can operate at pressures up to 1000 bar depending on the model chosen, and the material can resist the high impact pressure. Higher strength materials, such as stainless steel or ductile iron, were considered, but carbon steel was ultimately chosen for its consistency throughout the process and capital cost savings.

Table 6.7.ii Supercritical Pump Specifications

Specifications	Data
Electricity (kW)	52.9
Outlet Pressure (bar)	129
Outlet Temperature (°C)	103.9
Efficiency	0.30
Volumetric Flow Rate (m^3/hr)	4.4
Property Method	SRK

6.7.4 Methanol Water Distillation Column Distillate Stream Pump (P-5)

A pump is required to take the distillate stream from the methanol and water distillation column to 7 bar. This pump ensures that the recycle stream remains at 6 bar when mixed with the vapor stream leaving the flash evaporator, accounting for the pressure drop through the pipe.

Initially, this pump was designed as a compressor because the distillate stream from D-1 contained vapor. However, after implementing a total condenser in D-1, this stream is 100% liquid, thus requiring a pump. Table 6.7.iii shows the designed pump specifications.

Table 6.7.iii Methanol Water Distillation Column Distillate Pump Specifications

Specifications	Data
Electricity (kW)	0.53
Outlet Pressure (bar)	7
Outlet Temperature (°C)	26.0
Efficiency	0.3
Volumetric Flow Rate (m^3/hr)	0.95
Property Method	NRTL-RK

This pump will be a carbon steel reciprocating pump. Reciprocating pumps work well with lower flow conditions, which are present in this stream. Given that our process operates under high-pressure conditions following the recycle stream, the reciprocating pump will ensure reliable pressure buildup while minimizing pulsation effects.

6.7.5   Air Compressor for Biodiesel Drying and Absorption

A compressor increases the pressure of the air stream from atmospheric pressure to 1.5 bar before it enters the flash drum for biodiesel drying. This increases the inlet air temperature from 25°C to 73.7°C, which enhances stripping efficiency by reducing the biodiesel's viscosity. This promotes better interaction between the air bubbles and biodiesel (He et al., 2025). Compression ensures effective moisture removal, allowing the final biodiesel product to meet ASTM D6751-24 specifications for water, methanol, and free glycerol content. An isentropic compressor was modeled in ASPEN Plus. The specifications can be found in Table 6.7.iv. This compressor is a carbon steel blower. Blowers are commonly used for low-pressure air movement applications, making them a more cost-effective choice compared to a reciprocating or centrifugal compressor.

Table 6.7.iv Biodiesel Drying Compressor Specifications

Specifications	Data
Electricity (kW)	4.0
Outlet Pressure (bar)	1.5
Outlet Temperature (°C)	73.7
Efficiency	0.72
Inlet Volumetric Flow Rate (m^3/hr)	243.8
Outlet Volumetric Flow Rate (m^3/hr)	191.6
Property Method	NRTL-RK

Furthermore, a blower was added on the vapor exit stream of the biodiesel dryer to account for frictional pressure losses from the pipes moving the vapor stream into the absorption column. ASPEN Plus was used to model an isentropic compressor. The specifications for this compressor are listed in Table 6.7.v.

Table 6.7.v Absorber Inlet Compressor Specifications

Specifications	Data
Electricity (kW)	4.16
Outlet Pressure (bar)	1.5
Outlet Temperature (°C)	88.5
Efficiency	0.72
Inlet Volumetric Flow Rate (m^3/hr)	256.7
Outlet Volumetric Flow Rate (m^3/hr)	201.6
Property Method	NRTL-RK

6.7.6 Heat Integration and Heat Exchangers

Heat exchangers were used to reach the required temperatures and phases for optimal operating conditions. Initially, the process utilized more heat exchangers at intermediate points, such as after the feed stream pump, in the recycle stream, and prior to the glycerol distillation column. While these heat exchangers were originally designed to maintain single-phase flow in pipes and ensure the distillation column feed was near the bubble point, they were deemed redundant because their high cost outweighed the small decrease in duty for other heat exchangers.

Heater blocks in ASPEN Plus were used to determine the required heating duty for each heat exchanger. A plot of temperature and heat duty for each heating block was used to determine the potential for heat integration in the system. Due to the primary need for cooling and the low heat duties required for the downstream heat exchangers, the only opportunity for heat integration was for the reactor feed and effluent streams. The heat exchanger before the reactor only required 341.0 kW to heat the stream, while the heat exchanger after the reactor required 421.4 kW of cooling. Therefore, because the heat duties of the streams are not equal, an additional 80.4 kW of cooling was required for the reactor effluent stream. This cooling was supplied through a heat exchanger with cooling water prior to the flash drum.

Equation 6.7.ii Cooling Water Flow Heat Transfer Equation

Water: $Q = mC_p\Delta T$

Q = Heat duty
m = Overall coefficient
C_p = Specific Heat Capacity
ΔT = Temperature difference

For each heat exchanger, the required heat transfer area and the heat transfer fluid flow rate were calculated. Heat transfer area was calculated using Equation 6.5.ii. The heat transfer fluid flow rate was determined using Equation 6.7.ii for cooling water as the process fluid. When calculating the heat transfer area, the overall heat transfer coefficient, U, was approximated using component viscosities and Table 14-5 in the 5th edition Plant Design and Economic for Chemical Engineering textbook by Peters, Timmerhaus, and West (2003). The lowest reasonable overall heat transfer coefficient was chosen to provide a conservative estimate for utility costs. The information for each heat exchanger (not including the distillation column condensers and reboilers) is summarized in Table 6.7.vi.

Table 6.7.vi Heat Exchanger Summary

Heat Exchanger	HX-1	HX-2	HX-5	HX-6	HX-9
Fluid 1	Reactor Inlet	HX-1 effluent	D-1 Bottoms	F-2 Bottoms	D-2 Bottoms
Fluid 2	Reactor Effluent	Cooling Water	Cooling water	Cooling water	Cooling water
Duty (kW)	341.0	80.4	63.0	8.0	9.6
Hot T in (°C)	283.7	161.7	112.7	37.9	159.7
Hot T out (°C)	161.7	120	35	25	35
Cold T in (°C)	103.9	20	20	20	20
Cold T out (°C)	280.0	40	40	35	40
U (W/m^{2}K)	375	650	425	300	20
T$_{lm}$	19.7	110.5	36.6	3.8	50.4
Area (m^2)	57.6	1.5	6.9	83.6	9.2
Type	Double pipe	Double pipe	Double pipe	Floating Head Shell & Tube	Double pipe
Fluid flow rate (kg/hr)	x	1,152.7	45,192.3	7,684.1	6,656.8

6.8   Storage

6.8.1   Feedstock Storage Tanks

The input streams of WCO and methanol are supplied from two pre-process storage tanks, one for each feedstock. These two tanks are designed to allow a four-week hold-up of feedstock. The four-week production volume acts as a safeguard against supply chain issues that may result in varying feedstock availability. The WCO feedstock storage tank is designed to hold 900 m^3 of WCO, and the methanol feedstock storage tank is designed to hold 125 m^3 of methanol. All the calculations are in Section 13.12. Current methods of WCO storage in industry utilize similar tanks made of carbon steel or stainless steel. No heating is required as WCO is expected to remain liquid at 25°C. The WCO should be kept out of the light to prevent photo-oxidation (Lopresto et al., 2024).

Both tanks are made of carbon steel because the stored materials are not corrosive and will minimize the cost of the tanks. A cone-top tank was chosen for the WCO tank because there are no concerns about the vaporization of this compound within storage. However, a floating-roof tank was used for the methanol storage tank because methanol readily vaporizes at standard temperatures and pressures. Additional safety requirements for the methanol tank are listed in Section 8.4.1.

An additional tank was designed for plant shutdown scenarios. This tank will have a cone roof, be made of carbon steel, and is designed to hold 30 m^3 of material. This tank is needed when the plant is shut down for maintenance or other operations, as any material will need to be flushed out of the system before personnel can begin work. This tank's dimensions were determined by summing the various volumes of process operation blocks and multiplying that by two to ensure that all the process material within the system can fit within this specified tank. The material held in this tank will be the methanol and propane usually present in the recycle stream, and although these materials have high vapor pressures, which normally would require a floating roof tank, the low storage volume required in this case means only a cone roof is necessary.

6.8.2 Product Storage Tanks

There will be two post-process storage tanks for the biodiesel and pharmaceutical-grade glycerol. These tanks were designed to allow for a four-week hold-up to allow for continued operation in the case of supply chain variability.

The biodiesel product storage tank has a volume of 900 m^3, and the pharmaceutical-grade glycerol product storage tank has a volume of 125 m^3. The biodiesel product storage tank is made of carbon steel. The tank has a floating roof, as concerns exist about the vaporization of this product within storage. The glycerol tank will be constructed of 304 stainless steel to maintain its pharmaceutical-grade quality. Furthermore, the tank will have a cone roof because there are no concerns about its vaporization within storage at standard temperatures and pressures.

7 Economics

7.1 Feedstock and Product Revenue

The required raw materials include methanol, propane, WCO, and propylene glycol. The costs of the raw materials were estimated using wholesale prices. To maintain a conservative revenue estimate, high-end feedstock costs, market price B100, and low-end pharmaceutical grade glycerol prices were used. Table 7.1.i shows the feedstock costs during the start-up period and normal operations. The construction and start-up plan of our process is detailed fully in Section 10. During year -1, no revenue will be generated as the plant remains under construction and no biodiesel production occurs. Capital expenditures will dominate this period, with significant investments in permitting, equipment procurement, and site preparation. The ramp-up phase begins in month 14, starting at 50% of the plant operation capacity until reaching steady-state operations at month 18. Therefore, for year 0, WCO was priced at ¾ of the full capacity, steady-state quantity. The initial raw material costs are fully purchased in year 0 and are shown in the table below. Table 7.1.ii details the revenue associated with product production.

Table 7.1.i Feedstock Costs

Feed	Price (USD/t)	Year 0 Quantity (t)	Year 0 Price (USD)	Year 1+ Quantity (t)	Year 1+ Price (USD)
Methanol	$417	7,987	$3,330,579	1,048	$437,016
WCO	$441	7,117	$3,138,597	9,490	$4,185,090
Propane	$799	568	$453,832	-	-
Propylene Glycol	$4,046	2.1	$8,497	-	-
Total			**$6,931,505**		**$4,622,106**

Table 7.1.ii Product Revenue

Product	Price (USD/t)	Year 0 Quantity (t)	Year 0 Revenue (USD)	Year 1+ Quantity (t/yr)	Year 1+ Revenue (USD/yr)
Biodiesel	$1,165	6,904.6	$8,041,186	9,206.1	$10,721,582
Glycerol	$3,307	636.0	$2,103,133	848.0	$2,804,178
Total			**$10,144,319**		**$13,525,760**

7.2 Equipment Pricing

The tables below detail the pricing for each piece of equipment required for the process. Each table lists the equipment cost and operating cost when applicable. More details on operating costs are provided in Section 7.4. To account for price increases over time, the CEPCI cost correlation was used for all equipment costs calculated using Towler and Sinnott (2022)

46

(Equation 7.2.i). The CEPCI value for 2025 was approximated at 800, and the CEPCI value used for 2010 was 532.9.

Equation 7.2.i CEPCI Cost Correlation

$$C = \frac{C_2}{C_1} * C_e$$

C = adjusted cost
$C_{1,2}$ = CEPCI adjustment values
C_e = calculated cost estimate

The capital cost of the reactor is listed in Table 7.2.i. The cost was determined for a pressure vessel using Table 7.2 in Towler and Sinnott (2022). Based on the reactor dimensions in Table 6.4.iii, the shell mass was approximated to be 50,309 kg. There are no operating costs associated with the reactor because no external heating or cooling is required.

Table 7.2.i Reactor Capital Cost

Label	Reaction	Volume (m³)	Material	Capital Cost (USD)
R-1	Transesterification, Esterification, and Hydrolysis	13.4	CS	$629,471

The flash evaporators and decanter capital costs are listed in Table 7.2.ii. The equipment was priced as pressure vessels using the shell mass and Table 7.2 in Towler and Sinnott (2022). The shell mass was determined using an assumed wall thickness of 15 mm. This thickness was determined by applying a safety factor of 3 to the minimum wall thickness of 5 mm (Towler & Sinnott, 2022).

Table 7.2.ii Flash Drum and Decanter Capital Cost

Label	Description	Volume (m³)	Material	Capital Cost (USD)
F-1	Methanol and Propane Recycle	4.23	CS	$212,617
S-1	Biodiesel and Glycerol Decanter	0.54	CS	$25,059
F-2	Biodiesel Dryer	0.94	CS	$26,100
Total				**$263,776**

Storage tank capital costs are listed in Table 7.2.iii. These tanks were priced using Table 7.2 in Towler and Sinnott (2022) based on tank volume, roof type, and material of construction.

Table 7.2.iii Tank Capital Costs

Label	Contents	Volume (m³)	Roof Type	Material	Capital Cost (USD)
T-1	WCO	900	Cone	CS	$289,595
T-2	Methanol	125	Floating	CS	$282,180
T-3	Biodiesel	900	Floating	CS	$575,693
T-4	Glycerol	60	Cone	304 SS	$66,173
T-5	Propane/Methanol	30	Cone	CS	$34,682
Total					**$1,213,641**

The centrifugal pump and compressor costs listed in Table 7.2.iv were determined using Table 7.2 in Towler and Sinnott (2022). Pumps were priced as single-stage centrifugal pumps. For centrifugal pumps with flow rates below 0.2 L/s (P-2 and P-10) a flow rate of 0.2 L/s was used for cost determination. The price of reciprocating pumps was determined using Seider (2017). The cost of the compressors P-8 and P-12 were priced as blowers due to their low power requirements. Pumps 10 and 11 are made of 304 SS to comply with regulations regarding process conditions for the pharmaceutical grade glycerol product. For the pumps, the capital cost includes both the pump and the parallel in-line backup pump.

Table 7.2.iv Pump and Compressor Capital and Operating Costs

Label	Description	Quantity	Type	Material	Total Power (kW)	Capital Cost (USD)	Operating Cost (USD/yr)
P-1	WCO Feed	2	Centrifugal	CS	0.12	$24,564	$76
P-2	Methanol Feed	2	Centrifugal	CS	0.01	$24,189	$6
P-3	Before recycle	2	Reciprocating	CS	1.72	$26,241	$1,084
P-4	Before reactor	2	Reciprocating	CS	52.92	$48,192	$33,365
P-5	D-1 distillate to recycle	2	Reciprocating	CS	0.53	$25,890	$315
P-6	Before decanter	2	Centrifugal	CS	0.11	$24,366	$69
P-7	Before F-2	2	Centrifugal	CS	0.06	$24,338	$38
P-8	F-2 air in	1	Blower	CS	3.95	$13,629	$2,523
P-9	Biodiesel storage	2	Centrifugal	CS	0.10	$24,336	$63
P-10	Glycerol storage	2	Centrifugal	304 SS	0.02	$31,445	$13
P-11	Absorber water in	2	Centrifugal	304 SS	0.06	$24,327	$40
P-12	Absorber air in	1	Blower	CS	4.16	$13,921	$2,624
Total						**$305,438**	**$40,216**

The heat exchanger capital cost was determined using the heat transfer area and Table 7.2 in Towler and Sinnott (2022). The costs for double pipe and floating head shell and tube heat exchangers were compared. The cheaper heat exchanger was selected for the design. The heat exchanger capital and operating costs listed in Table 7.2.v exclude the condensers and reboilers for D-1 and D-2.

Table 7.2.v Heat Exchanger Capital and Operating Costs

Label	Description	Utility	Area (m²)	Type	Material	Capital Cost (USD)	Operating Cost (USD/yr)
HX-1	Reactor Inlet and Effluent	-	57.6	Double Pipe	CS	$61,653	-
HX-2	Before Flash 1	Cooling Water	1.5	Double Pipe	CS	$8,312	$8
HX-5	Before Decanter	Cooling Water	6.9	Double Pipe	CS	$28,736	$340
HX-6	Biodiesel Storage	Cooling Water	83.6	Floating Head Shell & Tube	CS	$69,339	$58
HX-9	Glycerol Storage	Cooling Water	9.2	Double Pipe	304 SS	$48,625	$50
Total						**$216,665**	**$456**

The costs associated with distillation columns are shown in Table 7.2.vi. These columns were priced in ASPEN Plus using the Process Economic Analyzer feature based on column sizing. The operating costs detailed in the table for the Methanol/Water Distillation column are based on calculations made by summing the condenser and reboiler utility costs with the reflux pump utility cost. The operating costs for the Glycerol Purification Column included the reflux pump electricity requirements and reboiler and condenser steam, and cooling fluid costs. The operating cost of D-2 also accounts for the refrigeration required for the propylene glycol in the condenser and the steam consumption of the steam jet ejector.

Table 7.2.vi Distillation Column Costs

Label	Description	Theoretical Stages	Capital Cost (USD)	Operating Cost (USD/yr)
D-1	Methanol and Propane Recycle	13	$604,546	$33,142
D-2	Glycerol Purification	12	$1,029,017	$172,494
Total			**$1,633,563**	**$205,636**

The price of the methanol absorber is shown in Table 7.2.vii. The absorber column was priced as a pressure vessel using the shell mass and Table 7.2 in Towler and Sinnott (2022). The shell mass was determined using an assumed wall thickness of 15 mm. This thickness was determined by applying a safety factor of 3 on the minimum wall thickness of 5 mm (Towler & Sinnott, 2022). The operating cost accounts for the use of process water.

Table 7.2.vii Absorber Costs

Label	Description	Stages	Capital Cost (USD)	Operating Cost (USD/yr)
A-1	Methanol Absorber	5	$32,652	$391

7.3   Total Plant Capital Costs

The plant capital costs are calculated using Table 6.9 from Peters, Timmerhaus, and West, which can be seen in Section 13.21 (2003). Our plant was modeled as a fluid processing plant and was calculated with the corresponding multipliers. These multipliers are all ratio factors of the total delivered equipment cost shown in Section 7.2.

7.3.1   Direct Capital Costs

Peters, Timmerhaus, and West model the direct capital costs as the expenses directly tied to the physical construction and equipment installation (2003). These are the basic factors to ensure the plant is operational. These costs amount to 360% of the delivered equipment cost, reflecting the significant infrastructure required for fluid processing.

Table 7.3.i Direct Plant Capital Costs

Expense	Multiplier	Price (USD)
Equipment	1.00	$4,315,704
Installation	0.47	$2,028,381
Instrumentation/Controls	0.36	$1,553,653
Piping	0.68	$2,934,679
Electrical Systems	0.11	$474,727
Buildings	0.18	$776,827
Yard Improvements	0.10	$431,570
Service Facilities	0.70	$3,020,993
Total	**3.60**	**$15,536,534**

7.3.2   Indirect Capital Costs

Peters, Timmerhaus, and West model the indirect capital costs as the expenses not directly tied to physical construction but necessary for project completion (2003). These costs amount to 144% of the delivered equipment cost. The substantial ratio of indirect costs highlights the

importance of thorough preparation outside of physical construction in capital-intensive processes.

Table 7.3.ii Indirect Plant Capital Costs

Expense	Multiplier	Price (USD)
Engineering/Supervision	0.33	$1,424,182
Construction Expenses	0.41	$1,769,439
Legal Expenses	0.04	$172,628
Contractor's Fees	0.22	$949,455
Contingency	0.44	$1,898,910
Total	1.44	**$6,214,614**

7.3.3 Overall Capital Investment

Peters, Timmerhaus, and West calculate the fixed capital investment as the sum of all direct and indirect costs required to establish operational capacity (2003). This encompasses all the expenditure needed to construct and commission the processing facility before production begins. Working capital is separate as it funds initial operations rather than physical assets.

Table 7.3.iii Total Capital Investment

Expense	Multiplier	Price (USD)
Fixed Capital Investment	5.04	$21,751,147
Working Capital	0.89	$3,840,976
Total	5.93	**$25,592,123**

7.4 Operating Costs

7.4.1 Utilities

The total utility cost for the biodiesel plant is depicted in Table 7.4.i. The main utilities contributing to operating costs in the plant are steam, electricity, and cooling water. Process water, wastewater treatment, and refrigeration costs were also determined.

Table 7.4.i Utility Costs

Utility Type	Energy Consumption (kW)	Consumption (kg/yr)	Operating Cost (USD/yr)
Electricity	63.8	-	$40,236
HP Steam	-	2,343,913	$27,001
LP Steam	-	37,609,833	$172,494
Cooling Water	-	13,747,473	$656
Process Water	-	781,714	$391
Wastewater Treatment	-	1,360,257	$1,836
Refrigeration	7.1	-	$4,473
Total			**$247,087**

All steam generated on site will be 15 bar to meet the steam pressure requirements for the glycerol-water distillation column reboiler. The high pressure steam (HPS) will be expanded through a turbine, so that a shaft work credit can be applied to the low-pressure steam (LPS) (3 bar). The design of a steam generation facility is outside the scope of this project. However, funds have been allocated to the construction of this facility as a part of the direct capital investment.

The price of 15 bar HPS was determined to be $5.23/Mlb using Equation 7.4.i. The shaft work generated from expanding the steam from 15 bar to 3 bar was calculated and priced as electricity to determine the discount for LPS using the methods in Towler & Sinnott (2022). With a credit of $3.13/Mlb, the cost of 3 bar steam was determined to be $2.10/Mlb. The full calculations are found in Section 13.13.

Equation 7.4.i Price of High-Pressure Steam

$$P_{HPS} = P_F \cdot \frac{dH_b}{\eta_B} + P_{BFW}$$

P_{HPS} = Price of HPS ($/Mlb)
P_F = Fuel Price ($/MMBtu)
dH_b = heating rate (MMBtu/Mlb steam)
η_B = boiler efficiency
P_{BFW} = Price of boiler feed water ($/Mlb)

The average cost of electricity for industrial use in Pennsylvania for December 2024 was $0.08/kWh (*State Energy Profile Data*, n.d.). This value was used to estimate operating costs for pumps.

The cost of cooling water was estimated as the price of 2 kWh/1000 gal in addition to $0.02/1000 gal for chemical treatment. Therefore, our team used $0.18/1000 gal for the total cost of cooling water. Cooling water will be recycled for 50 cycles. Therefore, the calculated cooling water cost is based on a consumption of 1/50th of the yearly value listed in Table 7.4.i. The cost of process water was estimated as $0.5/t, and the cost of wastewater treatment was estimated as

$1.5/t. All these estimations were based on recommendations in Towler and Sinnott (2022). This wastewater treatment cost includes the treatment of methanol to reduce the biochemical oxygen demand (BOD) of the water.

The cost of refrigeration for the glycol chiller was determined using Equation 7.4.ii and the methods in Towler & Sinnott (2022). Using an evaporator absolute temperature of 275 K, a condenser absolute temperature of 285 K, and an efficiency of 0.8, the actual coefficient of performance (COP) was found to be 22. A shaft work of 7.1 kW was calculated by dividing the condenser duty of 156 kW by the COP. This resulted in a total annual electricity cost of $4,473/yr for the glycol chiller.

Equation 7.4.ii Coefficient of Performance

$$COP = \frac{T_1}{T_2 - T_1}$$

T_1 = evaporator absolute temperature (K)
T_2 = condenser absolute temperature (K)

7.4.2 Labor Costs

To calculate the total number of operators per shift, the methods and Equation 7.4.iii were used from Turton et al. (2018). Because this process only involves fluid handling, there are no particulate processing steps to consider. The distribution of non-particulate processing operations are outlined in Table 7.4.ii. The four heat exchangers not included in the N_{np} value are factored into the distillation towers for condenser and reboiler duty.

Table 7.4.ii Non-Particulate Processing Steps

Equipment Type	Quantity	N_{np}
Compressors	2	2
Exchangers	9	5
Heaters/Furnaces	0	0
Reactors	1	1
Towers	2	2
Total	14	10

To determine the required workforce for continuous operation, the standard scaling factor from Turton et al. was applied (2018). The full calculation can be seen in Section 13.22. Based on this methodology, the final workforce requirement for the plant is 13 operating laborers (OLs). This is rounded down slightly from the calculated 13.09 value and will be accounted for through additional bonuses.

Equation 7.4.iii Operators per Shift

$$N_{OL} = \left(6.29 + 31.7P^2 + 0.23N_{np}\right)^{0.5}$$

P = Particulate Processing Steps
N_{np} = Non-Particulate Processing

53

The economic distribution model for petrochemical plants generally emphasizes high base salaries while maintaining lower benefits, as recommended by Towler and Sinnott (2022). This structure ensures competitive compensation to attract skilled labor while managing overall employment costs. To determine the appropriate salary for operating labor, historical data from 2001 was referenced, with a base salary of $50,000 (Turton et al., 2018). This value was then adjusted for inflation using the consumer pricing index. The specific cost factor used for 2001 was 193 and 323.38 for today's market (U.S Bureau of Labor Statistics, 2025). The ratio of these two values resulted in an updated operator salary of $83,777, reflecting the rising cost of labor and the economic conditions that have influenced wage growth over the past two decades. This salary ensures that our plant remains competitive in attracting skilled operators in the petrochemical sector.

Table 7.4.iii General Labor Costs

Labor Expense	Equation	Price (USD)
Operating Labor	Laborers * Yearly Salary	$1,089,104
Supervising Labor	OL * 0.2	$217,821
Overhead Costs	(OL + SL) * 0.3	$392,077
Total Labor Costs	OL + SL + Overhead Costs	$1,699,002
G&A Costs	Total Labor Costs * 0.65	$1,104,351
Total		**$4,502,355**

The supervising labor multiplier, used to scale up labor costs for management and oversight personnel, was selected based on recommendations from multiple literature sources. This multiplier accounts for the additional costs associated with managerial oversight, reflecting industry standards for labor allocation in chemical processing plants. Given the nature of our operations, where workflow is relatively stable with minimal variation in processing conditions, a moderate supervisory multiplier was chosen.

As previously discussed, the overhead cost multiplier was set at the lower end of the suggested range. Overhead costs include expenses such as utilities, maintenance, office administration, and facility management. Since our company primarily focuses on efficient chemical processing rather than extensive research and development (R&D), our overhead requirements are lower than those of pharmaceutical companies or research-intensive firms. Companies engaged in extensive R&D often require higher overhead costs due to laboratory equipment, specialized personnel, and regulatory compliance requirements.

General and administrative (G&A) costs represent the expenses necessary for corporate management and support functions. These costs encompass human resources, legal services, business development, and overall company administration. Effective management of G&A costs is crucial for long-term profitability, as excessive administrative overhead can reduce operational efficiency.

This overall labor cost strategy ensures that our plant operates with an optimized workforce while maintaining financial sustainability in a competitive market.

7.4.3   Miscellaneous Operating Costs

In addition to direct operating costs, several fixed and indirect expenses contribute to the overall cost structure of the plant. These costs are essential for maintaining plant operations, regulatory compliance, and long-term financial stability. The estimated costs for these factors are calculated based on a percentage of the Inside Battery Limits (ISBL) investment (Towler and Sinnott, 2022). The ISBL is modeled as the direct plant capital cost calculated in Table 7.3.i.

Table 7.4.iv Miscellaneous Operating Costs

Expense	ISBL Multiplier	Price (USD)
Maintenance	0.03	$466,096
Property Taxes/Insurance	0.015	$233,048
Rent of Land	0.01	$155,365
R&D Costs	0.005	$77,683
Environmental Charges	0.01	$155,365
Total	0.07	**$1,087,557**

Maintenance expenses, which include both materials and labor, are critical for ensuring long-term equipment reliability and process efficiency. Given that our process involves fluid handling with no solids processing, the lower end of the range was chosen. The property tax and insurance expenses account for liability protection, plant infrastructure insurance, and state or local property tax obligations. As our project assumes land is rented rather than purchased, an annual land lease cost is factored in. This estimation follows standard industry practices where long-term rental agreements are preferred over direct land purchases. While our facility is primarily focused on production rather than intensive R&D, a small allocation is made for process optimization and minor technological improvements. This is standard of the petrochemical industry (Towler and Sinnott, 2022). To ensure compliance with environmental regulations and contributions to applicable environmental funds, an environmental charge of 1% of ISBL investment is applied. This covers any regulatory fees, emissions management, and potential superfund contributions. Our project is modeled as a self-funded company without external loans or financial obligations, so no capital charges or debt-related interest payments are included in the operating costs. Additionally, since the process does not involve proprietary technologies requiring third-party licensing, no royalties or licensing fees are accounted for in this cost structure.

7.5   Summative Economic Analysis

7.5.1   After-Tax Cash Flow

The biodiesel production facility follows a structured timeline, beginning with year -1, which represents the plant's construction phase. During this period, all capital expenditures are incurred. Additionally, pre-operational costs such as preliminary maintenance, permits, and setup logistics are accounted for in this phase. This causes the year -1 costs shown in Figure 7.5.1 to be significantly negative.

Year 0 marks the commencement of plant commissioning, where the facility begins limited operations to test and optimize processes before reaching full-scale production. In year 0, the recycled raw materials including methanol, propane, and propylene glycol will be purchased. At this stage, utilities, WCO, consumable methanol, and revenue generation were modeled at 75% of plant capacity, reflecting the gradual ramp-up of operations. Full-phase production is scheduled to begin at month 18, requiring a phased approach to cost allocation and revenue estimation. Overall, limited revenue is accrued from production, but it is insufficient to offset the costs associated with operation, thus resulting in a negative cash flow.

Year 1 represents the plant's first year of full-scale production, during which all recurring operating costs, including raw material expenses, utilities, research and development (R&D) costs, and environmental compliance fees, are fully accounted for. From this point forward, the facility enters steady-state operation, ensuring consistent production levels and cost structures. At steady state, the raw materials, utilities, and product revenues are modeled at 90% capacity to account for periodic maintenance breaks for the plant. At this point, all modeled revenue should remain consistent year-to-year and presents a constant profit for the plant site.
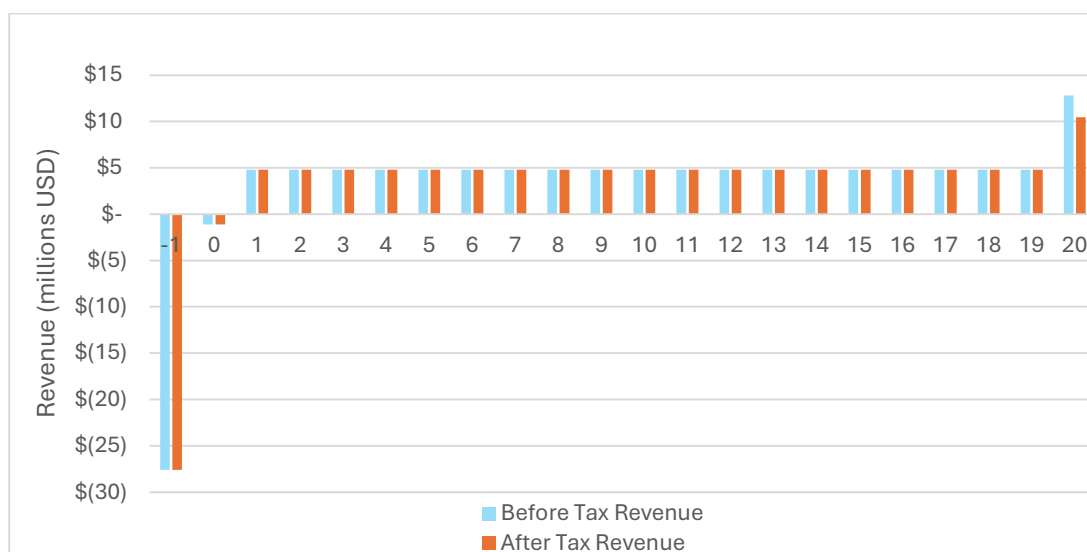

Figure 7.5.i After-Tax Cash Flow Model

For the subsequent twenty years, the plant operates at 90% production capacity, as reflected in Figure 7.5.i. A key financial advantage of this project is that the facility does not incur income tax liabilities. Under standard tax conditions, our taxable income would amount to $1.4 million annually, based on Pennsylvania's state income tax rate of 8.49% and the federal corporate tax rate of 21% (Crystal Stranger JD, EA, NTPI Fellow, 2024). However, the B100 biodiesel tax credit provides a $1.00/gal incentive for every gallon of biodiesel produced and distributed (Andre Tax Co., 2025). With an annual production of approximately 2.4 million gallons, this results in $2.4 million in tax credits, which fully offsets our taxable income. The salvaged equipment sold at the decommissioning of our plant is shown in year 20. This was slated to be $8 million factoring in piping, equipment and inflation. After taxes, we will recoup an additional $5.6 million in revenue.

The cash flow diagram visually demonstrates this tax exemption benefit, as well as the consistent revenue streams expected throughout the plant's operational lifespan. The long-term financial stability of the project is reinforced by favorable tax incentives, stable production rates, and efficient cost management, positioning it as an investment and can be seen in further detail in Figure 7.5.ii.

7.5.2   Cumulative Cash Flow

The cumulative cash flow model demonstrates strong financial viability, with the project breaking even between years 6 and 7 (Figure 7.5.ii). This early breakeven point is a promising indicator of profitability, as many large-scale industrial projects typically require longer payback periods.

The dip at the beginning of the diagram represents the initial costs associated with the capital investment necessary for the plant as well as the first year of operating or working costs for the plant to run, i.e. raw materials, utilities, labor, etc. After this point, even with the operating costs accounted for the revenue gained from the biodiesel and glycerol products are in excess of operating costs indicating a profitable chart for the overall site and resulting in the net worth of the plant continually increasing until the afore-mentioned break-even point detailed in Figure 7.5.ii.

By the end of the project's lifecycle, the cumulative net worth is projected to reach approximately $66.5 million. At decommissioning, an extra $5.6 million will be recovered from the sale of working capital and salvageable processing equipment after taxes. This recovery reduces the financial risk associated with plant closure, reinforcing the project's strong return on investment and long-term economic sustainability. A more comprehensive evaluation of the project's economic potential, along with the final recommendation can be found in Section 11.3.
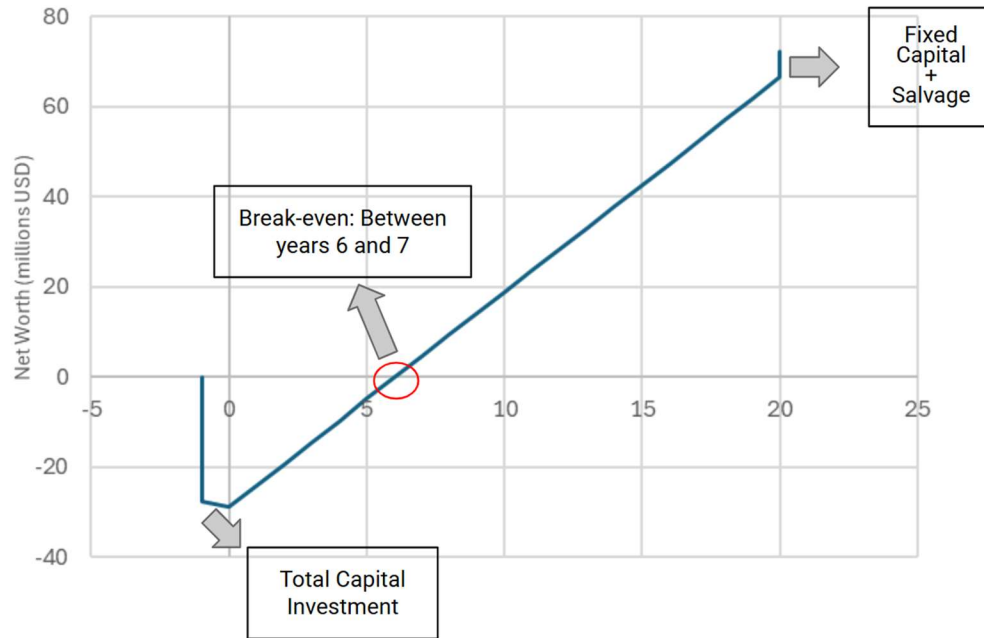
Figure 7.5.ii Cumulative Cash Flow Model

7.5.3   Financial Metrics

Return on Investment (ROI) is a financial metric used to measure the profitability of an investment relative to the cost of the investment. To calculate this, Equation 7.5.i was used (Towler & Sinnott, 2022). A higher ROI value indicates a more lucrative investment which makes it a crucial tool when looking at projected profits. As detailed in Section 13.14, the net profit has been calculated by subtracting the net worth of the plant after initial construction costs from the final net worth of the plant at the end of its operational cycle. For the purposes of calculation, a 22-year production cycle has been chosen and based on these values the ROI has been calculated to be 16.4% per annum, a promising return rate.

Equation 7.5.i Return on Investment

$$ROI = \frac{cumulative\ net\ profit}{plant\ life * initial\ investment} * 100\%$$

Internal Rate of Return (IRR) is another financial metric that achieves a similar goal to the ROI by determining the financial viability of a specific investment or venture. Specifically, the IRR represents the discount rate at which the net-present value (NPV) of an investment becomes zero. Analogously to ROI, a higher IRR value indicates a more attractive investment, making it a key tool for capital budgeting and strategic planning. IRR was calculated in Excel using the "IRR" function and came out to be 13.72%. This function models Equation 7.5.ii (Towler & Sinnott, 2022). The specific interpretation of this IRR value is expanded upon in Section 11.3.

Equation 7.5.iiii Internal Rate of Return

$$IRR: \sum_{n=1}^{n=t} \frac{CF_n}{(1 + i')^n} = 0$$

n = each period (year)
t = total number of plant years
CF_n = cash flow for period
i' = internal rate of return

7.5.4   No Tax Credit Economics Scenario

In the scenario that there is a change in relevant legislation such that the tax credit currently in place that offers $1.00/gallon of biodiesel produced is eliminated entirely, the profitability of the site and overall financial metrics are dramatically impacted. As seen in Figure 7.5.iii, the new continuous cash flow diagram projects a break-even point between years 7 and 8, which is a shift by one year from the original scenario. Furthermore, the calculated IRR for a No Tax Credit scenario is drastically lower, dropping to around 5.20%, 8% lower than if a tax credit is in place. The effect of this changed IRR value compared to the original scenario is expanded upon in Section 11.3.
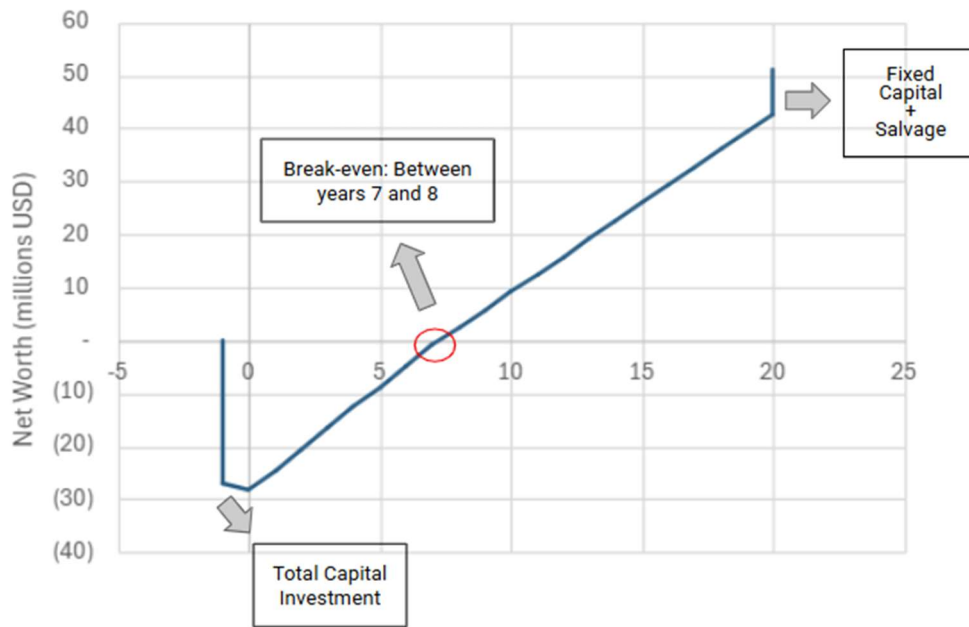

Figure 7.5.iii No Tax Credit CCF Diagram

8   Health, Safety, and the Environment

8.1   Health and Safety Pre-Modeling Analysis

Chemical hazards and potential release scenarios were analyzed to inform safety precautions for the plant. ALOHA software was used to create chemical release threat zone estimates for three potential events. The results of this analysis are outlined in the following section. The chemical hazards in the biodiesel plant are listed in Figure 8.1.i.

Chemical	Signal Word	NFPA Diamond	Hazard Pictograms	Chemical Hazard Statements	Stability and Reactivity
Methanol	Danger	3 / 1 0 /		H225: flammable liquids (cat. 2) H301: acute toxicity - oral (cat. 3) H331: acute toxicity - inhalation (cat. 3) H311: acute toxicity - dermal (cat. 3) H370: specific target organ toxicity - single exposure (cat. 1)	Highly flammable
Propane	Danger	4 / 2 0 /		H220: flammable gasses (cat. 1) H280: Gases under pressure - liquefied gas	Highly flammable
Oleic Acid (FFA)	Warning	1 / 1 0 /		H315: skin corrosion/irritation (cat. 2) H319: serious eye irritation (cat. 2b)	Peroxidizable compound
Triolein (Triglycerides)	n/a	n/a	n/a	n/a	n/a
Glycerol	Warning	1 / 1 0 /		H320: eye irritation (cat. 2b)	Air reactive (high temp)
Methyl Oleate (Biodiesel)	Danger	n/a		H227: flammable Liquid (cat. 4) H304: fatal if swallowed or enters airways H315: skin corrosion/irritation (cat. 2) H332: acute toxicity (cat. 4)	Air reactive (high temp)

Figure 8.1.i Chemical Hazard Information

8.1.1   Location Rationale

The biodiesel plant is in Lancaster, Pennsylvania. This location provides convenient access to feedstock sources and population centers for product distribution. Despite the infrastructure in this area, there are locations in this region that provide separation from public infrastructure and residential areas, making it less likely to affect the general population in the case of a toxic release. Plant siting away from nearby populations is the first step in ensuring the safety of the surrounding population.

8.1.2   Atmospheric Conditions

Another advantage of Lancaster, Pennsylvania is the relatively moderate climate. According to the Köppen climate classification, Lancaster falls within the hot-summer, humid continental climate, where summers tend to be warm, humid, and wet, but winters tend to be cold and snowy. This area is also characterized by partly cloudy weather year-round and moderate wind speeds. The average hourly wind speeds are about 4.7 mph from May to November and 6.4 mph from December to April. Average daily high temperatures from May to September are around 76˚F and from December to March are around 47˚F. Over half the year, the cloud cover ranges from clear to partly cloudy (Incorporated, n.d.)

The date used for safety scenario modeling was August 27, 2024, at 1300 hours EDT. which had an air temperature of 85˚F, a relative humidity of 53%, a two-tenths cloud cover, and 5.75 mph wind from the SE at 3 meters of height. These average summer conditions correspond to an atmospheric stability class of F, providing a conservative release estimation. However, outside of the summer months, temperatures are likely to be lower than 85˚F, so a C/D stability class was chosen for ALOHA modeling to better represent potential deviations during the colder season.

8.1.3   Leak Assumptions

As a result of the supercritical process conditions, assumptions on the fluid state were made to estimate the release quantity. The part of the process the leak occurred at, the pressure and temperature of the substances at that stage, and the relative volatility of chemicals were considered. For each release scenario, pipe diameters were calculated using the volumetric flow rates and an average flow velocity. For liquids, an industry-standard flow rate of 3 m/s was chosen, and for vapors at normal to medium pressure, a flow rate of 15 m/s was chosen. For streams at supercritical conditions, a liquid flow velocity was used because the fluid had a liquid-like density. The pipe diameter calculations are in Section 13.15.

8.2   Release Scenarios

8.2.1   Scenario 1: Pump 3 Seal Failure Resulting in Methanol and WCO Release

The first potential release scenario is a pump seal failure after the preliminary feed pump (P-3). Figure 8.2.i shows the location of the failure on the PFD. Because the pump effluent connects to the recycle stream, a pressurization issue at this juncture may result in a significant toxic release of both the WCO and the methanol at a pressure of 6 bar. Propane was not
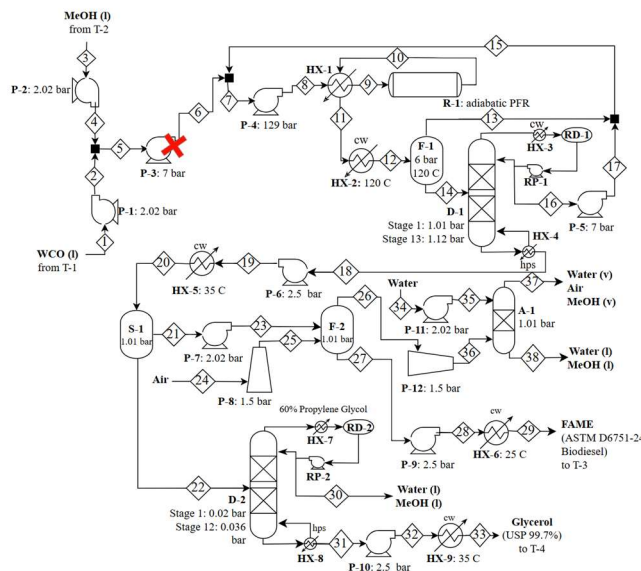
Figure 8.2.i Process Flow Diagram for Pump 3 Release

considered as a component of this release. While propane is initially fed into the system, during steady-state operating propane is fully recycled, eliminating it as a component in the feed stream.

A pump seal failure has a failure frequency from 10^{-1} to 10^{-2}/yr and the direct source model assumed a rupture of 20% of the pipe cross-sectional area. This equals 20% of the methanol stream flow rate. The calculations are shown in Section 13.15. This resulted in a release quantity of 206.9 kg/hr of methanol.

As observed in Figure 8.2.ii, the ERPG-1 exposure area extends over 80 yards. With this release area, it is unlikely that the toxic plume will extend far enough to cause harm to surrounding areas and businesses. However, due to the highly toxic and volatile nature of methanol, personnel on-site may be affected if they inhale or contact the release.
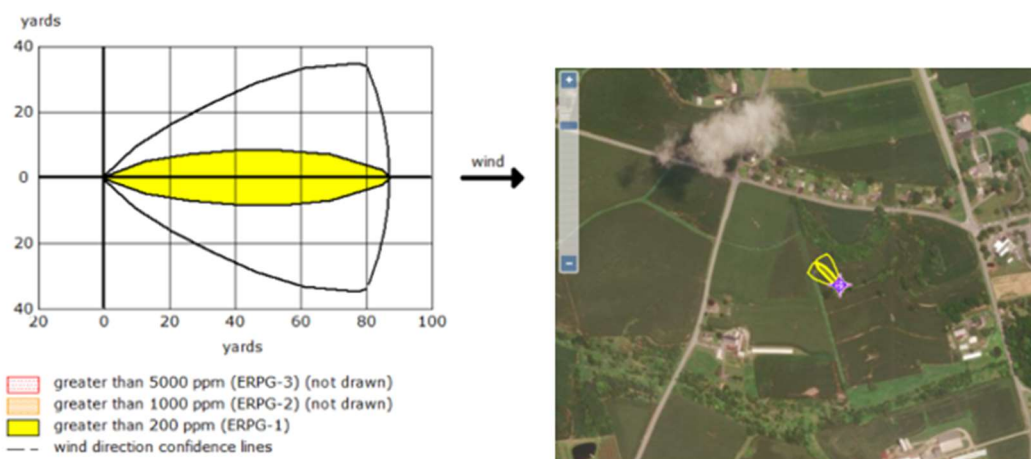
Figure 8.2.ii ERPG Zones of Methanol Release from P-3

8.2.2   Scenario 2: Gasket Seal Failure after Decanter resulting in large release of FAME
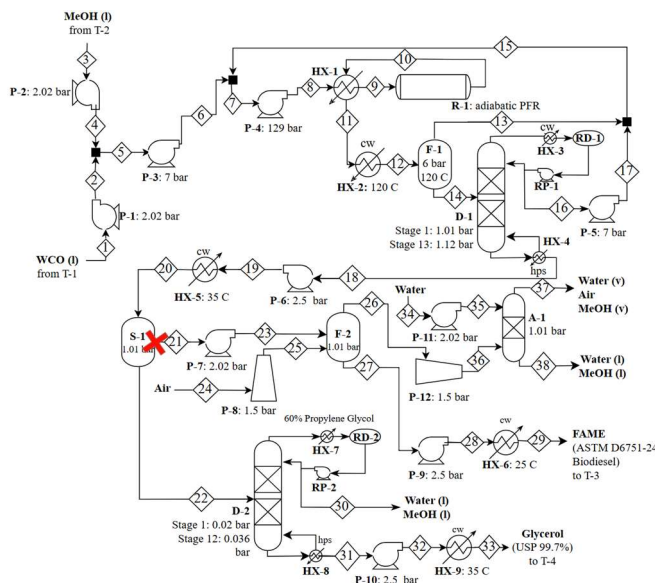
Figure 8.2.iii Process Flow Diagram for Decanter Release

This scenario considers a gasket failure leaving the decanter (S-1) resulting in a release of the light liquid take-off stream composed primarily of FAME (Figure 8.2.iii).

Due to limitations in physical and chemical property data available for biodiesel, petroleum-based diesel SDSs were utilized to determine the exposure limits and properties. Specifically, CAS 68476-34-6: No. 2 Diesel Fuel (Extra Low Sulfur) was used in place of FAME. As a result of this assumption, the toxicity zone approximations may be overestimated because biodiesel has a lower volatility and toxicity than petroleum-based diesel. However, exposure to vaporized FAME is still a health concern.

This simulation was modeled as a direct source and a puddle release. A gasket seal failure has a failure frequency rate of 10^{-2}/yr, and an assumed rupture of 20% of the cross-sectional area was used for the direct source simulation. Section 13.15 details the rupture flow rate calculations. This resulted in a release quantity of 232.1 kg/hr of FAME. The ERPG-1, 2, and 3 threat zones were determined using a 3x, 5x, and 10x multiple of the TWA release quantity of 100 mg/m^3. Figure 8.2.iv shows the ERPG limit exposure ranges. The ERPG-1 exposure area extended 80 yards, and the ERPG-2 exposure area extended 60 yards. This means that those within 60 yards could have severe health impacts within an hour of exposure, as ERPG-2 levels signify the maximum concentration an individual can be exposed to before facing serious lasting health effects. The threat zone is relatively limited, posing a significant health threat to operational staff on site if not evacuated promptly.
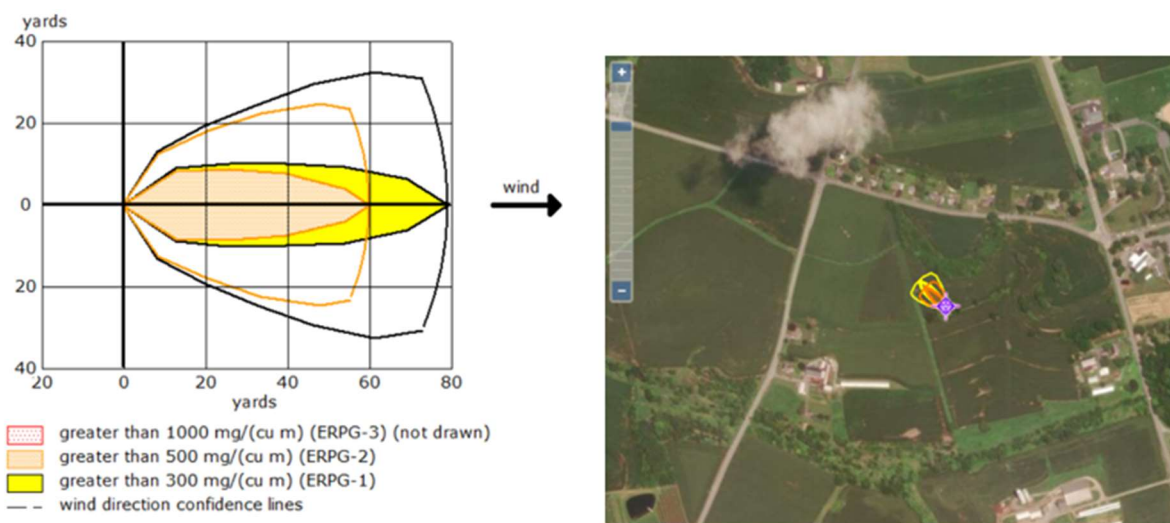
Figure 8.2.iv ERPG Zones for Decanter Release Direct Source

However, for this scenario, a blast force or overpressure would cause a larger impact from this release scenario is the blast force or overpressure consideration, as shown in Figure 8.2.v. Although diesel has a low volatility and vapor explosive limit, which reduces the chances of certain explosive scenarios, exposure to a heat source or spark may lead to an explosion.

Within a range of 10 meters from the leak source, serious injury is likely, and up to a radius of 40 meters site and building damage will occur, as well as potential harm to individuals.
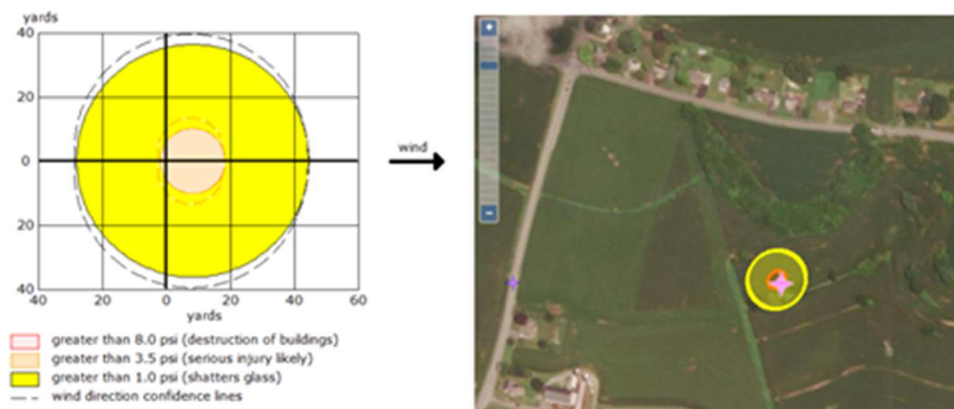
Figure 8.2.v Blast Force Zone for Decanter Release Direct Source

A puddle release is also a possibility. This assumes the leak of FAME from the decanter accumulates into a pool or puddle that then vaporizes or ignites. The overall volume of release was determined based on the volumetric flow rate of FAME and an average pooling depth of 4 cm (Chaudhary et al., 2019). This resulted in a pool of puddle area of 36.3 m^2. When modeled, an evaporating puddle posed no significant safety threat. However, if an ignition occurred it could generate a lethal threat zone within a radius of 10 yards, severe burns within 20 yards, and 1st degree burns or pain within a 35-yard range as shown in Figure 8.2.vi. However, this burning puddle scenario is unlikely due to the high flash point of the biodiesel and the low temperature at this juncture of 35 °C.
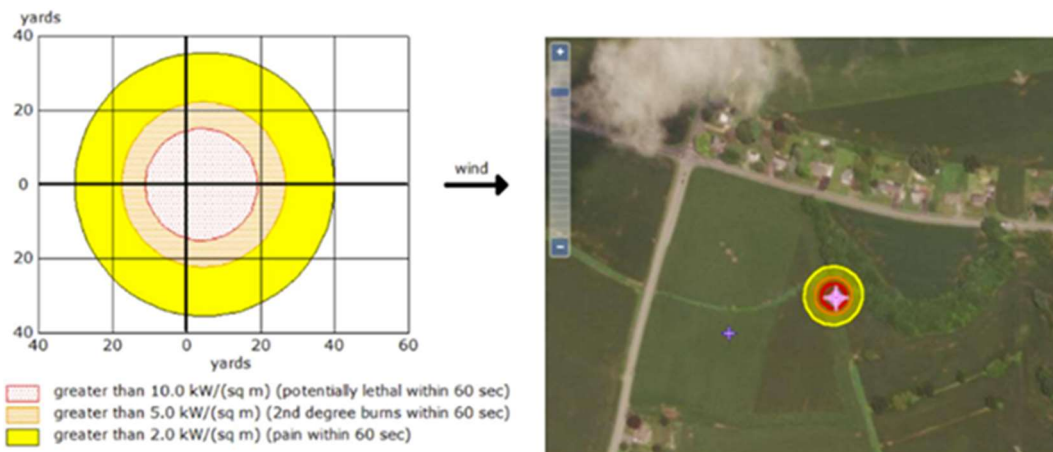
Figure 8.2.vi Burning Puddle Threat Zone for Decanter Release Scenario

8.2.3 Scenario 3: Gasket Failure or Pump 4 Seal Failure Resulting in Methanol Release

Scenario 3 models a gasket failure of the high-temperature, high-pressure methanol stream entering or leaving the PFR. This scenario is shown on the PFD below (Figure 8.2.vii).
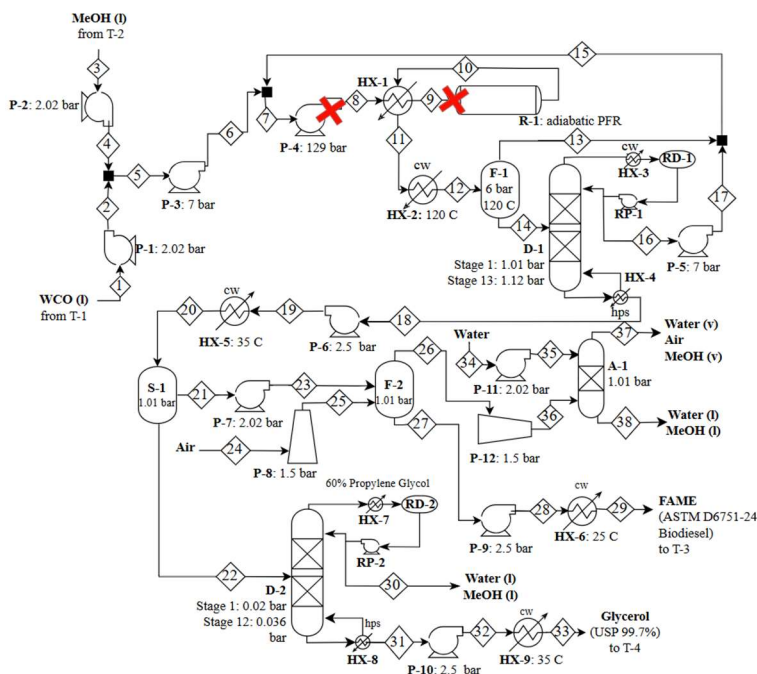
Figure 8.2.vii. Process Flow Diagram for Pump 4 or Gasket Seal Failure and Methanol Release

Gasket failures have a frequency failure rate of 10^{-2} /yr, but the high reactor pressure and temperature increase the likelihood of a gasket failure. Furthermore, due to the PFR's proximity to Pump 4, incomplete pressurization is likely in the event of a pump seal failure, which may spur a gasket failure. In addition to the toxicity, flammability, and explosivity hazards of methanol, the high temperature presents a serious potential for harm to operators in this area.

Designing a high-risk zone around the PFR would lower operator risk and exposure around the unsafe operating conditions. This zone should require additional PPE for heat protection and a water spray/deluge system to reduce the effect of a potential leak. Furthermore, insulated piping would reduce the risk for burns and increase operator safety.

ALOHA had limited modeling options for releases at supercritical temperatures and pressures. Thus, initially, pseudo-pipe sizing based on the specific flow rate of methanol at this point was modeled as both a liquid and a gas pipeline release. However, only the gas pipeline scenario was ultimately considered because at 280°C the liquid stream immediately vaporized. To model the liquid release, a 20% pipe cross-sectional area was assumed for the release area.

This resulted in a release quantity of 209.1 kg/hr of methanol, which is negligibly different from the model seen in Figure 8.2.ii.
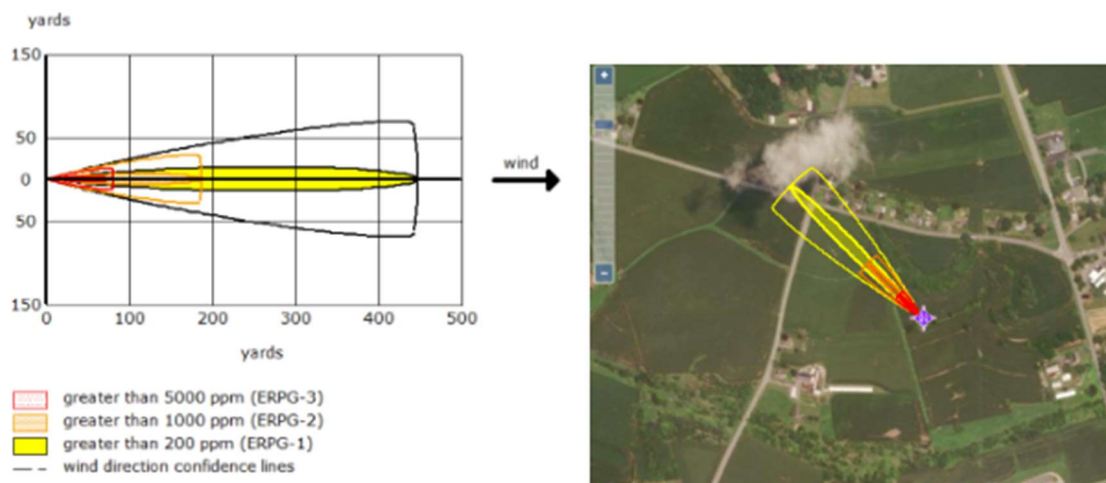
Figure 8.2.viii. ERPG Zones for PFR Material Stream Gas Pipeline Methanol Release

The gas pipeline model assumed a 2 in pipe diameter (Section 13.15). The ALOHA model simulated a gas release without the gas burning. The rupture area was assumed to be 20% of the pipe cross-sectional area. Figure 8.2.viii shows the ERPG limits. The ERPG-1 exposure area reached 450 yards, the ERPG-2 exposure area reached almost 200 yards, and the ERPG-3 exposure area reached 75 yards. This plume is significantly larger than in scenarios 1 and 2, illustrating how the high temperature and pressure around the PFR can lead to more harmful releases. The corresponding MARPLOT diagram in Figure 8.2.viii shows that the simulated release extends to neighboring roads and residential areas. This makes well-established public evacuation and safety procedures important. Furthermore, safety practices to minimize the risk to operators within the ERPG-2 and ERPG-2 zones are essential. It should be noted that this scenario also has corresponding flammability and explosive concerns. However, these scenarios were not detailed because the risks are minor and occur in only a limited range.

8.2.4   Maximum Credible Scenario

The maximum credible scenario is the methanol release prior to the PFR due to a gasket or pump seal failure. Compared to the other scenarios, the high pressure and temperature in Scenario 3 result in higher severity and likelihood. The exposure range for the methanol at ERPG-1 extends over 400 yards, while the other scenarios end within 100 yards. Furthermore, Scenario 3 is the only scenario where the ERPG-3 threat zones are of a non-negligible range. Methanol is a GHS category 3 Acute Toxicity via Oral (H301), Inhalation (H331), and Dermal (H311) hazard (Figure 8.1.i). Category 3 toxicity corresponds to TRC-3 and has a Tier 1 Outdoor threshold quantity (TQ) of 100 kg. The projected release quantity of methanol is 1045.6 kg/hr, which is 10 times the TQ. Due to the high temperature above its flashpoint, the methanol may combust when exposed to the atmosphere.

8.3 Most Credible Event and Inherently Safer Design

8.3.1 Most Credible Event and Risk Level

The methanol release prior to the PFR (Scenario 3) is also the most credible release scenario (MCE) because it has the highest potential frequency, 10^{-1}/yr for a gasket failure. In addition, this scenario has the greatest potential for harm to human health due to methanol's acute toxicity, the large release quantity, and flammability. Left unmitigated, this scenario is a Risk Level B as defined in Table 1-14 of the Chemical Process Safety textbook (Risk level determination reasoning is found Section 13.17).

8.3.2 Reducing Risk

Risk Level B is classified as an undesirable risk and requires additional safeguards to be put in place within a 3-month span. To reduce the risk level to a C or D, operational controls, equipment controls, consistent maintenance checks on the pump seal and gasket seal, and containment measures should be considered. Specifically, mitigation measures may include a higher rate of inspection for seals in the designated high-pressure instrumentation zone around the PFR, relief valves to prevent over-pressurization, and a wet scrubber or spray system that can absorb methanol vapor to minimize the spread of a release.

8.3.3 HAZOP for MCE

A pseudo hazard and operability study (HAZOP) around the PFR was conducted to identify factors that may increase the likelihood of the MCE (Section 13.18). This analysis is considered a pseudo-HAZOP because a full P&ID (Piping & Instrumentation Diagram) is typically utilized to ensure a thorough analysis is being conducted, but for the purposes of this safety simulation a more limited approach was taken. This pseudo-HAZOP analyzed flow and pressure parameter deviations. It determined that high flow rates and high-pressure situations had the highest risk of causing a pressure or gasket seal failure.

A high flow rate could be caused by an error in the feedstock pump or the flow rate sensor connected to the feedstock pump. In addition, deviations from normal operation in the distillation column or flash evaporator could increase the flow rate of the recycle stream and cause the PFR to overflow. Both scenarios could result in a pump seal failure. Higher flow rates may lead to incomplete stream pressurization once heated, increasing the fluid volume and leading to a gasket seal failure. Flow meters present after each pump going into the PFR (feedstock, compressors, etc.) and after the flash evaporator and distillation column in the recycle stream (F1 and D-1) could help ensure flow is operating under normal parameters and signal to any potential changes in the process.

To mitigate the risk of over-pressurization and high flow deviations, proper sizing and maintenance of pressure relief valves on the PFR, pressure vessels, pipes, and pumps is recommended. Furthermore, redundant pressure gauges and flow meters are recommended to reduce the risk of a significant release scenario. An activated charcoal scrubber or flare system should be connected to the relief valves to prevent releases into the plant environment or

atmosphere. Finally, it is important to ensure that regular maintenance is occurring to monitor corrosion progress and identify vulnerable areas for potential leaks.

8.3.4 LOPA for MCE

A Layer of Protection Analysis (LOPA) was conducted for the MCE (Scenario 3). The full calculations are shown in Section 13.20. The initiating event frequency (IEF) for a seal or gasket failure is 10^{-1}/yr. The severity level is "Very Serious" due to the release being 10 times the TQ. The existing safeguards for our design are described in Section 13.19 and include a pressure relief valve (PFD of 10^{-2}/yr), a rupture disk in the pipeline leading to the PFR (PFD of 10^{-2}/yr), excess flow valve to the control flow rate in the pipeline (PFD of 10^{-1}/yr), a basic process control system including various detectors, pressure gauges, and flow meters (cumulative PFD of 10^{-1}/yr), and operator response training in a high-stress scenario (PFD of 10^{-1}/yr). These independent protection layers (IPLs) result in a total calculated scenario frequency of 10^{-8}/yr, which is below the corresponding target mitigated event frequency (TMEF) of 10^{-5}/yr. Therefore, no additional layers are required, and the current risk is considered acceptable.

8.4 Relevant Codes and Regulations

The codes and regulations applicable to the chemicals and conditions of our process design will be outlined in the following section.

8.4.1 Methanol

OSHA 29 CFR 1910.1200 defines methanol as a hazardous chemical and requires appropriate labeling, employee safety training, and accessible SDS to communicate the risks. Also, under the National Fire Protection Association (NFPA) *30*, methanol is classified as a Class IB flammable liquid and requires specific storage and handling precautions. According to these guidelines, methanol storage tanks are required to have, "liquid and vapor containment, electrical grounding, cathodic protection, protection from stray currents, in-tank vapor control, vapor space fire suppression, and management of inhalation, ingestion, and dermal contact." (Methanol Institute, n.d.).

Furthermore, the Environmental Protection Agency (EPA) Toxic Substances Control Act (TSCA) *40 CFR Parts 702, 711, 720, and 721* states that manufacturers must report any manufacturing, importing, or utilization and inventory of methanol. This includes subsequent review processes that may require additional investigation into other appropriate regulations that may apply depending on use conditions and criteria.

The EPA Clean Water Act (CWA) *Sections 303, 307, and 402*, set water quality standards for surrounding bodies of water, general toxic pollutants that must fall within *National Pollutant Discharge Elimination System (NPDES)* standards, as well as release limits. These limits apply to the wastewater streams leaving our process. More detail on wastewater treatment is outlined in 8.6.1.

8.4.2 Biodiesel

The production and utilization of biodiesel are subject to many environmental and worker safety standards to ensure safe handling, minimized environmental impact, and sustainability. Under OSHA 29 CFR 1910.1200, biodiesel is classified as a hazardous chemical in certain workplace conditions, requiring appropriate labeling to communicate potential risks to workers.

The EPA regulates biodiesel manufacturing under the TSCA 40 CFR Part 702, 711, 720, and 721, requiring manufacturers to report production, importation, and utilization data for regulatory review. Additionally, the transportation and storage of biodiesel must comply with Department of Transportation (DOT) 49 CFR Parts 171-180, ensuring safe handling during distribution. Fire safety regulations under NFPA 30 classify biodiesel as a Class IIIB combustible liquid, necessitating proper storage and fire prevention measures to mitigate risks.

The Clean Air Act (CAA) 42 U.S.C. 7401 et seq. regulates air emissions from biodiesel production, particularly volatile organic compounds (VOCs) and particulate matter, to under 2.7 t/yr. Furthermore, CWA Sections 303, 307, and 402 impose water quality standards and effluent limitations under the National Pollutant Discharge Elimination System (NPDES), ensuring that biodiesel byproducts, including glycerol and residual methanol, do not contaminate water bodies. Waste management regulations under the RCRA 40 CFR Part 261 apply to byproducts such as glycerol and any hazardous residues requiring proper disposal. More details on wastewater compliance are detailed in Section 8.6.

8.4.3 Glycerol

Glycerol, a byproduct of biodiesel production, is subject to various regulatory standards to ensure safe handling, environmental compliance, and proper disposal. Under OSHA 29 CFR 1910.1200, glycerol mist must be appropriately labeled to communicate potential hazards. OSHA 29 CFR 1910.1000 establishes permissible exposure limits to protect workers from respiratory irritation. If airborne concentrations exceed these limits, OSHA 29 CFR 1910.134 mandates respiratory protection.

The EPA's TSCA 40 CFR Part 702, 711, 720, and 721 requires reporting of glycerol production, importation, and use for regulatory review. At large quantities, emissions regulations under the CAA 42 U.S.C. 7401 et seq. may apply. Additionally, under the Comprehensive Environmental Response, Compensation, and Liability Act 42 U.S.C. 9601 et seq., releases of contaminated glycerol in significant quantities must be reported to the EPA. The CWA Sections 303, 307, and 402 mandate that glycerol-containing wastewater meet NPDES standards before discharge to prevent excessive organic loading in water bodies, which can lead to oxygen depletion and ecological imbalances. The disposal of crude glycerol and glycerol wastewater is not a concern of our plant design because the glycerol is purified and sold, rather than discarded.

Transportation and storage must comply with DOT 49 CFR Parts 171-180, though pure glycerol is generally not classified as hazardous unless mixed with flammable or toxic substances. Additionally, the NFPA 30 classifies glycerol as a Class IIIB combustible liquid,

necessitating proper storage and handling procedures to mitigate fire hazards. For applications in food, pharmaceuticals, and cosmetics, glycerol must meet purity standards set by the Food and Drug Administration (FDA) 21 CFR Part 184.1324. Furthermore, Good Manufacturing Practices 21 CFR Part 110 applies to facilities handling glycerol for food and pharmaceutical use to ensure sanitary processing. This is important in this specific context where glycerol is intended to be sold further on as a byproduct of the process and thus must abide by these standards and regulations.

8.4.4   Propane

Propane is a highly flammable liquefied petroleum gas and is regulated under multiple federal and industry-specific standards to ensure its safe handling, transportation, and environmental compliance.

Under *OSHA 29 CFR 1910.1200*, propane is classified as a hazardous chemical, requiring proper labeling to communicate risks such as fire, explosion, and asphyxiation. Additionally, *OSHA 29 CFR 1910.110* establishes workplace safety requirements for propane storage and handling, including container design, pressure relief devices, and ventilation. OSHA exposure limits for propane are set at 1,000 ppm under *OSHA 29 CFR 1910.1000*, with additional recommendations from NIOSH and ACGIH to prevent asphyxiation risks. Fire safety regulations fall under *NFPA 58 (Liquefied Petroleum Gas Code)* and *NFPA 30*, which establish guidelines for propane storage, transfer, and fire prevention.

The EPA regulates propane under the *TSCA 40 CFR Part 702, 711, 720, and 721*, requiring manufacturers and importers to report production and distribution data. If stored above 10,000 lbs, facilities must comply with the *EPA* Risk Management Program *40 CFR Part 68*, ensuring accidental release prevention and emergency planning. Under the Emergency Planning and Community Right-to-Know Act *40 CFR Part 355*, propane is classified as an Extremely Hazardous Substance when stored in large quantities, requiring Tier II chemical inventory reporting for emergency response coordination. These two regulations will not apply to our design since propane will not be stored on-site and the total amount in the process is below these limits.

The *CAA 42 U.S.C. 7401 et seq*. regulates propane as a VOC and defines emission control measures. The propane in this system is completely recycled, so this does not apply to our design. Water contamination risks are addressed under *CWA Sections 303, 307, and 402*, ensuring compliance with *NPDES* standards if propane leaks into water bodies.

Transportation is regulated under DOT Hazardous Materials Regulations *49 CFR Part 172*, requiring placarding, proper shipping classifications, and handling standards to mitigate transportation hazards.

Lastly, for confined space entry where propane may accumulate, OSHA mandates compliance with *29 CFR 1910.146*, ensuring proper ventilation and worker protection. If

inspection of the D-1 distillation column or flash evaporator F-1, which handle propane, must occur, these regulations must be followed.

8.5   Relevant PPE for Chemicals in Operation

The required PPE within the plant is flame-resistant clothing, eye protection, and gloves when working with machinery or transporting chemicals. Most of the process is continuous, so the direct handling of chemicals is often not required. However, due to the potential toxicity of the chemicals, adequate PPE considerations are listed by chemical if contact is necessary.

The biodiesel product is relatively non-volatile but can cause skin and respiratory irritation upon prolonged exposure. To mitigate these risks, workers should wear nitrile rubber gloves over latex gloves to ensure chemical resistance and prevent skin absorption. A NIOSH-approved half-face respirator with a dust/mist filter is recommended to protect against inhalation of mist or fine droplets.

Methanol is a highly volatile, flammable, and toxic solvent widely used in industrial processes. It can be absorbed through the skin and inhaled, leading to severe health effects such as central nervous system depression and metabolic acidosis. Due to its ability to permeate many glove materials, butyl rubber gloves are recommended for optimal protection against skin exposure.

Propane, typically encountered as a gas, presents risks primarily related to flammability and asphyxiation. However, in liquid form, it can cause severe cold burns upon contact. When handling liquid propane, workers should use splash-resistant goggles to prevent eye exposure, as well as thermal insulating gloves to protect against frostbite. In high-temperature environments, a face shield may be necessary for added protection. Additionally, a NIOSH-approved respirator is required in cases where propane may displace oxygen or reach hazardous concentrations.

Oleic acid, representing the WCO utilized in this process, is a naturally occurring fatty acid with low toxicity. However, it can cause irritation if inhaled in high concentrations or in mist form. Although respiratory protection is not typically required, it should be used when working in environments where aerosolized oleic acid is present, which would be the case during a release scenario as the WCO is in a vapor phase when entering the PFR. Impermeable gloves are necessary to prevent skin contact, and safety goggles with side shields provide eye protection against splashes.

Glycerol, a viscous and hygroscopic compound, is widely used in food, pharmaceuticals, and industrial applications. Although generally regarded as low in toxicity, exposure to its vapors or aerosols can cause respiratory discomfort. If vapors or aerosols are generated, respiratory protection meeting DIN EN 143 or DIN 14387 standards with an A(P2) filter is recommended. Nitrile rubber gloves should always be worn to prevent direct skin contact, and NIOSH-approved safety glasses are required to protect the eyes from accidental exposure.

8.6   Waste Disposal

 8.6.1   Methanol

In our process, methanol is released in both vapor and liquid waste streams. 2.3 t/yr of methanol exists in the absorber column as a vapor. This quantity is below the 2.7 t/yr limit for VOC emissions defined in Section 8.4.1. There are two liquid methanol-containing waste streams: the absorber bottoms stream and the distillate from the glycerol distillation column. The combined liquid waste has a methanol concentration of 42.4 kg/m^3, with a total methanol output of 53.1 t/yr.

Local regulations limit the discharge of waste streams with BOD concentrations greater than 250 mg/L (*Borough of Ephrata, PA*, n.d.). The concentration of the BOD in our plant's wastewater stream is significantly larger than this limit. Therefore, internal wastewater treatment is required. Biological oxidation will be used to lower the BOD concentration to permissible limits before discharge through the sewer to a Publicly Owned Treatment Works for final treatment. While the design of a wastewater treatment system is out of the scope of this project, an estimate for wastewater treatment costs has been determined. Specific details on treatment costs are outlined in Section 7.4.1.

 8.6.2   Other contaminants

While the major contaminant of our plant's wastewater is methanol, traces of other contaminants are present. Local regulations limit the amount of oil sent to Publicly Owned Treatment Works to 100 mg/L (*Borough of Ephrata, PA*, n.d.). The combined oil concentration of the wastewater is 5.7 mg/L, well below the allowable value. Therefore, no additional treatment is required to remove the oil contents. The outlet glycerol concentration is negligible. Furthermore, any remaining glycerol is biologically oxidized with the methanol in the required wastewater pretreatment.

8.7   Environmental Considerations and Impact

The construction and operation of the WCO plant also have an impact on the environment and local ecosystems. The plant is located in a primarily rural area of Lancaster, Pennsylvania. However, there are some nearby residential areas and businesses. The plant is also in the Susquehanna River Watershed and may have an impact on the quality of waterways and groundwater.

In case of an accidental release of hazardous chemicals, as discussed in Section 8.2, damage to the environment may occur due to the toxicity and other health hazards presented by the chemicals used in our process. Specifically, methanol is toxic to both aquatic and land organisms and can cause a low growth rate in plants. It does not bind well to soil, allowing it to enter the groundwater (*Methanol - DCCEEW*, n.d.). Implementing proper containment systems, spill prevention plans, and emergency response protocols are essential in mitigating these risks.

Specific methods for preventing the release of methanol for the MCE are discussed in Sections 8.3.2 and 8.3.4.

Furthermore, water usage and waste disposal are other key environmental considerations for the plant. Waste streams will be disposed of according to all relevant local and federal waste disposal laws, which are described in Sections 8.4. The methanol absorber column minimizes the amount of methanol that enters the environment as a vapor to levels below the allowable limit. The methanol-contaminated wastewater generated by the plant will be biologically treated, as described in Section 8.6, before being sent to a public sewer, thus further reducing the risk of groundwater contamination.

Outside of an accidental chemical release, the daily operation of the WCO plant is not expected to have a significant impact on the environment. The use of WCO as a biofuel feedstock promotes sustainable waste management. Traditional biofuels rely on crops such as corn or soybeans for feedstocks, whose cultivation can lead to deforestation, soil depletion, excessive water consumption, and competition with food sources. These problems are minimized by using a second-generation feedstock, WCO. The purification and sale of the glycerol byproduct minimizes waste and creates an additional revenue stream, which enhances the plant's sustainability.

Biodiesel is inherently cleaner than conventional diesel fuel because it recycles carbon that is already in the environment instead of releasing underground carbon stores. Thus, the plant helps reduce fossil fuel dependence, which boosts regional energy security and supports the transition to renewable energy. Biodiesel also burns cleaner than petroleum-based diesel, producing lower levels of carbon dioxide, sulfur dioxide (SO_2), and particulate matter. Therefore, biodiesel use will reduce the GHG emissions of the transportation industry and may contribute to improved air quality in Lancaster.

However, product transportation and the energy consumption of the plant, including electricity and steam use, may offset some of the environmental benefits. To mitigate this, the use of renewable energy sources such as solar or wind should be evaluated. Finally, the physical footprint of the plant raises environmental concerns. Constructing a new industrial facility may require clearing land, which could disrupt local ecosystems and displace wildlife. Careful site selection and environmental impact assessments would be necessary to minimize habitat destruction.

8.8   Social Impact

There are several social impacts associated with the establishment of the proposed biodiesel plant in Lancaster, Pennsylvania. One benefit is the creation of jobs related to plant construction, production, transportation, and plant maintenance. These jobs are expected to provide stable incomes for local workers, improve financial security for families, and may reduce unemployment in the area. This would also help stimulate Lancaster's local economy, as

employees would spend their earnings at local businesses, supporting restaurants, shops, and other services. Additionally, while the plant intends to source waste cooking oil from local potato chip factories, this can be expanded to include other nearby restaurants and food service providers. This would provide them with an additional revenue stream by selling their waste cooking oil. This type of collaboration strengthens the economic foundation of the region and encourages sustainable business practices.

Although there are many economic benefits, there are potential challenges that need consideration. Industrial operations come with inherent risks, and workplace safety is a major concern. In the event of an accident or injury at the plant, employees and their families would be directly impacted, both financially and emotionally. Furthermore, the proposed plant handles highly toxic and flammable chemicals, which, in the event of the release scenarios described in Section 8.2 may harm the local community. Therefore, ensuring strict safety protocols and emergency response plans would be crucial to protecting workers and minimizing disruptions to their livelihoods.

Another potential issue is the plant's impact on the surrounding community's quality of life. Industrial facilities often generate noise from machinery, truck traffic, and daily operations, which could be disruptive to nearby residents. Increased transportation of waste oil into the plant and biodiesel out of it may also lead to congestion on local roads, affecting daily commutes and businesses in the area. Furthermore, community members may raise concerns about having an industrial facility in their neighborhood, as they may fear negative changes to the character of their town. However, we do not anticipate large concerns due to the concentration of existing manufacturing within the region. Addressing these concerns through community engagement and transparent communication would be essential to gaining public support.

9 Final Recommended Design

The following section outlines the final design recommendations including stream compositions, equipment specifications, and process conditions. All stream numbers and equipment labels are depicted in the PFD (Figure 6.3.ii).

9.1 Storage and Feed Transport

9.1.1 Feedstock Storage

The WCO and methanol feeds will be supplied from two pre-process storage tanks that both hold four weeks' worth of feed. The WCO storage tank T-1 is a cone roof tank constructed using carbon steel. It is designed to hold 900 m^3 of WCO. The methanol storage tank, T-2, is a floating-roof carbon steel tank. It is designed to hold 125 m^3.

Propane is not stored on-site due to the achieved 99.9% propane recycle rate. The required propane will be added during process start-up, and levels will be checked during maintenance cycles. During shut down, the methanol-propane mixture currently in the process equipment will be stored in Tank T-5, a 30 m^3 cone roof carbon steel tank.

9.1.2 Product Storage

The biodiesel and pharmaceutical-grade glycerol product (streams 29 and 33 respectively) will be sent to two post-process storage tanks that each hold four weeks' worth of product. The biodiesel storage tank, T-3, is a floating-roof carbon steel tank designed to hold 900 m^3 of product. The glycerol storage tank, T-4, is a cone roof tank constructed of 304 stainless steel, designed to hold 60 m^3 of product. The biodiesel product stream (stream 29) is sent towards its respective storage tank through pump P-9, which operates at 2.5 bar, while the glycerol product stream (stream 33) is sent towards its respective storage tank through pump P-10, which also operates at 2.5 bar. Both product streams are cooled to 25°C before storage.

9.1.3 Feed Transport

The WCO feed (stream 1) will be moved from storage container T-1 using pump P-1 and combined with the methanol feed, which is pumped (stream 3) from storage T-2 by pump P-2. Both pumps operate at 2.02 bar. The combined stream 5 enters pump P-3, which increases the pressure to 7 bar and raises the stream temperature to 29.4°C to promote mixing with the recycle stream. The flow rates of these streams are shown in Table 9.1.i.

Table 9.1.i Storage Block and Transport Stream Flow Rates

	1&2	3&4	5	6
Temperature (°C)	25.0	25.0	27.7	29.8
Pressure (bar a)	1	1	1	7
Flow Rate (kg/hr)				
Water	48.1	0.0	48.1	48.1
Propane	0.0	0.0	0.0	0.0
Methanol	0.0	132.8	132.8	132.8
Triolein	1,034.4	0.0	1,034.4	1,034.4
FFA	120.3	0.0	120.3	120.3
FAME	0.0	0.0	0.0	0.0
Glycerol	0.0	0.0	0.0	0.0
Total	**1,202.8**	**132.8**	**1,335.6**	**1,335.6**

9.2 Reactor

Stream 6 exits P-3 and is combined with the methanol and propane recycle stream (stream 15) before entering pump P-4. P-4 raises the process fluid to the supercritical pressure (129 bar) required for the reaction. Stream 8 exits P-4, enters heat exchanger HX-1 at 103.9°C and leaves at 280°C. The reactor product stream (stream 10) is used as the heating fluid in HX-1 to reduce utility costs for the plant. The reactor feed is now under supercritical conditions and is prepared to enter reactor R-1.

Stream 9 enters R-1 where the transesterification, hydrolysis, and esterification reactions take place. R-1 is an adiabatic PFR that operates at 280°C and 128 bar. The reactor contains four, 17 m long tubes with an internal diameter of 0.50 m resulting in a total reactor volume of 13.4 m³. The residence time within the reactor is 79 minutes. The reactor achieves a WCO conversion of over 99%. The reactor products enter HX-1 at 284°C and exit at 162°C. This stream then passes through heat exchanger HX-2 which cools stream 12 to 120°C before entering flash evaporator F-1 to begin separations. The stream flowrates for the reactor block are found in Table 9.2.i.

Table 9.2.i Reactor Block Stream Flowrates

Flow Rate (kg/hr)	6	7	8	9	10	11	12
Temperature (°C)	29.8	78.0	103.9	280.0	283.7	161.7	120.0
Pressure (bar a)	7	6	129	128	128	128	128
Flow Rate (kg/hr)							
Water	48.1	55.6	55.6	55.6	55.6	63.0	63.0
Propane	0.0	72.0	72.0	72.0	72.0	72.0	72.0
Methanol	132.8	1,045.6	1,045.6	1,045.6	1,045.6	920.2	920.2
Triolein	1,034.4	1,034.4	1,034.4	1,034.4	1,034.4	0.1	0.1
FFA	120.3	120.3	120.3	120.3	120.3	4.4	4.4
FAME	0.0	0.05	0.05	0.05	0.05	1,160.7	1,160.7
Glycerol	0.0	0.0	0.0	0.0	0.0	107.6	107.6
Total	**1,335.6**	**2,328.0**	**2,328.0**	**2,328.0**	**2,328.0**	**2,328.0**	**2,328.0**

9.3   Separations

9.3.1   Methanol and Propane Recovery

The cooled reactor products (stream 12) enter flash evaporator F-1, where it is adiabatically expanded from 128 bar to 6 bar to recover methanol and propane. The carbon steel flash evaporator has a total height of 2.0 m, a diameter of 1.0 m, and operates at 120°C. The feed location is halfway up the vessel. The full vessel dimensions are depicted in Figure 6.5.i. The overhead vapor product (stream 13), containing primarily methanol and propane, is mixed with the liquid methanol and propane recovered from distillation column D-1 (stream 17). The mixed liquid recycle stream (stream 15) is sent back to the beginning of the process and mixed with the methanol and propane feeds (stream 6). The bottoms product of flash F-1 (stream 14) is sent to distillation column D-1 to recover the remaining methanol and propane.

Stream 14 enters column D-1 at 114°C and 6 bar at a height of 5.7 m. The column has 13 total theoretical stages and a diameter of 0.5 m. Due to the presence of two liquid phases, the column is packed with 1.5" stainless steel 304 Pall rings. There is 4.73 m of packing below the feed and 2.7 m of packing above the feed. To allow for a 20-minute liquid hold-up time, 0.75 m of space is allowed below the packing. Additionally, there is 0.5 m of space between the packed sections and above the packing. This results in a total column height of 9.2 m. The column dimensions are depicted in Figure 6.5.ii.

The column uses a reflux ratio of 1.49 and a distillate-to-feed ratio of 0.734. The pressure at the top stage is 1.01 bar, and the condenser temperature is 25°C. The distillate (stream 16) contains primarily recovered methanol and exits the condenser at 25.2°C. Reflux pump RP-1 returns some distillate to the column, while the remainder of the stream is sent to pump P-5. Pump P-5 increases the pressure of Stream 17 to 7 bar to prepare it for mixing with the reactor feed. Stream 17 mixes with the overhead product from F-1 (stream 13) and is recycled at the beginning of the process. Overall, the flash evaporator and distillation column recycles 99.2% of the unreacted methanol and 99.9% of the propane in the system.

The bottoms product of D-1 contains primarily biodiesel (FAMEs) and glycerol. The pressure at the bottom stage is 1.12 bar, and the reboiler temperature is 113°C. The bottoms product (stream 18) is sent to the decanter. The flow rates of streams in this section of the process are shown in Table 9.3.i.

Table 9.3.i Separations Stream Table

Stream	12	13	14	15	16 & 17	18
Temperature (°C)	120.0	114.1	114.1	94.7	25.2	110.7
Pressure (bar a)	128	6	6	6	7	1
Flow Rate (kg/hr)						
Methanol	920.2	181.2	739.0	912.8	731.6	7.4
Triolein	0.1	0.0	0.1	0.0	0.0	0.1
FFA	4.4	0.0	4.4	0.0	0.0	4.4
FAME	1,160.7	0.1	1,160.7	0.1	0.0	1,160.7
Glycerol	107.6	0.0	107.6	0.0	0.0	107.6
Total	**2,193.0**	**181.3**	**2011.8**	**912.8**	**731.6**	**1,280.2**

9.3.2 Biodiesel Recovery

Stream 18, the bottoms product of the methanol-water distillation column (D-1), passes through P-6 at 2.5 bar before entering HX-5 to cool the stream to 35°C. Then, the fluid enters the decanter, S-1. The carbon steel decanter is maintained at atmospheric pressure and 35°C. The two-phase liquid stream (stream 20) entering the decanter is fed halfway up the vessel at a height of 0.7 m. The feed is fed through a 2.4 cm diameter pipe. The internal diameter of the decanter is 0.7 m. The continuous biodiesel phase interacts with the dispersed glycerol phase in the dispersion band for 2.07 min. The biodiesel take-off pipe is located at 1.2 m. The glycerol pipe is located at the bottom of the vessel, and the take-off pipe is at a height of 1.1 m. These vessel dimensions are depicted in Figure 6.5.iv.

The biodiesel take-off stream (stream 21) is sent to flash evaporator F-2 by pump P-7 at 2.02 bar. This stream is fed into the 1.2 m tall carbon steel vessel at a height of 0.62 m. Air, which is compressed to 1.5 bar and 73.7°C in P-8, is bubbled through a sparger at a height of 0.15 m above the base of the tank (stream 25). The vessel is 1 m in diameter and has a liquid hold-up time of 5 min. The flash evaporator operates at 35°C and atmospheric pressure. The biodiesel product exits at the bottom of the vessel (stream 27). It is pumped through P-9 at 2.5 bar, then cooled to 25°C in HX-6 using cooling water, and sent to the biodiesel storage tank T-3. The flow rates for streams in the biodiesel separation block are given in Table 9.3.ii.

The vapor stream leaves the top of the flash drum (stream 26) at 37.9°C and atmospheric pressure. The stream is compressed to 1.5 bar in P-12 before entering the bottom of absorber A-1, which operates at 27 °C. The pressure is 1.01 bar at the top stage and 1.02 bar at the bottom stage. Process water at 20 °C (stream 34) is pumped via pump P-11 at 2.02 bar into the top of the absorber column. The column is packed with 16 mm metal Pall rings and has a packed height of

2.0 m. The column diameter is 0.25 m, and there is 0.25 m of space above and below the packing. The column dimensions are shown in Figure 6.6.i. Stream 37, leaving the top of A-1, is vented to the atmosphere. Wastewater stream 38, leaving the bottom of A-1, is sent to an on-site wastewater treatment plant for disposal. Absorber block flow rates are shown in Table 9.3.iii.

Table 9.3.ii Biodiesel Recovery Stream Table

	18, 19 & 20	21 & 23	22	24 & 25	26 & 36	27, 28 & 29
Temperature (°C)	110.7	35.0	35.0	73.7	88.5	25.0
Pressure (bar a)	1	1	1	1.5	1	1
Flow Rate (kg/hr)						
Water	55.5	1.7	53.8	4.0	5.0	0.7
Propane	0.0	0.0	0.0	0.0	0.0	0.0
Methanol	7.4	1.9	5.5	0.0	1.5	0.4
Triolein	0.1	0.1	0.0	0.0	0.0	0.1
FFA	4.4	4.4	0.0	0.0	0.0	4.4
FAME	1,160.7	1,160.7	0.1	0.0	0.0	1,160.6
Glycerol	107.6	0.4	107.2	0.0	0.0	0.4
Air	0.0	0.0	0.0	281.2	280.9	0.3
Total	**1,335.7**	**1,169.2**	**166.6**	**285.2**	**287.4**	**1,166.9**

Table 9.3.iii Absorber Block Flow Rates

	26 & 36	34 & 35	37	38
Temperature (°C)	88.5	20.0	33.7	36.9
Pressure (bar a)	1	1	1	1
Flow Rate (kg/hr)				
Water	5.0	99.1	9.6	94.5
Propane	0.0	0.0	0.0	0.0
Methanol	1.5	0.0	0.3	1.3
Triolein	0.0	0.0	0.0	0.0
FFA	0.0	0.0	0.0	0.0
FAME	0.0	0.0	0.0	0.0
Glycerol	0.0	0.0	0.0	0.0
Air	280.9	0.0	280.5	0.3
Total	**287.4**	**99.1**	**290.4**	**96.1**

9.3.3 Glycerol Purification

The bottoms product of the decanter (stream 22) is fed to vacuum distillation column, D-2, at 35°C and atmospheric pressure. The column is constructed of 304 stainless steel and has 12 theoretical stages, with the feed entering above stage 8. The distillation occurs in a vacuum due to glycerol's high boiling point at atmospheric pressure. A two-stage steam jet ejector is used to pull a vacuum on the column. To minimize pressure drop, the column is packed with Koch Flexipac HC 1Y structured packing. The packed height below the feed is 0.84 m, and the packed height above the feed is 1.27 m. 0.5 m of space below the packing, at the feed location, and above the packing was allowed, resulting in a total column height of 3.75 m. These dimensions are depicted in Figure 6.5.v.

A reflux ratio of 3 and a bottoms-to-feed ratio of 0.272 achieved a glycerol product purity of 99.75%. The pressure at the top stage is 0.02 bar, and the distillate exits the condenser at 12°C. The cooling fluid in this condenser is a 60% propylene glycol, 40% water mixture that will be cooled in a glycol chiller. The distillate (stream 30), containing water and methanol, is a waste stream and is disposed of in the on-site wastewater treatment plant.

The pressure at the bottom stage is 0.036 bar, and the bottoms product exits the reboiler at 165°C. The bottoms glycerol product (stream 31) is pumped at 2.5 bar via P-10 to heat exchanger HX-9. The heat exchanger cools the stream to 35 °C, which is then sent to storage tank T-4. The flow rates for streams in the glycerol separation block are shown in Table 9.3.iv.

Table 9.3.iv Glycerol Block Stream Flows

Stream	22	30	31, 32 & 33
Temperature (°C)	35.0	12.0	35.0
Pressure (bar a)	1	0.02	1
Flow Rate (kg/hr)			
Water	53.8	53.6	0.2
Propane	0.0	0.0	0.0
Methanol	5.5	5.5	0.0
Triolein	0.0	0.0	0.0
FFA	0.0	0.0	0.0
FAME	0.1	0.0	0.1
Glycerol	107.2	0.0	107.2
Total	**166.6**	**59.1**	**107.5**

9.3.4 Ancillary Equipment

The process outlined above requires nine heat exchangers, and twenty-six pumps (13 spare pumps). Table 9.3.v outlines the process temperatures, required process fluid flow rates, duties, and heat transfer areas for all the heat exchangers in the process. Table 9.3.vi included the

type, material, volumetric flow rate, and power requirement for the pumps. Specifications on the reflux pumps are included in Sections 6.5.3 (RP-1) and 6.5.4 (RP-2).

Table 9.3.v Heat Exchangers Summary

Heat Exchanger	HX-1	HX-2	HX-3	HX-4	HX-5	HX-6	HX-7	HX-8	HX-9
Fluid	Reactor Effluent	Cooling Water	Cooling Water	3 bar steam	Cooling water	Cooling Water	60% Propylene Glycol	15 bar steam	Cooling Water
Duty (kW)	341.0	80.4	615.4	542.5	63.0	8.0	155.5	160.7	9.6
Hot T in (˚C)	283.7	161.7	64.6	133.5	112.7	37.9	16.7	198.0	159.7
Hot T out (˚C)	161.7	120.0	25.2	133.5	35.0	25.0	12.0	198.0	35.0
Cold T in (˚C)	103.9	20.0	20.0	78.4	20.0	20.0	2.0	187.9	20.0
Cold T out (˚C)	280.0	40.0	40.0	110.7	40.0	35.0	6.0	187.9	40.0
Area (m^2)	57.6	1.5	98.6	32.9	6.9	83.6	51.7	79.6	9.2
Type	Double Pipe	Double Pipe	Floating Head Shell & Tube	U-tube	Double Pipe	Floating Head Shell & Tube	Floating Head Shell & Tube	U-tube	Double Pipe
Fluid flow rate (kg/hr)	-	1,152.7	26,500.0	903.6	45,192.3	7,684.1	267.6	297.3	6,656.8

Table 9.3.vi Pump Summary

Label	P-1	P-2	P-3	P-4	P-5	P-6	P-7	P-8	P-9	P-10	P-11	P-12
Pump/Compressor	P	P	P	P	P	P	P	C	P	P	P	C
Pressure (bar)	2.0	2.0	7.0	129.0	7.0	2.5	2.0	1.5	2.5	2.5	2.0	1.5
Total Power (kW)	0.11	0.01	1.72	52.9	0.53	0.10	0.06	3.95	0.09	0.02	0.06	4.16
Volumetric Flow Rate (m^3/hr)	2.6	0.2	3.1	4.4	1.0	1.6	1.5	191.6	1.4	0.1	1.4	256.7
Type	CF	CF	R	R	R	CF	CF	Blower	CF	CF	CF	Blower
Material	CS	CS	CS	CS	CS	CS	CS	CS	CS	304 SS	CS	CS

Pump (P), Compressor (C), CF (centrifugal), R (reciprocating), Carbon Steel (CS)

10 Plant Construction Timeline Scenario

For this proposed biodiesel plant, which will produce 9,206.1 tons/yr of biodiesel at full capacity, the construction timeline scenario is scheduled to last 18 to 19 months. This timeline spans from initial permitting and confirmation of project feasibility to initial production start-up and ramp-up to full capacity.

The project will commence with the feasibility, design, and permitting phase, which is projected to last around 3-4 months. During this phase, the full feasibility of the project will be evaluated through regulatory approval (Lawry et al., 2013). Documents such as construction blueprints will be mapped out, and any permitting for land, utility, and environmental release will be procured as well (Koeva, 2000). As this phase is carried out, the procurement and site preparation phase will begin in tandem, around the 2nd to 3rd month, and last around 2-3 months. This phase involves land clearing at the designated site, utility access preparation, and ordering of long-lead equipment such as reactors, distillation columns, and complex instrumentation systems.

Following the preliminary steps of preparing the land for construction, around months 4-5 in, then the civil works can begin on site. This phase involves laying foundations, erecting the structural steel, and constructing equipment pads, which will last approximately 4-5 months (Lawry et al., 2013). Once the civil works are nearing the end of construction, then the mechanical installation phase can begin. This is the bulk phase of construction for the process, as piping networks will be established and all process equipment placed and interconnected. This installation will proceed over 6-7 months and should commence by month 7. In tandem with the mechanical installation, the electrical and instrumentation installation will begin around month 8 and will span across the next 3 months. This phase involves all the wiring of electric equipment such as control panels, instrumentation for process automation, and emergency shutdown systems (Lawry et al., 2013). Control instrumentation such as flow meters, temperature probes, and level sensors are also installed during this phase.

Once these major construction phases are completed and the process equipment is ready to operate, then the pre-commissioning phase can begin. This phase is projected to begin around month 11-12 and will last 1-2 months. It includes testing the mechanical integrity of all process equipment, pressure testing of piping systems, flushing of lines, and dry runs of motors and pumps (Lawry et al., 2013). All the control systems and instrumentation are tested to ensure their functionality prior to the introduction of process fluids as well. Identifying and addressing any issues with equipment during this stage will minimize future operational disruptions during the start-up and ramp-up phases.

Once the pre-commissioning is completed around month 13, then the plant will start its initial operation in the start-up phase, which will last around a month. Feedstocks will be introduced to the system under controlled conditions, and conversion efficiency, separation performance, and product quality will all be tested (Lawry et al., 2013). Adjustments to process

parameters will be made in real time to achieve target product qualities, and the plant's safety systems will also be validated during this phase. This period serves as training for plant personnel under real operational settings as well.

Following the start-up phase, the plant then enters the ramp-up phase around months 14-15, which will last until the plant operates at full capacity around 18-19 months. During the first few months, the plant will operate at half capacity until reliable performance is ensured and variability in process parameters is minimized (Lawry et al., 2013). The operating capacity is then slowly increased over the course of around 3 months to reach the plant's full operating capacity of 9,206.1 t/yr. This entire projected timeline is summarized in 10.i.
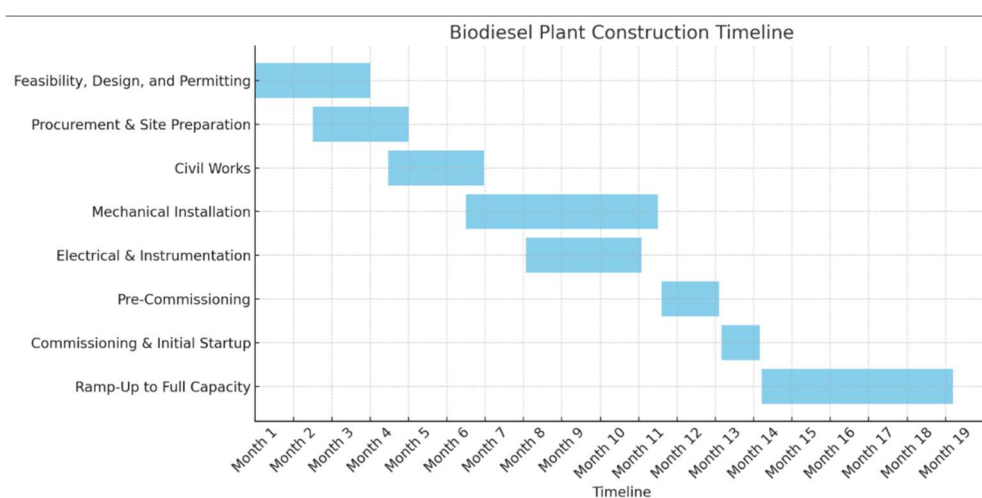
Figure 10.i Plant Construction Timeline

11 Recommendations and Conclusions

The production of supercritical biodiesel production is an emerging field; therefore, our team recognizes that several aspects of this design could be improved. In the following sections, our team will provide future work suggestions, design improvements, and a decision on whether this plant is viable for real-world construction and investment.

11.1 Future Research Suggestions

11.1.1 Increasing Plant Design Scale

Future work may consider increasing the production capacity of the plant. Previous research on supercritical methanol biodiesel production found that a larger plant, 128,000 t/yr, resulted in a comparatively lower payback period and breakeven selling price due to the impact of economies of scale (Nagapurkar & Smith, 2023). A larger product revenue compared to the required increase in capital cost investment may improve the economic viability of the design.

11.1.2 Kinetic Data & Reactor Design

The largest assumption made in the design of our plant is the use of kinetic data that uses weight percentage as each reaction compound unit. Although it is difficult to measure the density and concentration of compounds at supercritical conditions, weight percentage-based kinetic data may not accurately represent the reactions occurring in the PFR. Therefore, it is possible that the conversion presented here would not match results obtained from real-world implementation of this design. We recommend that future research focus on obtaining concentration-based kinetic data to model the supercritical reactor and verify the validity of our team's assumption.

Furthermore, when designing the PFR for our process, our team elected to use a single reactor with three competing reactions: hydrolysis, esterification, and transesterification (Section 6.4.1). This posed a challenge in finding kinetic data where each reaction was modeled separately or where all three reactions were modeled together. Most of the kinetic data available was either hydrolysis and esterification modeled in one reactor, hydrolysis and esterification modeled in a series of two reactors, or transesterification modeled separately (Kusdiana & Saka, 2004; Peters et al., 2022). While the kinetic data our team chose modeled all three reactions in a single reactor, concerns over concentration units affect the legitimacy of our results (Okoro et al., 2018). Therefore, we recommend that future groups consider the use of two separate reactors and forgo the transesterification reaction to improve access to kinetic data.

11.2 Design Improvements

Due to time constraints, some aspects of the design may have benefited from additional optimization. These areas are discussed in the following sections.

11.2.1 Increase Methanol Recycling

For the methanol/water distillation column (D-1), as previously described in Section 6.5.2, a 99.2% recovery of unreacted methanol was obtained. Our team focused on optimizing

the reflux ratio and distillate-to-feed ratio. However, additional optimization around the feed temperature and feed tray, as well as column pressure, may increase methanol recovery. Furthermore, designing a distillation column to replace the first flash drum may also increase recovery. Increased methanol recovery would not only reduce feedstock costs but also lower the quantity of methanol in the waste streams, which would reduce the wastewater treatment cost, and potentially, remove the need for the methanol absorber. The current plant design sends approximately $22,000/yr of methanol into the wastewater stream. Furthermore, the capital cost of the absorber is $32,652. When prorated to the total capital investment, the absorber column amounts to nearly $200,000 in capital. Therefore, due to the high capital and raw material costs associated with the current design, future work should consider the optimization of methanol recycling.

11.2.2 WCO Filtering On-Site

The WCO feed used in our process is purchased pre-filtered, which increases the raw material cost. Future work should consider designing a WCO filtration system on-site to reduce the purchasing price of WCO, thus lowering raw material costs. Because waste cooking oil is the most expensive recurring cost in our process, $4,184,154/yr, reducing the overall cost would significantly increase the plant's IRR.

11.2.3 Biodiesel Washing

An additional area of improvement would be replacing the biodiesel flash evaporator (F-2) with a washing and drying system. The current flash evaporator requires the addition of a methanol-absorbing column to strip methanol from the vapor stream, leaving the flash evaporator into a wastewater stream for processing. However, due to the high miscibility of water and methanol, a washing step would directly transfer the methanol into a wastewater stream, removing the need for an absorption column. The specific parameters that need to be explored are the temperature and flow rate of the water in the washing step and the temperature and flow rate of air into the dryer to ensure the biodiesel product meets ASTM standards. The potential benefits of the washing step should be weighed based on the equipment costs, operating costs, operating efficiency, and potential environmental and safety benefits of directly transferring the methanol to a wastewater stream.

11.3 Final Recommendation

Our team conditionally supports the design of the proposed biodiesel plant. The proposed plant has an IRR of 13.7%, which presents an economically desirable opportunity for investors interested in experimental technologies. However, due to the experimental nature of the design, we propose a pilot-scale reactor be constructed first to obtain real-world kinetic data. This pilot plant would verify the proposed kinetics, product yield, and product quality prior to the decision on a full-scale plant based on the updated economic value. While an IRR of 13.7% presents a desirable investment opportunity, this value was determined by assuming the continuation of current government policies that provide tax credits for producing biodiesel. Therefore, the

economic viability of this is subject to changes depending on US government policy initiatives. Without a tax credit, the IRR falls to 5.2%. In this case, our team would not recommend the construction of a full-scale or pilot plant because this value does not portray an economically attractive opportunity to invest in, especially when uncertainty lies with the true yield and product quality.

12 Acknowledgements

First, we would like to extend our thanks to Professor Eric Anderson for his continuous guidance these past two semesters on this capstone project. The direction and assistance that Professor Eric Anderson provided were instrumental to this project's completion. Additionally, we would like to thank Professor Ron Unnerstall for his guidance on process safety and the release scenario modeling for this project.

Finally, we would like to thank all professors within the University of Virginia Department of Chemical Engineering for their teaching and guidance over the last four years. This capstone project would not be possible without their dedication to education and support.

13 Appendix

13.1 Design Basis Calculation: Waste Cooking Oil Feedstock Quantity

<u>Per 4,000 kg/hr potatoes:</u> ("The Ultimate Guide to Fry Potato Chips," 2020)
Potato Chip Factory Oil Input: 412.5 L/hr
Volume Oil in Chips: 35%
Potato Chip Factory Oil Output: 412.5 * 0.65 = 268.13 L/hr or 6,435 L/day
* Assume oil is added to account for evaporation and filtration losses *

<u>Lays Factory San Antonio, TX (21,500 lbs potatoes/hr)</u>: (*Open Sourcemap - Development Environment*, n.d.)
Weight Conversion: 21,500 lbs * 0.453592 kg/lb = 9750 kg potatoes/hr
Oil Output: 6,435 L/day * (9750/4000) = 15,700 L/day

Density of B100 biodiesel: 0.9164 g/cm^3 at 0.1MPa and 293.15 K (NguyenThi et al., 2018)
Density of WCO: 0.92 g/mL (Salihu et al., 2021)
<u>Yearly Output (1 factory):</u> 15,700 L/day * 0.92 g/mL * 1000 mL/L * 1 tonne/1*10^6 g *365 = 5272 t/yr

13.2 USP Grade Glycerol Specifications

Specification	USP Grade Glycerin
Glycerin Content	99.7%
Ash	N/A
Water	0.3% Max
Chlorides	10 ppm Max
Color	10 Max. (APHA)
Specific Gravity	1.2612 Min
Sulfate	20 ppm Max
Assay	99.0 - 101.0% (on dry basis)
Heavy Metals	5 ppm Max
Chlorinated Compounds	30 ppm Max
Residue on Ignition	100 ppm Max
Fatty Acid & Ester	1.000 Max
pH (10% solution)	N/A
DEG and Related Compounds	Pass
Organic Volatile Impurities	Pass
Organic Residue	N/A

Copied from SRS International, n.d.

13.3 ASTM D6751-24 Biodiesel Purity Standard

Property	ASTM Method	Limits	Units
Calcium & Magnesium, combined	EN 14538	5 maximum	Ppm (ug/g)
Flash Point (closed cup)	D 93	93 minimum	°C

Alcohol Control (Must meet one)
  1. Methanol Content
  2. Flash Point
	1. EN 14110
	2. D 93
		1. 0.2 maximum
		2. 30 maximum
			1. % volume
			2. °C

Water & Sediment	D 2709	0.05 maximum	% vol
Kinematic Viscosity, 40 C	D 445	1.9 - 6.0	mm^2/sec
Sulfated Ash	D874	0.02 maximum	% mass
Sulfur S 15 Grade S 500 Grade	D 5453 D 5453	0.0015 max. (15) 0.05 max. (500)	% mass (ppm) % mass (ppm)
Copper Strip Corrosion	D 130	No. 3 maximum	
Cetane	D 613	47 minimum	
Cloud Point	D 2500	report	°C
Carbon Residue, 100% sample	D 4530*	0.05 maximum	% mass
Acid Number	D 664	0.5 maximum	mg KOH/g
Free Glycerin	D 6584	0.020 maximum	% mass
Total Glycerin	D 6584	0.240 maximum	% mass
Phosphorus Content	D 4951	0.001 maximum	% mass
Distillation, T90 AET	D 1160	360 maximum	°C
Sodium/Potassium, combined	EN 14538	5 maximum	ppm
Oxidation Stability	EN 14112	3 minimum	hours
Cold Soak Filtration For use in temperatures below -12 C	Annex to D 6751 Annex to D 6751	360 maximum 200 maximum	Seconds Seconds

(U.S. Department of Energy, n.d.)

13.4 Flash Evaporator Dimension Calculations

The maximum design vapor velocity was calculated using the Souders-Brown equation. Density and volumetric flow data were taken from ASPEN Plus.

$$u_v = 0.035\sqrt{\frac{722.609 - 6.181}{6.181}} = 0.377 \text{ m/s}$$

The vapor volumetric flow rate was determined by dividing the mass flow rate of the vapor stream by its density.

$$\text{Vapor volumetric flow rate} = \frac{198.888\frac{kg}{h}}{6.18063\frac{kg}{m^3} \cdot 3600\ s} = 0.0089 \text{ m}^3\text{/s}$$

The minimum tank area was determined by dividing the vapor volumetric flow rate by the maximum vapor velocity. This area was used to find the minimum tank diameter.

$$\text{Minimum vessel area} = \frac{0.0089\frac{m^3}{s}}{0.377\frac{m}{s}} = 0.0237 \text{ m}^2$$

$$\text{Minimum diameter} = \sqrt{\frac{4 \cdot 0.0237}{\pi}} = 0.174 \text{ m}$$

To maintain a 2:1 height to diameter ratio, a diameter and disengagement space of 1.4 m was selected. The liquid flow rate was calculated by dividing the mass flow rate of the liquid stream by its density. The liquid volume was calculated by multiplying the flow rate by the 30-minute liquid hold up time. Dividing this by the selected tank area resulted in a liquid level of 0.95 m.

$$\text{Liquid volumetric flow rate} = \frac{2121.5\frac{kg}{h}}{722.609\frac{kg}{m^3} \cdot 3600\ s} = 8.005*10^{-4} \text{ m}^3\text{/s}$$

Volume for 30-minute liquid hold up time: $8.005*10^{-4}$ m^3/s * 1800 s = 1.47 m^3

Liquid Depth: $\frac{1.47\ m^3}{\pi \cdot 0.5^2} = 0.95$ m

13.5 Recycle Stream and Biodiesel Distillation Column Design

Condenser:

$$\Delta T_{lm} = \frac{(T_1 - t_2) - (T_2 - t_1)}{\ln\left[\frac{T_1 - t_2}{T_2 - t_1}\right]} * Ft = \frac{(64.576 - 40) - (25.204 - 20)}{\ln\left[\frac{64.576 - 40}{25.204 - 20}\right]} = 12.47\ °C$$

The area of heat transfer was calculated to be 98.6 m^2 using the condenser heat duty of 615.388 kW and a U overall heat coefficient of 500 W/ m^2°C determined because of the hot and cold fluids in the heat exchange. The work for this equation is seen below.

$$Q = UA\Delta T_{lm}$$

$$A = \frac{Q}{U\Delta T_{lm}} = \frac{615.388*1000\ W/kW}{500\cdot12.47} = 98.6\ m^2$$

Heat capacity for water of 4.18 kJ/kg°C was used to determine the cooling water flow rate

$$Q = mc\Delta T$$

$$m = \frac{Q}{c\Delta T} = \frac{615.388}{4.18*(40-20)} * 3600 = 26{,}500\ kg/hr$$

Reboiler:

The LMTD for the kettle reboiler was calculated to be 36.24 °C. A slight difference in this situation compared to the calculation utilized for the condenser, is that the hot fluid is saturated steam at 3 bar that delivers energy for the heat transfer via heat of vaporization. Thus, the entry and exit temperatures were both noted to be 133.5 °C. The temperature of the cooler FAME and glycerol stream was 78.413 °C as it entered and 110.691 °C as it exited.

$$\Delta T_{lm} = \frac{(T_1 - t_2) - (T_2 - t_1)}{\ln\left[\frac{T_1 - t_2}{T_2 - t_1}\right]} = \frac{(133.5 - 110.691) - (133.5 - 78.413)}{\ln\left[\frac{(133.5 - 110.691)}{(133.5 - 78.413)}\right]} = 36.24\ °C$$

The area of heat transfer was calculated to be 33.27 m^2 using the condenser heat duty of 542.523 kW and a U overall heat coefficient of 450 W/ m^2°C determined because of the hot and cold fluids in the heat exchange. The work for this equation is seen below.

$$Q = UA\Delta T_{lm}$$

$$A = \frac{Q}{U\Delta T_{lm}} = \frac{542.523*1000\ W/kW}{450\cdot36.24} = 33.27\ m^2$$

To determine the specific mass flow rate of the saturated steam necessary for the reboiler, a simple heat of vaporization was utilized, as seen below, to determine a mass flow rate of 0.251 kg/s given a heat of vaporization of 2162.1 kJ/kg or 903.6 kg/hr.

$$m = \frac{Q}{\Delta H^{fg}} = \frac{542.523 \; kW}{2162.1 \; kJ/kg} = 0.251 \frac{kg}{s} = 903.6 \; kg/hr$$

13.6 Methanol/Water Distillation Column Liquid Depth Calculations

Liquid volumetric flow rate $= \dfrac{1335.65 \frac{kg}{h}}{760.417 \frac{kg}{m^3} \cdot 3600\ s} = 4.878 \times 10^{-4}$ m³/s

Volume for 20-minute liquid hold-up time: 4.878×10^{-4} m³/s * 1200 s = 0.5854 m³

Liquid Depth: $\dfrac{0.5854\ m^3}{\pi \cdot 0.5^2} = 0.745$ m

13.7 Methanol/Water Distillation Column Reflux Drum Calculations

Reflux drum volume for 30-minutes $= \dfrac{1.379 \frac{m^3}{h}}{2} = 0.6898\ m^3$

Reflux drum height & diameter based on 3:1 height-to-diameter ratio:

$h = 3d = 6r$

$V = \pi r^2 h = 6\pi r^3$

$r = \sqrt[3]{\dfrac{V}{6\pi}} = \sqrt[3]{\dfrac{0.6898\ m^3}{6\pi}} = 0.33$ m

$h = 6r = 6 \cdot 0.33\ m = 1.99$ m ~ 2 m

Reflux drum shell mass calculation:

$m = \rho \cdot \pi \cdot d \cdot h \cdot t = 7850\ \dfrac{kg}{m^3} \cdot \pi \cdot 0.66\ m \cdot 2\ m \cdot 0.015\ m = 491.25\ kg$

13.8 Decanter Dimensions Calculations

Density and viscosity data was taken from ASPEN Plus

Droplet Settling Velocity using Stokes Law:

$$u_d = \frac{d_d^2 * g * (\rho_d - \rho_c)}{18 \mu_c} = \frac{(150*10^{-6})^2 * 9.81 * (116.89 - 80.148)}{18(0.003972)} = 1.13 * 10^{-3}\ m/s$$

Continuous phase volumetric flow rate:

$$L_c = \frac{\dot{m}_c}{3600 \rho_c} = \frac{1169.11}{3600(805.148)} = 4.03 * 10^{-4}\ m^3/s$$

Area of interference:

$$A_i = \frac{L_c}{u_d} = \frac{4.03 * 10^{-4}}{1.13 * 10^{-3}} = 0.358\ m^2$$

Vessel diameter:

$$d_t = 2 * \sqrt{\frac{0.358}{\pi}} = 0.675 \ m \ \approx 0.7 \ m$$

Vessel height: 2:1 ratio of height to diameter

$$h_t = 2 * d_t = 1.351 \ m \approx 1.4 \ m$$

Dispersion band height: 10% of vessel height

$$h_d = 0.1 * h_t = 0.135 \ m$$

Dispersion band residence time:

$$\tau_d = \frac{h_d}{u_d} = \frac{0.135}{1.13*10^{-3}} = 119.94 \ s = 1.99 \ min$$

Entrainment velocity check:

$$u_c = \frac{\dot{m}_d}{3600*\rho_d*A_i} = \frac{166.548}{3600*1169.89*0.358} = 1.10 * 10^{-4} \ m/s$$

Droplet diameter check:

$$d_d = \sqrt{\frac{u_d 18 \mu_c}{g(\rho_d - \rho_c)}} = \sqrt{\frac{1.13*10^{-3}*18*0.00397}{9.81(1169.89-805.148)}} = 4.84 * 10^{-4} \ m$$

Feed flow rate:

$$L_f = \left(\frac{\dot{m}_c}{\rho_c} + \frac{\dot{m}_d}{\rho_d}\right)\frac{1}{3600} = \left(\frac{1169.11}{805.148} + \frac{166.548}{1169.89}\right)\frac{1}{3600} = 4.43 * 10^{-4} \ m^3/_s$$

Feed pipe diameter:

$$d_f = \sqrt{\frac{4\left(\frac{L_f}{v_f}\right)}{\pi}} = \sqrt{\frac{4\left(\frac{4.43*10^{-4}}{1}\right)}{\pi}} = 2.375 \ cm$$

Biodiesel take-off height:

$$z_1 = 0.9 h_t = 0.9 * 1.4 = 1.2 \ m$$

Interface height:

$$z_3 = 0.5 h_t = 0.5 * 1.4 = 0.7 \ m$$

Glycerol take-off height:

$$z_2 = \frac{(z_1 - z_3)\rho_c}{\rho_d} + z_3 = \frac{(1.2-0.7)*805.148}{1169.89} + 0.7 = 1.1 \ m$$

13.9 Biodiesel Flash Drum Dimensions Calculations

The maximum design vapor velocity was calculated using the Souders-Brown equation.

Density was taken from ASPEN Plus

$$u_v = 0.05 \sqrt{\frac{807.025 - 1.15}{1.15}} = 1.324 \text{ m/s}$$

The vapor volumetric flow rate was determined by dividing the mass flow rate of the vapor stream by its density.

$$\text{Vapor volumetric flow rate} = \frac{1028.88 \frac{kg}{h}}{1.15 \frac{kg}{m^3} \cdot 3600 \, s} = 0.249 \text{ m}^3/\text{s}$$

The minimum tank area was determined by dividing the vapor volumetric flow rate by the maximum vapor velocity. This area was used to find the minimum tank diameter.

$$\text{Minimum vessel area} = \frac{0.249 \frac{m^3}{s}}{1.324 \frac{m}{s}} = 0.188 \text{ m}^2$$

$$\text{Minimum diameter} = \sqrt{\frac{4 \cdot 0.188}{\pi}} = 0.489 \text{ m}$$

To maintain a 2:1 height to diameter ratio, a diameter and disengagement space of 1 m was selected. The liquid flow rate was calculated by dividing the mass flow rate of the liquid stream by its density. The liquid volume was calculated by multiplying the flow rate by the 5-minute liquid hold up time. Dividing this by the selected tank area resulted in a liquid level of 0.153 m.

$$\text{Liquid volumetric flow rate} = \frac{1166.92 \frac{kg}{h}}{807.025 \frac{kg}{m^3} \cdot 3600 \, s} = 4.017 * 10^{-4} \text{ m}^3/\text{s}$$

Volume for 5-minute liquid hold up time: $4.017 * 10^{-4}$ m^3/s * 300 s = 0.121 m^3

Liquid Depth: $\frac{0.121 \, m^3}{\pi \cdot 0.5^2} = 0.153$ m

13.10 Vacuum Distillation Column Condenser and Reboiler Design

Condenser:

The LMTD for the total condenser was calculated to be 10.34℃. The temperature of the hot fluid entering (16.7℃) and the hot fluid leaving (12.0℃) was taken from the ASPEN Plus model. The temperature of the propylene glycol water mixture was chosen to enter at 2℃ and exit at 6℃ to achieve an LMTD of at least 10℃.

$$\Delta T_{lm} = \frac{(T_1 - t_2) - (T_2 - t_1)}{\ln \left[\frac{T_1 - t_2}{T_2 - t_1}\right]} = \frac{(16.7159 - 6) - (11.9756 - 2)}{\ln \left[\frac{16.7159 - 6}{11.9756 - 2}\right]} = 10.34℃$$

The area of heat transfer was calculated to be 50.14 m² using the heat duty calculated in ASPEN Plus (155.545 kW) and an overall coefficient of 300 W/ m²℃.

$$Q = UA\Delta T_{lm}$$

$$A = \frac{Q}{U\Delta T_{lm}} = \frac{155,545}{300 \cdot 10.34} = 50.14 \text{ m}^2$$

The mass flow rate of the propylene glycol water mixture required for the condenser was calculated using the specific heat capacity equation, with the specific heat capacity of 3.371 kJ/kg℃ (*Propylene glycol based heat-transfer fluids*, n.d.).

$$Q = mc\Delta T$$

$$m = \frac{Q}{c\Delta T} = \frac{155.545}{3.371 \cdot 4} = 11.54 \text{ kg/s}$$

Reboiler:

The saturation temperature of steam at 15 bar is 198℃ and the boiling point of glycerol at 0.036 bar is 187. 9℃ were used to determine ΔT_m.

$$\Delta T_m = 198 - 187.9 = 10.1℃$$

$$A = \frac{Q}{U\Delta T_{lm}} = \frac{160.743}{200 \cdot 10.1} = 79.58 \text{ m}^2$$

Determination of mass flow rate of steam required using a heat of vaporization for saturated steam at 15 bar of 1946.4 kJ/kg:

$$m = \frac{Q}{\Delta H^{fg}} = \frac{160.743 kW * 3600}{1946.4 \, kJ/kg} = 297.3 \text{ kg/hr}$$

13.11 Steam Jet Ejector Design

Calculation of steam consumption for stage 1:

$$Q = A_2 \sqrt{\frac{2}{\rho} \cdot \frac{P_1 - P_2}{1 - (\frac{A_2}{A_1})^2}} = 0.010261 \ m^2 \sqrt{\frac{2}{1.6508} \cdot \frac{2000 - 15000}{1 - (25)^2}} = 185.58 \ m^3/h$$

$$Q_{mass} = \rho Q = 1.6508 * 185.58 = 306.4 \ kg/h$$

Calculation of steam consumption for stage 2:

$$Q = A_2 \sqrt{\frac{2}{\rho} \cdot \frac{P_1 - P_2}{1 - (\frac{A_2}{A_1})^2}} = 0.0089383 \ m^2 \sqrt{\frac{2}{1.6508} \cdot \frac{12300 - 101325}{1 - (5)^2}} = 2157.13 \ m^3/h$$

$$Q_{mass} = \rho * Q = 1.6508 * 2157.13 = 3561 \ kg/h$$

13.12 Storage Tank Dimension Calculations

WCO feedstock storage tank calculations:

$Q_{mass} = 1202.4$ kg / h

$$Q = \frac{Q_{mass}}{\rho} = \frac{1202.4 \ kg \ / \ h}{915.82 \ kg \ / \ m^3} = 1.3129 \ m^3 \ / \ h$$

$V = Q \cdot t = 1.3129 \ m^3/ \ h \cdot 672 \ h = 882.29 \ m^3$

Final tank design selection $= 900 \ m^3$

Methanol feedstock storage tank calculations:

$Q_{mass} = 132.8$ kg / h

$$Q = \frac{Q_{mass}}{\rho} = \frac{132.8 \ kg \ / \ h}{792 \ kg \ / \ m^3} = 0.16768 \ m^3 \ / \ h$$

$V = Q \cdot t = 0.16768 \ m^3/ \ h \cdot 672 \ h = 112.68 \ m^3$

Final tank design selection $= 125 \ m^3$

Biodiesel post-process storage tank calculations:

$Q_{mass} = 1166.9$ kg / h

$$Q = \frac{Q_{mass}}{\rho} = \frac{1166.9 \; kg \; / \; h}{874 \; kg \; / \; m^3} = 1.3351 \; m^3 \; / \; h$$

$V = Q \cdot t = 1.3351 \; m^3 / h \cdot 672 \; h \; = 897.2 \; m^3$

Final tank design selection $= 900 \; m^3$

Glycerol post-process storage tank calculations:

$Q_{mass} = 107.48$ kg / h

$$Q = \frac{Q_{mass}}{\rho} = \frac{107.48 \; kg \; / \; h}{1261.3 \; kg \; / \; m^3} = 0.085215 \; m^3 \; / \; h$$

$V = Q \cdot t = 0.085215 \; m^3 / h \cdot 672 \; h \; = 57.264 \; m^3$

Final tank design selection $= 60 \; m^3$

13.13 Steam Cost Calculations

High Pressure Steam Price

The price of fuel used was \$4.30/MMBtu (*Natural Gas Futures Contracts*, n.d.) The heating rate was calculated as the enthalpy of 15 bar steam at the superheat temperature minus the enthalpy of saturated water at 15 bar. The boiler efficiency was assumed to be 0.8, and the price of boiler feed water was assumed to cancel with the condensate credit. The steam conditions shown in the table below were obtained from the ASME International Steam Tables (Harvey et al., 2014).

	HPS	LPS
Pressure (bar)	15	3
Saturation Temperature (°C)	198	134
Superheat Temperature (°C)	330	140
Specific Entropy (kJ/kg)	7.0324	7.0269
Specific Enthalpy (kJ/kg)	3104.4	2739.4

$$P_{HPS} = \frac{\$4.30}{MMBtu} \cdot \frac{0.972 MMBtu/Mlb}{0.8} = \$5.23/\text{Mlb steam}$$

Low Pressure Steam Price

Difference in enthalpy levels for isentropic expansion: 365 kJ/kg

Nonisentropic enthalpy of expansion: 310.25 kJ/kg

Shaft work in kWh/Mlb: 39.09

Shaft work credit (using a price of electricity of $0.08/kWh): $3.13/Mlb

Price of 3 bar steam: $2.10/Mlb

13.14 ROI Calculation

$$ROI = \frac{\$72{,}183{,}746 \ (Y_{20}) - \$(27{,}589{,}439) \ (Y_{-1})}{(-22 \ years) * (27{,}589{,}439)} * 100\% = 16.44\%$$

13.15 Pipe Diameter Calculations for Release Scenario Simulation

Scenario 1: Pump 3 Seal Failure resulting in Methanol Release

$$m = 1160.62 \ kg/hr * 0.2 \ = 232.124 \ kg/hr$$

Scenario 2: Gasket Failure Exiting Decanter (S-1) for release of FAME

$$Q = 1.45204 \ m^3/hr \ \rightarrow 0.0004033 \ m^3/s$$

$\boldsymbol{Q = Av, A = \frac{\pi D^2}{4}, Q = \frac{\pi D^2}{4} v}$, where v is defined as 3 m/s because flow velocity for a liquid is between 1 m/s to 5 m/s.

$$D = \sqrt{\frac{4Q}{\pi v}} = \sqrt{\frac{4*(0.0004033 \ \frac{m^3}{s})}{\pi*(3 \ m/s)}} = 13.08 \ mm \sim 14 \ mm \ , \text{this is sized up to a 2 in pipe for the}$$

advantages in real-world planning on usage.

A schedule 40 (Sch 40) pipe is used for material to correspond with this pipe diameter.

Scenario 3: Flow from Pump 4 entering the PFR

$$Q = 11.8665 \ m^3/hr \ \rightarrow 0.003296 \ m^3/s \ \text{ for overall flow in pipe, of which } \sim 50\% \text{ is methanol}$$

$\boldsymbol{Q = Av, A = \frac{\pi D^2}{4}, Q = \frac{\pi D^2}{4} v}$, where v is defined as 3 m/s because methanol is supercritical here and thus a flow velocity for a liquid is chosen, i.e. a value between 1 m/s to 5 m/s.

$$D = \sqrt{\frac{4Q}{\pi v}} = \sqrt{\frac{4*(0.003296 \frac{m^3}{s})}{\pi*(3 \ m/s)}} = 37.4 \ mm \sim 40 \ mm \sim 1.5 \ in, \text{this is sized up to a 2 in pipe for the}$$

advantages in real-world planning on usage.

A schedule 80 (Sch 80) pipe is used for material to correspond with this pipe diameter. It should also be noted that for the simulation release, the flow rate was defined to just methanol and not the entire flow for the pipe sized here.

13.16 Reactivity Matricies

NFPA				Capstone Compatibility Chart	GLYCERINE	METHANOL	OLEIC ACID	OLEIC ACID METHYL ESTER	PROPANE	WATER
Health	Flammability	Instability	Special							
1	1	0		GLYCERINE						
1	3	0		METHANOL	Y					
1	1	0		OLEIC ACID	N	N				
				OLEIC ACID METHYL ESTER	Y	Y	Y			
2	4	0		PROPANE	Y	Y	Y	Y		
				WATER	Y	Y	Y	C	Y	

Y : Compatible
N : Incompatible
C : Caution
SR : Self-Reactive
*: Changed by user

	Glycerol	Methanol
Oleic Acid	Reaction products may be flammable Reaction liberates gaseous products and may cause pressurization Exothermic reaction at ambient temperatures (releases heat) Reaction may be particularly intense, violent, or explosive Polymerization reaction may become intense and may cause pressurization	Reaction products may be flammable Reaction liberates gaseous products and may cause pressurization Exothermic reaction at ambient temperatures (releases heat) Reaction may be particularly intense, violent, or explosive Polymerization reaction may become intense and may cause pressurization

	Methyl Oleate
Water	Reaction products may be corrosive Reaction liberates gaseous products and may cause pressurization

13.17 MCE Risk Level Mapping

Risk Matrix

1. Select the severity from the highest box in either of columns 1, 2 or 3. Read the Category and Safety Severity Level from the same row.
2. Select the likelihood from columns 4 thru 7.
3. Read the Risk Level from the intersection of the severity row and the likelihood column.

TMEF: Target mitigated event frequency
TQ: Threshold Quantity

	1 Human Health Impact	2 Fire, Explosion Direct Cost in $	3 Chemical Impact	Severity Category	Safety Severity Level	Likelihood 4 LIKELY — Expected to happen several times over the life of the plant. — 0 to 9 years	5 UNLIKELY — Expected to happen possibly once over the life of the plant. — 10 to 99 years	6 IMPROBABLE — Expected to happen possibly once in the division over the life of the plant. — ≥ 100 years	7 IMPROBABLE BUT NOT IMPOSSIBLE — Not expected to happen anywhere in the division over the life of the plant — > 1000 years
Severity	Public fatality possible, employee fatalities likely	Greater than $10 MM	≥ 20x TQ	CATASTROPHIC	4 TMEF = 1×10^{-6}	Risk Level A	Risk Level A	Risk Level B	Risk Level C
	Employee fatality possible. Major injury likely	$1 MM to < $10 MM	From 9x to < 20x TQ	VERY SERIOUS	3 TMEF = 1×10^{-5}	Risk Level A	Risk Level B	Risk Level C	Risk Level D
	Lost time injury (LTI) likely[a]	$100K to < $1 MM	From 3x to < 9x TQ	SERIOUS	2 TMEF = 1×10^{-4}	Risk Level B	Risk Level C	Risk Level D	Negligible Risk
	Recordable Injury[b]	$25K to < $100K	From 1x to < 3x TQ	MINOR	1 TMEF = 1×10^{-3}	Risk Level C	Risk Level D	Negligible Risk	Negligible Risk

Risk Level A: Unacceptable risk, additional safeguards must be implemented immediately.
Risk Level B: Undesirable risk, additional safeguards must be implemented within 3 months.
Risk Level C: Acceptable risk, but only if existing safeguards reduces the risk to As Low as Reasonably Practicable (ALARP) levels.
Risk Level D: Acceptable risk, no additional safeguards required.

[a]Lost time injury (LTI): The injured worker is unable to perform regular job duties, takes time off for recovery, or is assigned modified work duties while recovering.
[b]Recordable injury: Death, days away from work (DAW), restricted work or transfer to another job, medical treatment beyond first aid, or loss of consciousness.

13.18 MCE HAZOP Analysis

Parameter	Deviation	Cause	Consequence	Action
Flow	No	Prior pump becomes inoperational (for feedstock or initial mixing pump 3) Pump seal rupture for P-4	Flow rate of methanol/triolein mixture into the reactor is too low or zero, resulting not only in impacts for biodiesel conversion but also can cause severe damage to pump if it is running dry or under capacity. In the situation of a pump seal rupture, could directly result in toxic release	Install pressure gauge(s) on material stream going from pump 3 onwards so if there is low flow as detailed by low pressure, it can be detected quickly Regular line maintenance to monitor corrosion progress and potential leaks or pump seal failures
	High	Error in feedstock pump leading to overflow could directly cause a pump seal failure prior to the PFR Improper pressurization could result in stream behaving less liquid-like and thus having a higher flow velocity which impacts subsequent pumps and processes	Directly lead to a pump seal failure if too much material is flowing into a pump aiming to compress to a higher pressure, i.e. with pump 3 or pump 4. High flow rate could also overwhelm connection to PFR which is being conducted in a relatively small pipe and may cause a burst at a connection point, i.e. a gasket seal failure	Add pressure relief valve to piping system and potentially reactor (relief valve should vent to scrubber or some methanol processing ideally because of component composition) Install flow meter on pipe system going into PFR, either for volumetric or flow velocity or both

Parameter	Deviation	Cause	Consequence	Action
Pressure	Low	Improper pressurization from one of the compressor pumps on the line prior to the PFR High flow rates resulting in either ineffective pressurization of material stream	Direct consequence is that high pressures and supercritical methanol are crucial to the biodiesel conversion process, so transesterification may be impacted or directly reduced	Regular line maintenance to monitor corrosion progress and potential leaks, install redundant pressure gauges and alarms.
	High	Overpressurization from inadvertent reaction or contamination of material streams. (i.e. methanol reacts with oleic acid or glycerol somewhere along the process or after recycle stream begins) Increased flow amounts with a constant flow velocity could lead to an overpressuriziation because of pumps' inability to move material stream. In addition, blockages in stream from particulate or too much liquid could result in limited flow through pipe system causing a backup and over pressuring.	Damage to process equipment. Potential rupture of process piping, reactor, or valves causing a loss of containment of methanol stream. Direct failure for pump seals, gasket seals, and any other connective equipment that serve as weak/failure points for pipe system.	Ensure proper sizing and maintenance of pressure relief valves on the plug flow reactor and on the distillation column (D-1) in the case of overpressure events. Install a flow meter on the feed to the PFR and monitor feed composition. Have redundant pressure gauges and alarms. Add pressure relief valve to piping system.

13.19 IPL Identification for MCE Risk Mitigation

Type of IPL	Description	IPL Credits
Pressure Relief Valve	Helps to prevent a system from exceeding a specific pressure level and leading to over pressurization. The effectiveness of this system depends on the amount of service and experience it's used for as well as the type of system it is working in and the level of exposure to corrosion, dirt, or a polymerizing product.	2
Rupture Disk	Helps to prevent a system from exceeding a specific pressure level and leading to over pressurization. The effectiveness of this system depends on the amount of service and experience it's used for as well as the type of system it is working in and the level of exposure to corrosion, dirt, or a polymerizing product.	2
Excess Flow Valve	In-line valves through which pressurized liquids or vapors run and can be shut off if there's an excessive discharge of vapor or liquid resulting in a break in a hose or piping system, in this situation the latter.	1
Basic Process Control System	Leak detectors, automatic feed shut-off system, pressure gauges, flow meters	1
Operator response	Routine operation under high stress following established procedures and practices	1

13.20 LOPA for MCE

1. Initiating Event (IE) Frequency (Table 12-2)
   a. **10^{-1}/year**
2. Severity Level (Table 1-14 – Risk Matrix)
   a. **Very Serious**
3. Likelihood (from 1 and Table 1-14)
   a. **Unlikely**
4. Risk Level (from 2 and 3 and Table 1-14)
   a. **Risk level B**
5. Target Mitigated Event Frequency (TMEF) (Table 1-14 – Risk Matrix)
   a. **10^{-5}/year**
6. Enabling Conditions
   a. The material inflow line for the PFR and the methanol running through this line operate constantly when site is in operation so the enabling conditions are not a limiting factor.
7. Conditional Modifiers:
   a. No conditional modifiers in this situation.
8. Adjusted Initiating Event Frequency (Multiply 1 x 6 x 7)
   a. $1.0 * 10^{-1} = \mathbf{10^{-1}}$ **/year**.
9. Existing Layers of Protection (type and PFD from Table 12-3, 12-4)
   a. Total: $10^{-2} * 10^{-2} * 10^{-1} * 10^{-1} * 10^{-1} = \mathbf{10^{-7}}$**/year**
10. Frequency with Existing Layers of Protection (Multiply 8 x 9)
    a. $10^{-1} * 10^{-8} = \mathbf{10^{-8}}$
11. Additional Layers of Protection Required
    a. $1 * 10^{-5} / (10^{-8}) = 1000$, **no additional layers required**

Table 6-9 Ratio factors for estimating capital investment items based on delivered-equipment cost

Values presented are applicable for major process plant additions to an existing site where the necessary land is available through purchase or present ownership.[†] The values are based on fixed-capital investments ranging from under $1 million to over $100 million.

	Percent of delivered-equipment cost for		
	Solid processing plant[‡]	Solid-fluid processing plant[‡]	Fluid processing plant[‡]
Direct costs			
Purchased equipment delivered (including fabricated equipment, process machinery, pumps, and compressors)	100	100	100
Purchased-equipment installation	45	39	47
Instrumentation and controls (installed)	18	26	36
Piping (installed)	16	31	68
Electrical systems (installed)	10	10	11
Buildings (including services)	25	29	18
Yard improvements	15	12	10
Service facilities (installed)	40	55	70
Total direct plant cost	269	302	360
Indirect costs			
Engineering and supervision	33	32	33
Construction expenses	39	34	41
Legal expenses	4	4	4
Contractor's fee	17	19	22
Contingency	35	37	44
Total indirect plant cost	128	126	144
Fixed-capital investment	397	428	504
Working capital (15% of total capital investment)	70	75	89
Total capital investment	467	503	593

[†]Because of the extra expense involved in supplying service facilities, storage facilities, loading terminals, transportation facilities, and other necessary utilities at a completely undeveloped site, the fixed-capital investment for a new plant located at an undeveloped site may be as much as 100 percent greater than that for an equivalent plant constructed as an addition to the existing plant.

[‡]See Table 6-6 for descriptions of types of process plants.

(Peters et al., 2003)

13.22 Operators Needed for Continuous Operation

1. Determine shifts per operator per year

   - Operators work 49 weeks/year, 5 8-hour shifts/week

   - Total shifts per operator per year: 49×5=245 shifts/year

2. Calculate total plant shifts per year

   - The plant operates 24/7 with 3 shifts/day

   - Total plant shifts per year: 365×3=1095 shifts/year

3. Determine total operators required

   - Operators needed to cover all shifts: 1095 shifts/year / 245 shifts/year = 4.469

13.23 Theoretical Calculations for Change in Methanol Recovery Rate

$Entering\ Separator: 7.3897\frac{kg}{hr}MeOH\ ; Exiting\ Separator\ into\ Biodiesel\ Stream: 1.9338\frac{kg}{hr}MeOH$

$1.9338\frac{kg}{hr} \div 7.3897\frac{kg}{hr} * 100\% = \sim26.16\%\ of\ methanol\ is\ sent\ into\ biodiesel\ stream$

$Entering\ Flash\ 2: 1.9338\frac{kg}{hr}\ MeOH; Exiting\ Flash\ 2: 1.5301\frac{kg}{hr}MeOH$

$1.5301\frac{kg}{hr} \div 1.9338\frac{kg}{hr} * 100\% = \sim79.15\%\ of\ methanol\ is\ released\ as\ a\ vapor$

$Allowable\ Methanol\ VOC\ release\ Quantity: 2.7\frac{tons}{yr} = \frac{2700\frac{kg}{yr}}{90\%\ est\ uptime} = 3000\frac{kg}{yr}$

$3000\frac{kg}{yr} = 0.3425\frac{kg}{hr} \div 0.7915\ (79.15\%) = 0.4327\frac{kg}{hr}entering\ Flash\ 2$

$0.4327\frac{kg}{hr}into\ F2 \div 0.2616\ (26.16\%) = 1.654\frac{kg}{hr}entering\ separator$

$Methanol\ Recycle\ Stream\ (curr.): 920.161\frac{kg}{hr}MeOH\ out\ of\ PFR; 912.771\frac{kg}{hr}MeOH\ recycled\ back\ in$

$912.771\frac{kg}{hr}MeOH \div 920.161\frac{kg}{hr}MeOH * 100\% = 99.2\%\ recovery\ currently$

Ideal MeOH Recycle Stream:

$920.161\frac{kg}{hr}MeOH\ out\ of\ PFR - 1.654\frac{kg}{hr}entering\ S1 = 918.507\frac{kg}{hr}MeOH\ gets\ recycled$

$918.507\frac{kg}{hr}MeOH\ \div 920.161\frac{kg}{hr}MeOH * 100\% = 99.8\%\ recycling\ rate$

14 Works Cited

20LB High Purity USA PROPANE R290 – 99.5% Guaranteed – Scientific Solutions. (n.d.). Retrieved March 20, 2025, from https://www.scisolinc.com/product/50-high-purity-usa-propane-lot-analysis-99-66-99-5-guaranteed/

Aboelazayem, O., Gadalla, M., & Saha, B. (2018). Biodiesel production from waste cooking oil *via* supercritical methanol: Optimisation and reactor simulation. *Renewable Energy*, *124*, 144–154. https://doi.org/10.1016/j.renene.2017.06.076

Advances in biotechnological applications of waste cooking oil. (2021). *Case Studies in Chemical and Environmental Engineering*, *4*, 100158. https://doi.org/10.1016/j.cscee.2021.100158

Alenezi, R., Baig, M., Wang, J., Santos, R., & Leeke, G. A. (2010). Continuous Flow Hydrolysis of Sunflower Oil for Biodiesel. *Energy Sources, Part A: Recovery, Utilization, and Environmental Effects*, *32*(5), 460–468. https://doi.org/10.1080/15567030802612341

Alenezi, R., Leeke, G. A., Winterbottom, J. M., Santos, R. C. D., & Khan, A. R. (2010). Esterification kinetics of free fatty acids with supercritical methanol for biodiesel production. *Energy Conversion and Management*, *51*(5), 1055–1059. https://doi.org/10.1016/j.enconman.2009.12.009

Alternative Fuels Data Center: Maps and Data - U.S. Biodiesel Production, Exports, and Consumption. (n.d.). U.S. Department of Energy. Retrieved October 27, 2024, from https://afdc.energy.gov/data/10325

Anantapinitwatna, A., Ngaosuwan, K., Kiatkittipong, W., Wongsawaeng, D., & Assabumrungrat, S. (2019). Effect of Water Content in Waste Cooking Oil on Biodiesel Production via Ester-transesterification in a Single Reactive Distillation. *IOP Conference Series: Materials Science and Engineering*, *559*(1), 012014. https://doi.org/10.1088/1757-899X/559/1/012014

Ashurst, J. V., Schaffer, D. H., & Nappe, T. M. (2025). Methanol Toxicity. In *StatPearls*. StatPearls Publishing. http://www.ncbi.nlm.nih.gov/books/NBK482121/

Attarakih, M., Abu Fara, D., & Sayed, S. (2001). Dynamic Modeling of a Packed-Bed Glycerol−Water Distillation Column. *Industrial & Engineering Chemistry Research*, *40*(22), 4857–4865. https://doi.org/10.1021/ie000430y

Aykas, D. P., & Rodriguez-Saona, L. E. (2016). Assessing potato chip oil quality using a portable infrared spectrometer combined with pattern recognition analysis. *Analytical Methods*, *8*(4), 731–741. https://doi.org/10.1039/C5AY02387D

Bauer, R. C., & German, R. C. (1961). *The Effect of Second Throat Geometry on the Performance of Ejectors without Induced Flow* (AEDC-TN-61-133). Arnold Engineering Development Center Air Force Systems Command.

Bautista, L., Vicente, G., Rodríguez, R., & Pacheco, M. (2009). Optimisation of FAME production from waste cooking oil for biodiesel use. *Biomass and Bioenergy*, *33*(5), 862–872. https://doi.org/10.1016/j.biombioe.2009.01.009

Beck, K. (2022, December 28). *The US State Known As The "Potato Chip Capital Of The World."* https://www.tastingtable.com/1150424/the-us-state-known-as-the-potato-chip-capital-of-the-world/

Blackwell, N. J. (U. Va. student). (2019). *Sustainability and Environmental Concerns of Biodiesel Production (STS Research Paper)* (By Request). (c)2019.

Bleviss, D. L. (2021). Transportation is critical to reducing greenhouse gas emissions in the United States. *WIREs Energy and Environment*, *10*(2), e390. https://doi.org/10.1002/wene.390

Borough of Ephrata, PA: Article VII Industrial Waste Pretreatment. (n.d.). Borough of Ephrata, PA Code. Retrieved March 21, 2025, from https://ecode360.com/6857723

Brahma, S., Nath, B., Basumatary, B., Das, B., Saikia, P., Patir, K., & Basumatary, S. (2022). Biodiesel production from mixed oils: A sustainable approach towards industrial biofuel production. *Chemical Engineering Journal Advances*, *10*, 100284. https://doi.org/10.1016/j.ceja.2022.100284

Canada, E. and C. C. (2010, June 11). *Appendix 1: Methanol - The Story of a Substance* [Not available]. https://www.canada.ca/en/environment-climate-change/services/canadian-environmental-protection-act-registry/historical/substances-lists/pollutants-environment-introduction-national-pollutant-release-inventory/appendix-1.html

Carbon Steel vs Stainless Steel. (n.d.). Retrieved February 11, 2025, from https://markforged.com/resources/blog/carbon-steel-vs-stainless-steel

Chai, M., Tu, Q., Lu, M., & Yang, Y. J. (2014). Esterification pretreatment of free fatty acid in biodiesel production, from laboratory to industry. *Fuel Processing Technology*, *125*, 106–113. https://doi.org/10.1016/j.fuproc.2014.03.025

Chaudhary, A., Gupta, A., Kumar, S., & Kumar, R. (2019). Pool fires of jatropha biodiesel and their blends with petroleum diesel. *Experimental Thermal and Fluid Science*, *101*, 175–185. https://doi.org/10.1016/j.expthermflusci.2018.10.021

Citra Dewi, A. S. & Slamet. (2019). Novel approach of esterification process using heterogeneous catalyst in biodiesel synthesis from waste cooking oil. *IOP Conference Series: Materials Science and Engineering*, *509*(1), 012012. https://doi.org/10.1088/1757-899X/509/1/012012

Code of Federal Regulations. (n.d.). Retrieved March 21, 2025, from https://www.govinfo.gov/content/pkg/CFR-2014-title40-vol29/xml/CFR-2014-title40-vol29-chapI-subchapN.xml

Consumer Price Index. (2025). [Dataset]. https://www.bls.gov/cpi/tables/supplemental-files/

Cox, A. W., Lees, F. P., Ang, M. L., & Loughborough University of Technology (Eds.). (1991). *Classification of hazardous locations: A report of the Inter-Institutional Group on the Classification of Hazardous Locations (IIGCHL)* (Repr). Institution of Chemical Engineers.

D02 Committee. (2024). *Specification for Biodiesel Fuel Blendstock (B100) for Middle Distillate Fuels*. ASTM International. https://doi.org/10.1520/D6751-24

Daud, N. M., Sheikh Abdullah, S. R., Abu Hasan, H., & Yaakob, Z. (2015). Production of biodiesel and its wastewater treatment technologies: A review. *Process Safety and Environmental Protection*, *94*, 487–508. https://doi.org/10.1016/j.psep.2014.10.009

Farobie, O., & Matsumura, Y. (2017). State of the art of biodiesel production under supercritical conditions. *Progress in Energy and Combustion Science*, *63*, 173–203. https://doi.org/10.1016/j.pecs.2017.08.001

Federal Tax Incentives: Biodiesel Fuel Credit § 40A. (n.d.). Retrieved March 7, 2025, from https://www.andretaxco.com/biodiesel-fuel-credit?

Flash Vessels: Calculation, Definition, Working Principle, Function, Design, and Sizing – JEFERSON COSTA. (n.d.). Retrieved February 13, 2025, from https://jefersoncosta.com/flash-vessels-calculation-definition-working-principle-function-design-and-sizing/

G Doná, Cardozo-Filho, L., Silva, C., & Castilhos, F. (2013). Biodiesel production using supercritical methyl acetate in a tubular packed bed reactor. *Fuel Processing Technology*, *106*, 605–610. https://doi.org/10.1016/j.fuproc.2012.09.047

Ghoreishi, S. M., & Moein, P. (2013). Biodiesel synthesis from waste vegetable oil via transesterification reaction in supercritical methanol. *The Journal of Supercritical Fluids*, *76*, 24–31. https://doi.org/10.1016/j.supflu.2013.01.011

Green approach for chemical production from waste cooking oils. (2023). *Sustainable Chemistry for Climate Action*, *2*, 100017. https://doi.org/10.1016/j.scca.2023.100017

Green, D. W., & Southard, M. Z. (2019). *Perry's Chemical Engineers' Handbook, 9th Edition* (9th edition). McGraw-Hill Education.

Greer, H. (2024, July 3). *Biodiesel Production Hits Record Highs as Demand and Adoption Surge*. ResourceWise. https://www.resourcewise.com/environmental-blog/biodiesel-production-hits-record-highs-as-demand-and-adoption-surge

Growth in global energy demand surged in 2024 to almost twice its recent average—News. (2025, March 24). IEA. https://www.iea.org/news/growth-in-global-energy-demand-surged-in-2024-to-almost-twice-its-recent-average

Gutiérrez Ortiz, F. J., & de Santa-Ana, P. (2017). Techno-economic assessment of an energy self-sufficient process to produce biodiesel under supercritical conditions. *The Journal of Supercritical Fluids*, *128*, 349–358. https://doi.org/10.1016/j.supflu.2017.03.010

He, L., Xie, H., Zong, Y., Zhao, L., & Dai, G. (2025, January 6). *Enhancing interfacial mass transfer for high-viscosity fluids: Hydrodynamic and mass transfer by twin-liquid film*. AICHE. https://aiche.onlinelibrary.wiley.com/doi/10.1002/aic.18708

Hearst Autos Research. (2020, April 22). *Biodiesel vs. Diesel: Everything You Need to Know*. Car and Driver. https://www.caranddriver.com/research/a31883731/biodiesel-vs-diesel/

Incorporated, C. L. V. (n.d.). *Climate and Average Weather Year Round in Lancaster*. Weatherspark. Retrieved March 18, 2025, from https://weatherspark.com/y/21992/Average-Weather-in-Lancaster-Pennsylvania-United-States-Year-Round

Is the biofuel industry approaching a feedstock crunch? – Analysis. (2022, December 6). IEA. https://www.iea.org/reports/is-the-biofuel-industry-approaching-a-feedstock-crunch

Karki, S., Sanjel, N., Poudel, J., Choi, J. H., & Oh, S. C. (2017). Supercritical Transesterification of Waste Vegetable Oil: Characteristic Comparison of Ethanol and Methanol as Solvents. *Applied Sciences*, *7*(6), Article 6. https://doi.org/10.3390/app7060632

Karmee, S. K., Patria, R. D., & Lin, C. S. K. (2015). Techno-Economic Evaluation of Biodiesel Production from Waste Cooking Oil—A Case Study of Hong Kong. *International Journal of Molecular Sciences*, *16*(3), Article 3. https://doi.org/10.3390/ijms16034362

Khan, N., Park, S. H., Kadima, L., Bourdeau, C., Calina, E., Edmunds, C. W., & Pursell, D. P. (2021). Locally Sustainable Biodiesel Production from Waste Cooking Oil and Grease Using a Deep Eutectic Solvent: Characterization, Thermal Properties, and Blend Performance. *ACS Omega*, *6*(13), 9204. https://doi.org/10.1021/acsomega.1c00556

Know the Differences Between 304 Stainless Steel vs 316. (2021, August 9). Kloeckner Metals. https://www.kloecknermetals.com/blog/304-stainless-steel-vs-316/

Kocsisová, T., Juhasz, J., & Cvengroš, J. (2006). Hydrolysis of fatty acid esters in subcritical water. *European Journal of Lipid Science and Technology*, *108*(8), 652–658. https://doi.org/10.1002/ejlt.200600061

Koeva Brooks, P., & Koeva Brooks, P. (2000). *The Facts About Time: To-Build*. International Monetary Fund. https://doi.org/10.5089/9781451855975.001

Kusdiana, D., & Saka, S. (2001). Kinetics of transesterification in rapeseed oil to biodiesel fuel as treated in supercritical methanol. *Fuel*, *80*(5), 693–698. https://doi.org/10.1016/S0016-2361(00)00140-X

Kusdiana, D., & Saka, S. (2004a). Effects of water on biodiesel fuel production by supercritical methanol treatment. *Bioresource Technology*, *91*(3), 289–295. https://doi.org/10.1016/S0960-8524(03)00201-3

Kusdiana, D., & Saka, S. (2004b). Two-step preparation for catalyst-free biodiesel fuel production: Hydrolysis and methyl esterification. *Applied Biochemistry and Biotechnology*, *113–116*, 781–791. https://doi.org/10.1385/abab:115:1-3:0781

Lawry, K., & Pons, D. J. (2013). Integrative Approach to the Plant Commissioning Process. *Journal of Industrial Engineering*, *2013*, 1–12. https://doi.org/10.1155/2013/572072

Lee, S., Posarac, D., & Ellis, N. (2011). Process simulation and economic analysis of biodiesel production processes using fresh and waste vegetable oil and supercritical methanol. *Chemical Engineering Research & Design: Transactions of the Institution of Chemical Engineers Part A*, *89*(12), 2626–2642. https://doi.org/10.1016/j.cherd.2011.05.011

Liu, J. (2013). *Biodiesel Synthesis via Transesterification Reaction in Supercritical Methanol: A) A Kinetic Study, b) Biodiesel Synthesis Using Microalgae Oil*. Syracuse University.

Lopresto, C. G., De Paola, M. G., & Calabrò, V. (2024). Importance of the properties, collection, and storage of waste cooking oils to produce high-quality biodiesel – An overview. *Biomass and Bioenergy*, *189*, 107363. https://doi.org/10.1016/j.biombioe.2024.107363

Ma, F., & Hanna, M. (1999). Biodiesel production: A review. *Bioresource Technology*, *70*(1), 1–15. https://doi.org/10.1016/S0960-8524(99)00025-5

Marchetti, J. M., & Errazu, A. F. (2008). Technoeconomic study of supercritical biodiesel production plant. *Energy Conversion and Management*, *49*(8), 2160–2164. https://doi.org/10.1016/j.enconman.2008.02.002

Methanol Institute. (n.d.). *Atmospheric Above Ground Tank Storage of Methanol*. https://www.methanol.org/wp-content/uploads/2016/06/AtmosphericAboveGroundTankStorageMethanol-1.pdf

Methanol—DCCEEW. (n.d.). Retrieved April 1, 2025, from https://www.dcceew.gov.au/environment/protection/npi/substances/fact-sheets/methanol#tabs-3

Miyatake, O., Hashimoto, T., & Lior, N. (1992). *The liquid flow in multi-stage flash evaporators*. *35*(12), 3245–3257.

Modi, D. N. (2010). *Biodiesel production using supercritical methanol*.

Monika, Banga, S., & Pathak, V. V. (2023). Biodiesel production from waste cooking oil: A comprehensive review on the application of heterogenous catalysts. *Energy Nexus*, *10*, 100209. https://doi.org/10.1016/j.nexus.2023.100209

Nagapurkar, P., & Smith, J. D. (2023). Techno-economic and life cycle analyses for a supercritical biodiesel production process from waste cooking oil for a plant located in the Midwest United States. *Environment, Development and Sustainability*. https://doi.org/10.1007/s10668-023-03064-9

Natural Gas Futures Contracts. (n.d.). OilPrice.Com. Retrieved March 26, 2025, from https://oilprice.com/futures/natural-gas

NguyenThi, T., Bazile, J.-P., & Bessières, D. (2018). Density Measurements of Waste Cooking Oil Biodiesel and Diesel Blends Over Extended Pressure and Temperature Ranges. *Energies*, *11*(5), 1212. https://doi.org/10.3390/en11051212

Nisworo, A. P. (2005). *Biodiesel by supercritical transesterification: Process design and economic feasibility* [EngD Thesis]. Technische Universiteit Eindhoven.

Okoro, O. V., Sun, Z., & Birch, J. (2018). Catalyst-Free Biodiesel Production Methods: A Comparative Technical and Environmental Evaluation. *Sustainability*, *10*(1), Article 1. https://doi.org/10.3390/su10010127

Oliveira, M., Ramos, A., Monteiro, E., & Rouboa, A. (2022). Improvement of the Crude Glycerol Purification Process Derived from Biodiesel Production Waste Sources through Computational Modeling. *Sustainability*, *14*(3), 1747. https://doi.org/10.3390/su14031747

Open Sourcemap—Development Environment. (n.d.). Open Sourcemap - Development Environment. Retrieved November 8, 2024, from https://127.0.0.1:3000/maps/61699b711c59e6e4501e8db9/things

Pasha, M. K., Dai, L., Liu, D., Guo, M., & Du, W. (2021). An overview to process design, simulation and sustainability evaluation of biodiesel production. *Biotechnology for Biofuels*, *14*(1), 129. https://doi.org/10.1186/s13068-021-01977-z

Pennsylvania Business Tax Guide. (2024, February 5). Optic Tax. https://optictax.com/pennsylvania-business-tax-guide/

Pennsylvania Code and Bulletin. (2024, December 28). Commonwealth of Pennsylvania. https://www.pacodeandbulletin.gov/Display/pacode?file=/secure/pacode/data/025/chapter129/s_rev129.1.html&d=reduce

Peters, M., Timmerhaus, K., & West, R. (2002). *Plant Design and Economics for Chemical Engineers* (5th ed.). McGraw Hill.

Peters, M. A., Alves, C. T., Wang, J., & Onwudili, J. A. (2022). Subcritical Water Hydrolysis of Fresh and Waste Cooking Oils to Fatty Acids Followed by Esterification to Fatty Acid Methyl Esters: Detailed Characterization of Feedstocks and Products. *ACS Omega*, *7*(50), 46870–46883. https://doi.org/10.1021/acsomega.2c05972

Pharma grade glycerin. (n.d.). Retrieved November 15, 2024, from https://www.sulzer.com/en/shared/applications/glycerin

Propylene glycol based heat-transfer fluids. (n.d.). Engineering Toolbox. Retrieved February 25, 2025, from https://www.engineeringtoolbox.com/propylene-glycol-d_363.html

Propylene Glycol USP. (n.d.). Retrieved March 31, 2025, from https://www.univarsolutions.com/propylene-glycol-usp-3903000

Quesada-Medina, J., & Olivares-Carrillo, P. (2011). Evidence of thermal decomposition of fatty acid methyl esters during the synthesis of biodiesel with supercritical methanol. *The Journal of Supercritical Fluids*, *56*(1), 56–63. https://doi.org/10.1016/j.supflu.2010.11.016

RDP Reciprocating Pumps. (2025). Ruhrpumpen. https://www.ruhrpumpen.com/en/products/reciprocating-pumps/rdp-pump.html

Rogers, D. W., & Choudhury, D. N. (1978). *Heats of hydrogenation of large molecules. Part 3—Five simple unsaturated triglycerides (triacylglycerols)*. *74*, 2868–2872.

Saka, S., Isayama, Y., Ilham, Z., & Jiayu, X. (2010). New process for catalyst-free biodiesel production using subcritical acetic acid and supercritical methanol. *Fuel*, *89*(7), 1442–1446. https://doi.org/10.1016/j.fuel.2009.10.018

Salihu, A., Mahmood, A. A., Gimba, S., Nzerem, P., & Okafor, I. (2021). Production of Biodiesel from Waste Cooking Oil by Transesterification Process using Heterogeneous Catalyst. Nigerian Journal of Environmental Sciences and Technology, 5(2), 501–510. https://doi.org/10.36263/nijest.2021.02.0308

Seider, W. D., Lewin, D. R., Seader, J. D., Widagdo, S., Gani, R., & Ng, K. M. (2017). *Product and process design principles: Synthesis, analysis, and evaluation* (Fourth edition). John Wiley & Sons Inc.

Serrano, L. M. V., & Silva, M. G. D. (2018). Study About Nitrogen Oxide Emissions and Fuel Consumption in Diesel Engines Fueled with B20. In K. Biernat (Ed.), *Biofuels—State of Development*. InTech. https://doi.org/10.5772/intechopen.74681

Sheehan, J., Camobreco, V., Duffield, J., Graboski, M., & Shapouri, H. (1998). *An Overview of Biodiesel and Petroleum Diesel Life Cycles*. https://www.nrel.gov/docs/legosti/fy98/24772.pdf

Sinnott, R. (with Coulson, J. M., & Richardson, J. F.). (2005). *Chemical Engineering Design: Chemical Engineering Volume 6* (4th ed). Elsevier Science & Technology.

Song, A., Zhao, S., Cao, Y., & Li, C. (n.d.). Effect of Sparger Characteristics on Bubble-Formation Dynamics under Oscillatory Air Pattern. *May 18, 2022*. https://www.mdpi.com/2227-9717/10/5/997

Structured Packing. (n.d.). Koch-Glitsch. https://www.koch-glitsch.com/technical-documents/brochures/structured-packing-brochure

The Cary Company. (n.d.). *Mica Band Heaters*. Retrieved March 31, 2025, from https://www.thecarycompany.com/catalogsearch/result/?q=Mica%20Band%20Heater

The Ultimate Guide to Fry Potato Chips. (2020, November 9). *Rosenqvists Food Technologies*. https://foodtechnologies.rosenqvists.com/articles/the-ultimate-guide-to-fry-potato-chips/

Towler, G., & Sinnot, R. (2021). *Chemical Engineering Design: Principles, Practice and Economics of Plant and Process Design Third Edition* (3eme éd). Elsevier.

Trejo-Zárraga, F., Hernández-Loyo, F. D. J., Chavarría-Hernández, J. C., & Sotelo-Boyás, R. (2018). Kinetics of Transesterification Processes for Biodiesel Production. In K. Biernat (Ed.), *Biofuels—State of Development*. InTech. https://doi.org/10.5772/intechopen.75927

Turton, R., Shaeiwitz, J. A., Bhattacharyya, D., & Whiting, W. B. (2018). *Analysis, synthesis, and design of chemical processes* (Fifth edition). Prentice Hall.

U.S. Department of Energy. (n.d.). *Alternative Fuels Data Center: ASTM Biodiesel Specifications*. Retrieved April 28, 2025, from https://afdc.energy.gov/fuels/biodiesel-specifications

U.S. Department of Energy. (2024). *Clean Cities and Communities Alternative Fuel Price Report, July 2024*. https://afdc.energy.gov/files/u/publication/alternative_fuel_price_report_july_2024.pdf

US EPA. (2015, August 25). *Fast Facts on Transportation Greenhouse Gas Emissions* [Overviews and Factsheets]. https://www.epa.gov/greenvehicles/fast-facts-transportation-greenhouse-gas-emissions

US EPA. (2023, February 9). *Why We Need to Decarbonize Transportation* [Guidance (OMB)]. EPA. https://www.epa.gov/greenvehicles/why-we-need-decarbonize-transportation

Van Kasteren, J. M. N., & Nisworo, A. P. (2007). A process model to estimate the cost of industrial scale biodiesel production from waste cooking oil by supercritical transesterification. *Resources, Conservation and Recycling*, *50*(4), 442–458. https://doi.org/10.1016/j.resconrec.2006.07.005

Verein Deutscher Ingenieure. (2010). *VDI Heat Atlas*. Springer Berlin Heidelberg. https://doi.org/10.1007/978-3-540-77877-6

Wen, Z., Yu, X., Tu, S.-T., Yan, J., & Dahlquist, E. (2010). Biodiesel production from waste cooking oil catalyzed by TiO2–MgO mixed oxides. *Bioresource Technology*, *101*(24), 9570–9576. https://doi.org/10.1016/j.biortech.2010.07.066

Woods, D. R. (2007). *Rules of Thumb in Engineering Practice* (1st ed.). Wiley. https://doi.org/10.1002/9783527611119

Zeng, D., Li, R., Wang, B., Xu, J., & Fang, T. (2014). A review of transesterification from low-grade feedstocks for biodiesel production with supercritical methanol. *Russian Journal of Applied Chemistry*, *87*(8), 1176–1183. https://doi.org/10.1134/S107042721408028X

Zhang, Y. (2003). Biodiesel production from waste cooking oil: 1. Process design and technological assessment. *Bioresource Technology*, *89*(1), 1–16. https://doi.org/10.1016/S0960-8524(03)00040-3